Speed Control of Sensor-less PMSM Drive using Chattering-free Sliding Mode Controller for Electric Vehicle Propulsion: (Three-wheeler Bajaj)

By: - Habtamie Geleta Tadele

A Thesis Submitted to

The Department of Electrical Power and Control Engineering

School of Electrical Engineering and Computing

Presented in Partial Fulfillment of the Requirement for the Degree of Master of Science in Electrical Power and Control engineering (Control Engineering)

Office of Graduate Studies

Adama Science and Technology University

July 2021

Adama, Ethiopia

Speed Control of Sensor-less PMSM Drive using Chattering-free Sliding Mode Controller for Electric Vehicle Propulsion: (Three-wheeler Bajaj)

By: - Habtamie Geleta Tadele
Advisor: Prof. Seungnam Kim
Co-advisor: Mr. Minyamer Gelawe Wase (MSc.)

A Thesis Submitted to
The Department of Electrical Power and Control Engineering
School of Electrical Engineering and Computing

Presented in Partial Fulfillment of the Requirement for the Degree of Master's of Science in Electrical Power and Control engineering (Control Engineering)

Office of Graduate Studies
Adama Science and Technology University

July 2021
Adama, Ethiopia

DECLARATION

I hereby declare that this Master Thesis entitled "Speed Control of Sensor-less PMSM Drive using Chattering-free Sliding Mode Controller for Electric Vehicle Propulsion: (Three-wheeler Bajaj)" is my original work. That is, it has not been submitted for the award of any academic degree, diploma, or certificate in any other university. All sources of materials that are used for this thesis have been duly acknowledged through citation.

Name of Student	Signature	Date

RECOMMENDATION

We, the advisors of this thesis, hereby certify that we have read the revised version of the thesis entitled "Speed Control of Sensor-less PMSM Drive using Chattering-free Sliding Mode Controller for Electric Vehicle Propulsion: (Three-wheeler Bajaj)" prepared under our guidance by **Habtamie Geleta** submitted in partial fulfillment of the requirements for the degree of Masters of Science in electrical power and control engineering (control). Therefore, we recommend the submission of the revised version of the thesis to the department following the applicable procedures.

Prof. Seungnam Kim		
Advisor	Signature	Date
Mr. Minyamer Gelawe Wase (MSc.)		
Co-advisor	Signature	Date

APPROVAL SHEET

We, the advisors of this thesis entitled "Speed Control of Sensor-less PMSM Drive using Chattering-free Sliding Mode Controller for Electric Vehicle Propulsion: (Three-wheeler Bajaj)" and developed by **Habtamie Geleta Tadele,** hereby certify that the recommendations and suggestions made by the board of examiners are appropriately incorporated into the final version of the thesis.

Prof. Seungnam Kim		
Advisor	Signature	Date
Mr. Minyamer Gelawe Wase (MSc.)		
Co-advisor	Signature	Date

We, the undersigned, members of the Board of Examiners of the thesis by **Habtamie Geleta** have read and evaluated the thesis entitled "Speed Control of Sensor-less PMSM Drive using Chattering-free Sliding Mode Controller for Electric Vehicle Propulsion: (Three-wheeler Bajaj)" and examined the candidate during open defense. This is, therefore, to certify that the thesis is accepted for partial fulfillment of the requirement of the degree of Master of Science in Electrical Power and Control Engineering (Control).

Chairperson	Signature	Date
Internal Examiner	Signature	Date
Dr. Beteley Teka		July 28 2021
External Examiner	Signature	Date

Finally, approval and acceptance of the thesis is contingent upon submission of its final copy to the Office of Postgraduate Studies (OPGS) through the Department Graduate Council (DGC) and School Graduate Committee (SGC).

Department Head	Signature	Date
School Dean	Signature	Date
Office of Postgraduate Studies, Dean	Signature	Date

ACKNOWLEDGEMENT

First and foremost, I would like to thank Almighty **God** for everything. Then my gratitude goes to my supervisor **Prof. Seungnam Kim** for his supervision, friendly attitude, and sharing of many good ideas. Regardless of his high workload, he always makes time to answer questions as well as giving encouraging advice. You are highly appreciated!

I am also very grateful to my co-advisor **Mr. Minyamer Gelawe Wase (MSc.)** for lots of advice and help in preparing the thesis documentation, but also for good ideas and discussions regarding everything from implementations of the system in Simulink in general.

I would moreover like to thank **Dr. Tefera Terefe Ytayew** for his patience, helpful advice, and sharing of his knowledge.

I want to give great gratitude to, the Department Head **Mr. Mesfin Merga** and department Postgraduate Coordinator **Dr. Milkias Brhanu** for their initiation for accomplishing the thesis in proper time.

Finally, I would like to thank my whole family and friends. Words cannot express how grateful I am to my Family and friends for their love, encouragement, and all of the sacrifices that they have made up to this time.

TABLE OF CONTENTS

LIST OF TABLES

TABLE OF FIGURES

LIST OF ACRONYMS

AC	Alternating Current
DC	Direct Current
SMC	Sliding Mode Controller
HOSMC	High Order Sliding Mode Controller
PMSM	Permanent Magnet Synchronous Motor
BLDCM	Brushless Direct Current Motor
IM	Induction Motor
EV	Electric Vehicle
SRM	Synchronous Reluctance Motor
IGBT	Insulated Gate Bipolar Transistor
MOSFET	Metallic Oxide Semiconductor Field Effect Transistor
FOSMC	Fractional Order Sliding Mode Controller
NFOSMC	Nonlinear Fractional Order Sliding Mode Controller
SMC-ERL	Sliding Mode Controller with Exponential Reaching Law
EMF	Electromotive Force
FOC	Field Oriented Control
GA	Genetic Algorithm
BJT	Bipolar Junction Transistor
PID	Proportional Integral Derivative
PI	Proportional Integral
PD	Proportional Derivative
SVPWM	Space Vector Pulse Width Modulation
V/F	Voltage Per Frequency
PWM	Pulse Width Modulation
VVS	Variable Voltage Source
FOPID	Fractional Order Proportional Integral Derivative
DTC	Direct Torque Control
ESO	Extended State Observer
NdFeB	Neodymium Iron Boron
FLC	Fuzzy Logic Controller
ISMC	Integral Sliding Mode Controller
d-q axis	Direct-Quadrature Axis

LIST OF SYMBOLS

A	Frontal area of the Bajaj
B	Coefficient of friction of the motor
C_r	Rolling resistance coefficient
E_{abc}	The three-phase induced EMF
G	Gravitational acceleration
i_{abc}	Three-phase current
J	Rotor moment of inertia
L	Inductance
L_d	Inductance of the d-axis
L_q	Inductance of q-axis
M	Gross mass of the vehicle
P	Number of poles
R_s	Stator resistance
T_e	Electromagnetic force
T_L	Load torque
V_{dc}	Dc link voltage
V_{abc}	Three-phase voltage
ω_r	Rotor speed of the motor
θ_r	Position of the rotor
i_d	d-axis current
i_q	q-axis current
V_d	d-axis voltage
V_q	q-axis voltage
F_r	Rolling resistance force
F_g	Gravitational force
F_a	Aerodynamic force
ρ	Density

ABSTRACT

Due to fast depletion of nonrenewable energy sources (fossil fuels), and their energy conversion efficiency, internal combustion engines are being replaced by electric vehicles (EVs) which uses renewable energy sources. There are different electric drives available to be used as propulsion system of EVs. PMSM drives are highly efficient as compared to other electric drives and is selected to be used in the three-wheeler Bajaj propulsion system. Because it didn't have rotor field windings, and brushes that will result in extra power loss in the system. Due to the magnetic saturation in the rotor, the PMSM motor is a nonlinear, multivariable coupled system that needs an appropriate and robust control technique to improve its dynamic performance features. A sliding mode controller (SMC) is a nonlinear controller which is known for its robustness for rejecting disturbances. However, it has a chattering problem. So, in order to use the robustness of this controller the chattering-free higher-order sliding mode controller (HOSMC) based on super twisting algorithm is used to control the speed of the motor. In order to achieve this, the vehicle dynamics, PMSM, and the SVPWM based inverter are modeled mathematically. To check the controller's performance, the entire system is implemented in MATLAB/Simulink. In order to accomplish sensorless speed control of PMSM drive, a nonlinear Extended State Observer (ESO) is performed. Various speed control techniques (such as PI, SMC, SMC-ERL, FOSMC, and HOSMC) are implemented. The comparison of these controllers is made with respect to their dynamic performance, robustness (with the addition of external disturbance to the system), and chattering phenomenon (for SMC types). Accordingly, all the controllers are simulated with a setpoint of 100rad/s and the response shows that the conventional SMC has a settling time of 0.1163sec and overshoot of 1.9928rad/s. SMC-ERL has a settling time of 0.0807sec and an overshoot of 0.1030, whereas FOSMC has a settling time of 0.6964sec and an overshoot of 3.8707rad/s. The proposed high order sliding mode controller has a settling time of 0.0619sec and an overshoot of 0.1507rad/s. Based on this; it can be concluded that the proposed–HOSM controller based on super twisted algorithm has better dynamic performance. However, SMC-ERL has a competitive performance but its disturbance rejection ability is lower compared to the proposed controller. The HOSM controller outperformed the other controllers with its better dynamic performance, higher disturbance rejection, and chattering elimination abilities.

***Key Words**: EV, Three-wheeler Bajaj, Sensor-less PMSM, SMC, HOSMC, and GA-PI*

2CHAPTER 1

INTRODUCTION

1.1. Background

The world's automotive industry has a fast-growing interest to replace traditional vehicles having internal combustion engines with electric and hybrid electric vehicles. This is due to two main factors: energy and the environment. [1]. Since conventional cars use fossil fuels as an energy source, pollutant gases such as Carbon dioxide and other greenhouse gases are released into the atmosphere causing a harsh environment for human beings and animals. In addition to this, conventional vehicles use non-renewable energy sources (i.e., fossil fuels) and there is a worldwide shortage of fossil fuel and its price is increasing, especially in countries like Ethiopia.

It is not questionable that pure electric vehicles have become one of the most appealing choices for energy conservation and pollution reduction. Thinking of the environment, EVs can offer pollution-free urban transportation. In terms of energy, EVs can provide a safe, comprehensive, and balanced energy choice by utilizing a variety of renewable energy sources efficiently.

EVs are highly efficient compared to internal combustion engine vehicles since the conversion efficiency of the traditional combustion engine vehicle is about 12%-30% whereas EVs convert about 40-70% of the energy from the source to power at the wheels [2].

In EVs, the core part that needs attention is the motor and has to be chosen properly. There are different motors available. However, the use of AC machine drives is growing in popularity in the last three decades. Induction Motor (IM) and PMSM become highly competitive. However, with features such as high efficiency, high power density, high reliability, small size, light weight, and a wide constant power region, PMSM drives are well suited to meet the major requirements of EVs, such as fast dynamic response, high power factor, and wide operating speed ranges [3], [4]. Compared to other motor types the cost of PMSM drive was higher. However, nowadays the cost is reduced because a permanent magnet with neodymium-iron-boron (NdFeB) becomes commercially available at a reasonable price [5]. Due to this, the use of PMSM drive is increasing gradually, and surely it will be a witness in the future for low and medium power applications [6].

Permanent magnet is used instead of DC field winding of rotor in PMSM drive to produce air gap magnetic flux. Electrical losses due to motor field winding are reduced, and thermal properties and efficiency of PM machines are improved by the lack of field losses. Mechanical components like as brushes and slip rings are not present, resulting in a motor that is lower in weight and has a high power-to-weight ratio, resulting in increased efficiency and reliability.

PMSM drive can be represented in different reference frames. This includes the three-vector a-b-c reference frame, the two vector representations in the α-β reference frame, and the d-q reference frame [7]. The three-vector representation makes machine parameters modeling unnecessarily complicated. However, transforming the system into a two-vector orthogonal reference frame simplifies the modelling of the system and its control. In addition to this, torque and flux would be indirectly controlled. The transformations used in this way are called Park and Clarke transformations.

The dynamic model of PMSM is highly non-linear because of the coupling between the speed of the rotor and the d-q currents of the motor due to the permanent magnet built in the rotor. To overcome this nonlinearity issue there is a natural control technique which is the exact feedback linearization control technique, in which the non-linear dynamic model of the motor is linearized by using a proper coordinate transformation. But the main problem is that, the exact dynamics of the motor is difficult to be known. Since, some parameters of the motor like resistance, inductance, and others may vary with time. feedback linearization can only avoid such linearity only partly. Then a robust and nonlinear controller which ensures good dynamic performances even in the existence of parameters uncertainties is designed to such a problem to avoid the need for exact feedback linearization. A sliding mode controller is such kind of controller which is robust to internal parameter variations and external load disturbances and has fast convergence.

SMC is a non-linear controller which has been widely used to control the position or speed of the PMSM motor. Because this controller has fast dynamic response, and high robustness characteristics, it is selected for speed control of the motor. The chattering phenomena caused by high frequency switching near the sliding surface by discontinuous control law in

SMC design is the main issue with the sliding mode controller. Chattering can have an impact on the system's performance by diminishing control accuracy and causing significant heat losses in electrical power circuits as well as increased wear on moving mechanical parts [8]. So, in order to suppress the chattering effect different mechanisms are available like composite controllers, different reaching methods, and high order sliding mode controller.

In this research work higher-order sliding mode controller, typically a second-order sliding mode controller based on a super twisting algorithm plus an improved extended state observer is used to control the speed of PMSM drive. The second-order sliding mode controller is one type of HOSM controller with a relative degree of 2. This controller also has all the advantages of an SMC controller like high robustness, high accuracy, and simplicity with an extra advantage of chattering suppression ability. GA-PI controller is used in this study to control the torque producing quadrature and flux producing direct currents of the motor.

The presence of position/ speed sensors in control of PMSM has several disadvantages, such as reduced reliability, susceptibility to noise, extra weight and cost, and increased complexity in the drive system. So, the sensorless control used in this study will give reduced hardware complexity, noise immunity, higher reliability, and reduced maintenance to the control system. In order to accomplish sensorless control in the system, an improved extended state observer (ESO) is designed with a novel nonlinear function. This function has highly continuous and derivable compared to the functions used in the previous times and it can effectively reduce the high-frequency flutter phenomenon. The rotor speed of the PMSM drive is extended to a new state.

1.2. Statement of the Problem

Energy and the environment are the two major factors in the development of human civilization in the world. Conventional vehicles use non-renewable fossil fuels as a source of energy which leads to air pollution and might deplete someday. Additionally, the cost of gasoline is increasing from time to time. Electric vehicles are alternative solutions for the reduction of global warming. The electric motor drive is the main part of EVs. According to the current research status, PMSM drives are highly competent with other electric drives. PMSM is typically a nonlinear, multivariable coupled system, which is sensitive to internal parameter variations and external load disturbances, as well as some parameters that are not incorporated in its modeling. To come up with these problems a robust and non-linear control technique SMC is used in this study.

The conventional SMC has a chattering problem. There are different mechanisms available to suppress this issue. In order to mitigate this phenomenon, higher-order SMC (HOSMC) technique is implemented. This controller has the advantage of strong robustness of traditional SMC plus an additional chattering elimination ability. In the closed-loop control of PMSM drive, the speed or position of the rotor has to be measured and fed back to the control system using sensors. However, using sensors in systems like EVs has many disadvantages. This issue can be overcome using sensorless control of the PMSM drive by applying observers. In this research work, an improved extended state observer is used to replace sensors for estimating the angular speed of the rotor.

1.3. Research Questions

- How to model and optimize the speed and current controllers of the system?
- How to reduce the chattering in the SMC controller?

1.4. Objectives of the Study

1.4.1. General Objective

The general objective of this research thesis is to design and simulate the chattering free sliding mode controller for speed control of sensor less permanent magnet synchronous motor (PMSM) drive for three-wheeler electric Bajaj propulsion.

1.4.2. Specific Objectives

The following are the specific objectives of the study.

- To design an optimized current controller for the system.
- To design chattering-free SMC for sensorless (using ESO) speed control of PMSM drive.
- To simulate the system using MATLAB software and make a relevant conclusion based on the result.

1.5. Scope of the Study

The focus of this research thesis is to design and simulate a sensorless permanent magnet synchronous motor (PMSM) and control its speed using a chattering free sliding mode controller with MATLAB/Simulink software for three-wheeler electric Bajaj propulsion.

1.6. Limitations of the Study

Because of the limited time I had, the complexity of the system, and the cost of the materials used in the research thesis, preparing the prototype is very difficult. So, this thesis work is limited to simulation by using MATLAB/Simulink software.

1.7. Motivations of the Study

Automotive industries are working to replace conventional internal combustion engine vehicles with electric vehicles due to their energy and environmental effect. In electric vehicles motors are used for traction purposes and there are requirements that the motor needs to have like, high-speed range, good dynamic performance, high efficiency, etc. Different motor drives are available but PMSM is better due to its high efficiency, smaller size and compact weight, better torque-speed characteristics, wide speed range, longer life, etc. PMSM drive can be used in different application areas such as electric vehicles, robotics, aerospace engineering, and industries.

The control of PMSM drive especially in electric vehicles is influenced by different uncertainties like parameter variations external load disturbances, unmodeled and nonlinear dynamics of the system. So, in order to get good dynamic performance in the system robust controllers have to be implemented. The sliding mode controller is one of those controllers, with a chattering issue in it. to overcome this issue higher-order sliding mode controller based on super twisting algorithm is implemented to the speed loop of the system.

1.8. Significance of the Study

The waste of energy and air pollution due to the emission of gases are the major issues in the world as well as in our country. Fossil fuels are nonrenewable sources of energy that someday it will deplete. But using an electric motor for traction purpose is very advantageous in many aspects such as:

- It is pollution-free or it is environmentally friendly.
- It has a lower operating cost.

- It uses renewable sources which is electricity.
- Its efficiency is higher compared to fossil fuel cars.

For countries like Ethiopia, electric vehicles have a positive economic effect especially in the case of reduction of the cost given to fossil fuels.

In Adama, Ethiopia, fossil fuel powered three-wheeler Bajajs are the main transportation mechanisms. So, this research work is helpful to transform the conventional fossil fuel powered Bajaj to electric Bajaj. The members of ASTU center of transportation and vehicle engineering are working to develop and provide electric vehicles to Ethiopian market.

In this study, sensorless speed control of PMSM using a HOSM controller with an improved ESO is implemented. The HOSM controller is designed in order to eliminate the chattering effect that occurs in traditional SMC, and the improved ESO is used in this study to implement sensorless control of the PMSM drive.

1.9. Thesis Organization

This thesis work is organized into 5 chapters as shown below.

Chapter 1: Includes introduction, statement of problem, objectives, research questions, significance, and scope of the research.

Chapter 2: Includes comparison of PMSM with different motor types, discussion of different control techniques as well as literature review on PMSM motor and different control mechanisms

Chapter 3: In this chapter, the general methods used to accomplish the objectives of the study, dynamics as well as the selection of components of the 3-wheeler vehicle, dynamic modeling of the PMSM drive, and its controller design are discussed.

Chapter 4: The results of the proposed controller are discussed and compared with some related works.

Chapter 5: Presents conclusions of the whole work and recommendations for future works.

CHAPTER 2

THEORETICAL BACKGROUND AND LITERATURE REVIEW

2.1. Chapter Overview

In this chapter, the performance evaluation of PMSM is compared with different electric motor types. The common control techniques of the PMSM motor are explained. Finally, various papers related to the speed control of PMSM are reviewed and discussed.

2.2. Electric Vehicles

EVs are types of vehicles that use one or more electric motors or traction motors for propulsion and battery as a source of energy. Electric motors used for electric vehicles must satisfy the most common requirements like high torque generating capacity, high acceleration, and high power-density.

When a vehicle climbs up a hill, it needs higher torque at low speed. So, high torque capability is needed for climbing uphill, acceleration, and high torque for short time is needed for starting. The maximum torque of the motor is normally twice as large as the rated torque and designed to last for 20 to 40 seconds [9].

In order to select an appropriate type of motor for the vehicle a comparison of different motors based on electric vehicle requirements is needed. Among the requirements, propulsion devices should have the most important properties that are high power density and high efficiency. The following are the most common requirements of the motor in electric vehicles [10].

- Reliability and robustness of the motor for various operating conditions.
- High power and torque to size ratio.
- High torque at lows speed for starting and climbing hills, as well as high power and high speed for cruising.
- Higher efficiency
- Smaller size and weight of the motor
- Lower maintenance cost and longevity of its life span
- Low noise/ low current harmonics and torque ripple

- High power density.
- Reasonable cost.

The comparison of different electric motors that can be used for traction purposes of EVs is discussed in the following section.

2.3.1. Various Electric Motor Types

There are various types of electric motors classified based on their structure, and power sources. And from those motors, permanent magnet synchronous motor (PMSM) is categorized under AC motor types. The classification of motors is described in Figure 2.1 as shown below:

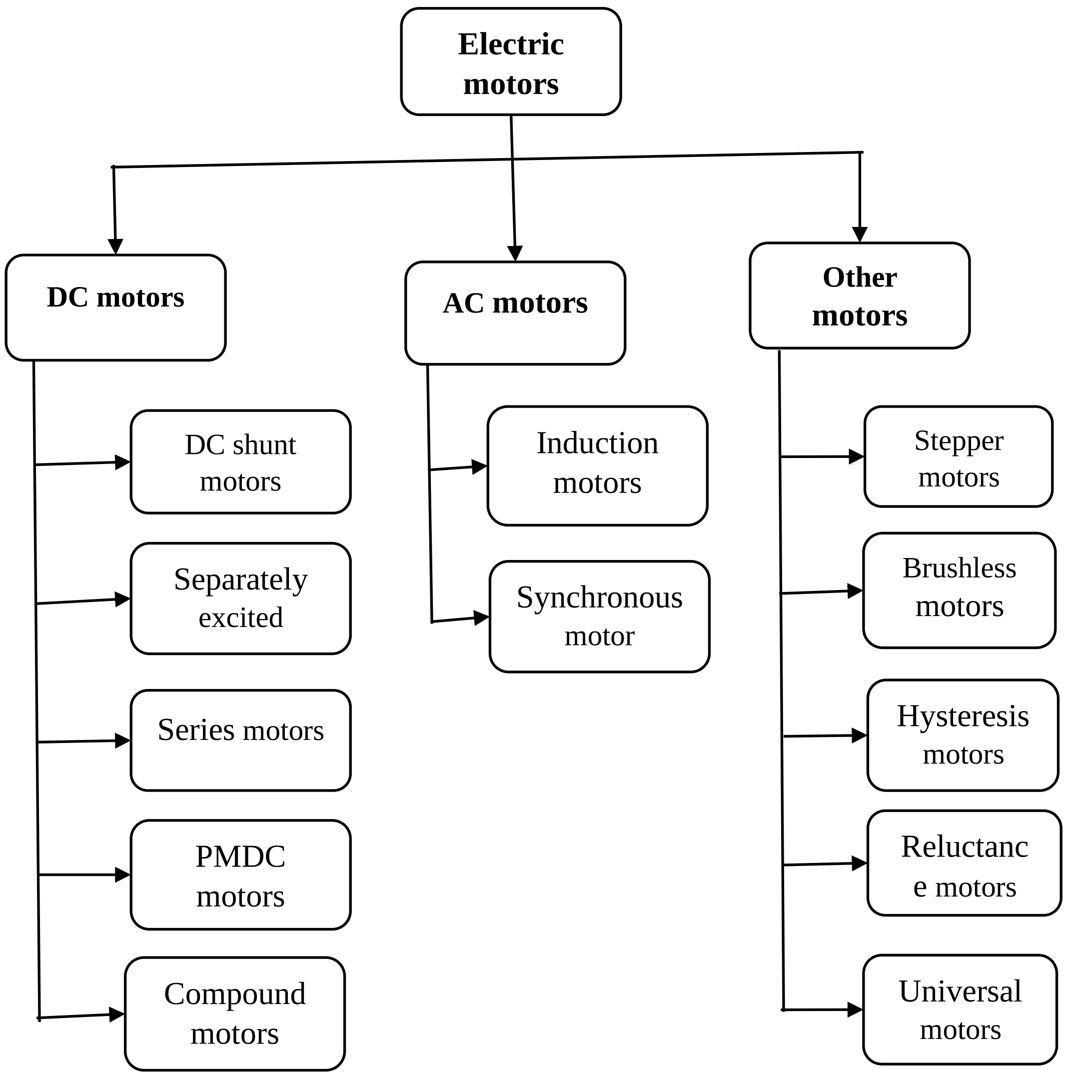

Figure 2.1. classification of motors

2.3.1.1. Performance Comparison of Motors

The common performance comparisons of PMSM with IMs, BLDC motors, and DC motors are discussed in the following section in tabular form. The performance of the PMSM drive is better compared to DC and IMs. However, it is known that the cost of permanent magnet motors is higher than other motor types. But the significant reduction of cost is seen nowadays as can be seen as discussed in Table 2.6. Because of its numerous advantages, PMSM would be the most preferable motor in different application areas in the future [9].

PMSM drive is better than induction motors in its efficiency, torque to volume ratio, weight, and compactness as well as its lower maintenance as described in Table 2.1.

Table 2.1.Comparison between PMSM and induction motors (IM) [11].

Criteria	PMSM	IM
Efficiency	Higher efficiency at low speeds when compared to AC IMs because PMSM doesn’t have field windings in its rotor	Lower efficiency at no load, light load, and low speeds. But it is competitive at higher speed regions.
Torque/volume ratio	Higher ratio with smaller sizes and lighter weight of the motor	Lower when compared to PMSM
Reliability, longevity	High reliability, longevity, low noise, and ease of control.	High reliability but Low stability and overheating at low speed.
Construction	More Complex construction	Simple construction
Dynamic response	Fast	Slow
Torque, power density	Higher	Lower
Weight, compactness	Has lesser weight since it is highly compact	Has higher weight, less compact
Maintenance	Less maintenance	More frequent maintenance

Similarly, in the following Table 2.2, PMSM and BLDCM drives are compared. PMSM motor is better in its efficiency, absence of torque ripple and current harmonics, lower noise, and higher speed range.

Table 2.2. Comparison between PMSM and BLDC [L1].

Criteria	PMSM	BLDCM
Efficiency	High because it has no field winding losses	Highly competitive
Torque ripple	No torque ripple at commutation	There is torque ripple at commutation
Current harmonics	Fewer current harmonics due to sinusoidal excitation	Low order current harmonics in the audible range
Back EMF	Sinusoidal back emf	Trapezoidal back emf
Current to be fed	Fed with sinusoidal currents	Fed with trapezoidal currents
Core loss	Lower core loss	Higher core loss due to harmonic content
Noise	Low noise	Noisy
Control algorithm	Mathematically intensive Relatively complex control (continuous 3 phase sine wave)	Relatively easy Easier to control (six trapezoidal states)
Speed range	Higher	Lower

In the same manner, the comparison of PMSM and DC motors is made in Table 2.3. DC motors have more bulky construction since they have a brush, slip ring, and field windings that add an extra power loss to the system that results in reduced efficiency.

In addition to this, they require frequent maintenance. This motor also has poor thermal performance, lower speed range, lower efficiency, etc. because of these factors, using DC drives as a propulsion system for electric vehicles is not recommended.

Table 2.3. Comparison between PMSM and DC motors [L5]

Criteria	PMSM	Conventional DC
Efficiency	High	Moderate (because of the friction between the brushes and commutator power will be lost in the form of heat and spark)
Maintenance	Less/almost none	Periodic maintenance is needed
Power to size ratio	High (the size and the weight of the motor is lower for the same power rating)	Moderate/low
Dynamic response	Fast	Slow
Speed range	High	Low
Electric noise	Low	High because of the brushes (which produces an arc) or commutators
Thermal performance	Good	Poor
Life span	Longer	Shorter because of its bulky construction (containing brushes, commutators, etc.). because brushes create friction with the commutator heat will produce and damage the motor through time.
Brushes	No brushes used	There are brushes and it has different side effects on the motor since it produces a spark and it will cause a fire hazard

2.3.2. Performance Evaluation of Different Traction Motors.

As it is shown in Table 2.4, PM motors have the highest power density due to the usage of a permanent magnet rotor, and the highest efficiency because there is no rotor copper loss. DC and induction motors (IM) are easier to control and their flux and torque can be controlled separately [11]. Induction motors are highly reliable compared to other motors due to their robust and rigid construction. The comparison in the following table is made out of 5.

Table 2.4. Performance evaluation of different motors [11].

Parameters	DC	(IM)	(PM)	(SRM)
Power density	2.5	3.5	5	3.5
Efficiency	2.5	3.5	5	3.5
Controllability	5	5	4	3
Reliability	3	5	4	5
Technological maturity	5	5	4	4
Cost	4	5	3	4
Total	22	27	25	23

In the following Table 2.5 efficiency in (%) and weight of, DC motor, induction motor, synchronous reluctance motor, and permanent magnet motor is presented based on literature [11]. As can be seen in the following table the efficiency of the PM motor drive is the best PM motors don’t have field windings on their rotor so the copper loss caused by field windings is eliminated. Besides PM motors don’t have brushes that causes power loss in the form of sparks. The comparison of the weight is based on an assumption of the weight of PM drive as 100. It is shown that the PMSM motor has the smallest weight and the weight of IM is two times and the weight of DC motors is four times the weight of PM motors.

Table 2.5. Efficiency and weight comparison of different traction motors [11].

Types of motor	Efficiency in %	Weight (based on PM=100)
PM	97	100
SRM	94	150
IM	90	200
DC	80	400

And the following Table 2.6 contains the cost comparison of different electric motors including the electronics used with them at different times. This comparison is based on an assumption of DC as 100. It is shown that the cost of PM motors and SRMs decreases at a fast rate with time. However, the cost of DC motors and induction motors is not reducing significantly.

Table 2.6. Cost comparison of different types of motors at different times [11].

Type	1993	1998	2003
DC	100	105	110
IM	100	90	80
SRM	150	90	70
PM	150	90	60

2.4. Different Control Techniques of PMSM Motor

To control the speed of PMSM drive different control methods like scalar control, direct torque control (DTC) and field-oriented control can be used. These control techniques are summarized in the following section.

2.4.1 Scalar Control of PMSM Drive

In this control technique, only the magnitude of the speed is used. The main drawback of this control technique is its poor performance because of lack of feedback, but the time it takes to implement is less. The easiest method of controlling a PMSM is scalar control, which maintains a constant relationship between voltage or current and frequency across the motor's speed range (i.e., v/f is kept constant) and it is also known as volt/frequency control [12].

The frequency is set according to the needed synchronous speed and the magnitude of voltage/current is adjusted to keep the v/f ratio constant [12]. This method uses an open-loop control technique with no parameters of the motor used as feedback. So, it is advantageous because no sensors are used. The synchronous speed of the motor is given by:

$$\omega_s = \frac{2\pi f_s}{p} \tag{2.1}$$

The motors used in electric vehicles need to have a traction motor with a good control technique. But scalar control has a poor dynamic performance. So, it won't be a good choice to control permanent magnet motors used in electric vehicles. The block diagram of v/f control is shown in Figure 2.2.

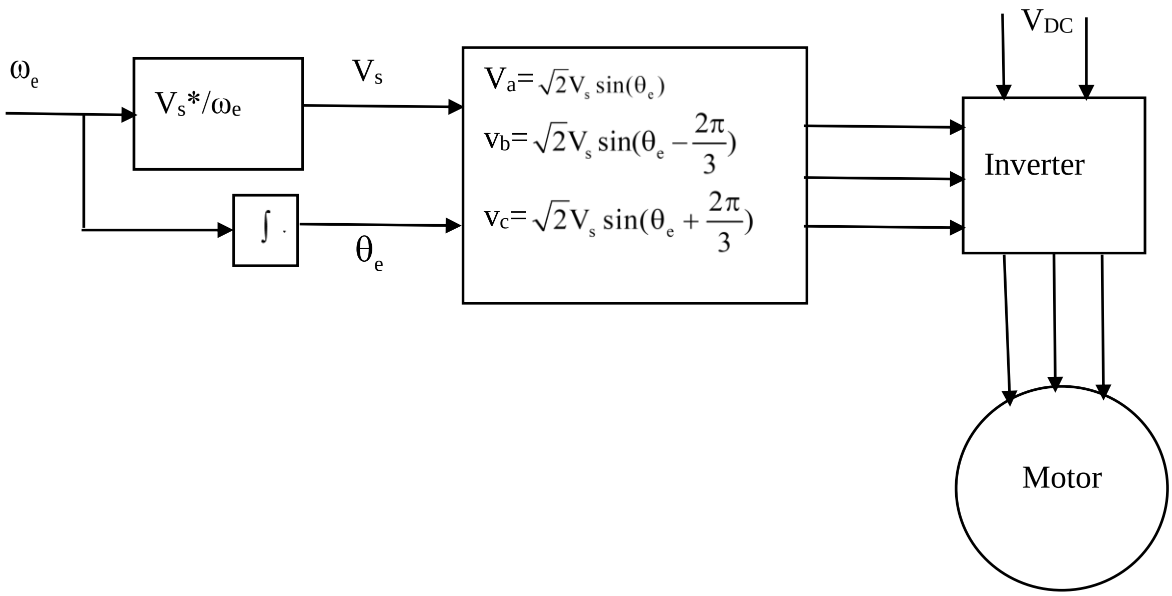

Figure 2.2. Block diagram of v/f control [12].

2.4.2. Vector Control Technique for PMSM Drive

This control technique mainly consists of the motor, inverter, speed controller, and different coordinate transformation to build the PMSM drive and its speed control [13]. This control technique is characterized by its fast dynamic response, high accuracy, and wide speed range, but its control performance is easily affected by the variation of motor parameters [14]. This control technique uses some parameters of the motor like position or speed of the motor as feedback.

Vector control also known as field-oriented control utilizes a certain transformation technique (Park and Clarke transformations) to get the d and q axis components of the motor. It has two closed control loops. These are the outer loop to control the speed or position of the motor and the inner loop to control the direct and quadrature current of the motor. The block diagram of field-oriented control is shown in Figure 2.3.

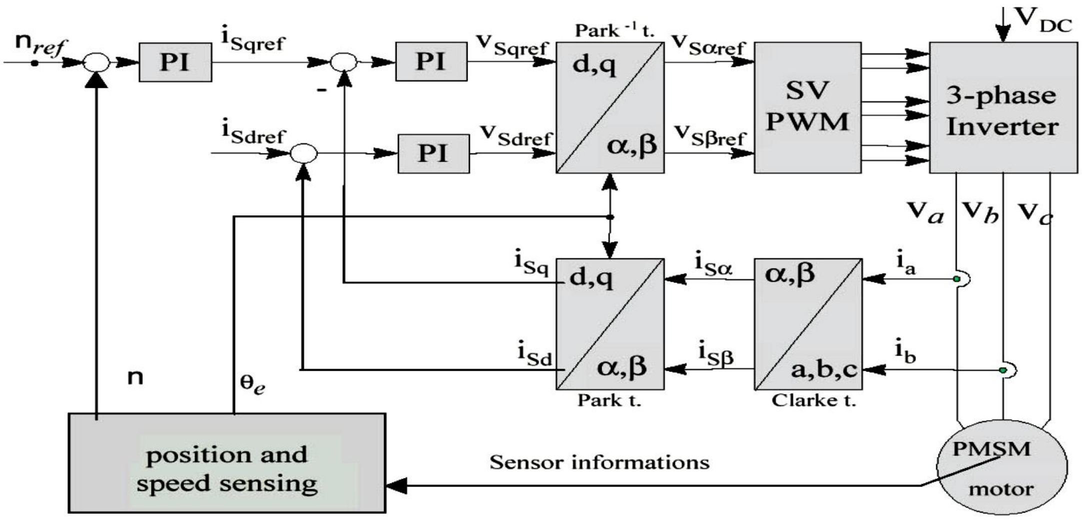

Figure 2.3. structure diagram of vector control of PMSM [14].

There are three types of vector control, these are filed oriented control, direct torque control, and voltage vector control. Field-oriented control (FOC) and direct torque control (DTC) are now recognized as the two high-performance control strategies for PMSM drive[15].

2.4.2.1. Direct Torque Control (DTC)

One of the most popular methods for controlling various types of AC motors is direct torque control. [16]. In this method, the control of stator flux and electromagnetic torque is achieved separately in the stationary frame (α, β), allowing the machines to have an accurate and fast electromagnetic torque response. It uses a switching table in order to select an appropriate voltage vector.

Unlike FOC with stator current as inner control objective, DTC governs the stator flux using hysteresis controls. In hysteresis control, Flux and torque errors are the inputs and its outputs determine the appropriate voltage vector for each commutation period. When compared to FOC control it possesses high torque dynamics but it has variable switching frequency which might cause switching loss and it also has higher torque ripple [17]. The following figure shows the direct torque control of PMSM using a hysteresis controller. The following Figure 2.4 shows the classical scheme of direct torque control scheme of PMSM drive.

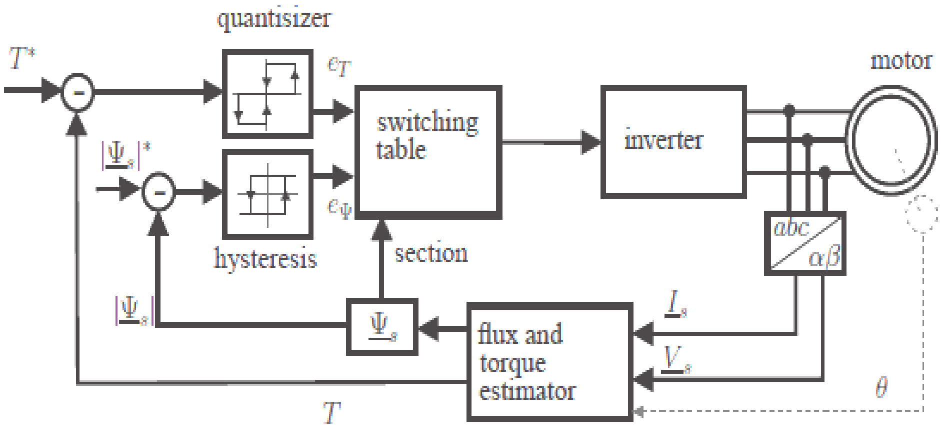

Figure 2.4. Classical DTC scheme [18].

2.4.2.2. Field-Oriented Control of PMSM

The control of PMSM drive is basically depending on the principle of field orientation [15]. This control method is utilized to attain independently decoupled torque and flux control based on the transformation of the three-phase current components (stage streams) into a two-phase torque and flux creating current components in a rotating outline of reference rather like dc machine [19].

The FOC is a method to control the currents represented by a two-phase d-q vector form. This method provides the benefits of smooth starting and acceleration, as well as good dynamic response with minimum torque ripples [20]. Field oriented control has the following advantages [19]:

- Transforms the coupled nonlinear AC models to a linearized system.
- The torque as well as the flux of the motor can be controlled separately.
- Fast response and good transient and steady-state performance.
- High torque at the start as well as low start-up current.
- Highly Efficient.
- Wide speed range through field weakening.

Due to the above advantages, FOC is used in this study to control the speed of PMSM drive. The following figure shows the field-oriented control of the PMSM drive. The block diagram of field-oriented control of PMSM drive is shown in Figure 2.5.

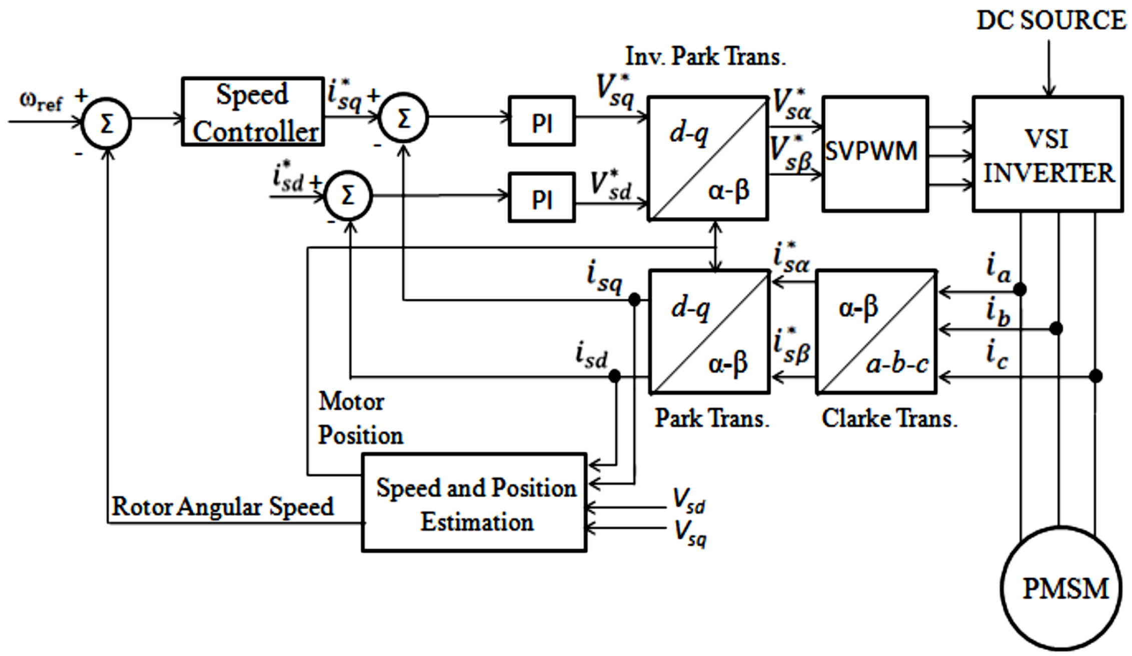

Figure 2.5. field-oriented control of PMSM drive [18].

2.5. Related Works on PMSM Drive

For the past thirty years, PM motor drives have piqued the interest of researchers [21]. Different researchers have been working on PMSM drives on its analysis, simulation, and modeling. This portion of the paper presents a brief review of some of the papers published at different times on permanent magnet synchronous motors. The cascade control system of PMSM control contains two control loops, the outer loop to control speed and the inner loop to control the d-q current of the system.

The authors in [13] analyzed the performance of PMSM drive using vector control technique and they used different speed controllers like PI, PID, SMC, and SMC plus PID. The simulation of the PI controller is performed under a reference speed of 100rpm. The result of this controller shows that there are some oscillations that took 5 seconds to settle down. It also has a high overshoot. But when the speed is controlled using a PID controller the settling time becomes twice better than the PI controller. The sliding mode controller is used as a speed regulator and fed to a vector control unit which produces switching pulses for PMSM drive. SMC has very less settling time and overshoot compared to PI and PID speed regulators. Even though the SMC controller has better control performance than other controllers mentioned above, there is a chattering problem, and the authors didn't discuss it.

The authors in [22] simulated a fractional-order sliding mode controller with PID (FOSMC-PID) for speed control of PMSM drive at a reference speed of 500rpm and 2Nm load torque. Then they made a performance comparison with the conventional integral sliding mode controller (ISMC). As the result shows that ISMC has 10 times higher overshoot (9.22%) and 30 times longer settling time than FOSMC. In this study, the performance comparison of FOSMC controllers under different sliding surface designs (PI, PD, PID) is made as shown in the following Table 2.7. They concluded that FOSMC with PID is better compared to others. The main drawback of this work is that the chattering effect isn't reduced significantly.

Table 2.7. Comparison of performance indices of FOSMC with different sliding surfaces and SMC controller [20].

Performance indices	SMC	FOSMC-PI	FOSMC-PD	FOSMC-PID
Overshoot [%]	9.22	5.52	0	0.8593
Settling time (sec)	0.0288	0.0094	0.096	0.0096
Speed drop (V)	1.28	4.3	1.5	1.16
Steady state error (rpm)	0.02	0.04	0.06	0.02
Torque ripple	12	11	10	10
Speed ripple	0.16	0.12	0.014	0.014

A comparative analysis of speed control schemes for PMSM drive with PI, PID, and adaptive PID controllers has been made in the literature [23]. The control performance of the traditional PI and PID methods can seriously be affected when the parameters of the motor vary. So, in order to deal with the motor parameter and load torque variations, an adaptive control algorithm was introduced in this paper. But adaptive controllers didn't deal with the convergence condition of the system error. The dynamic performance of an adaptive PID controller is better than conventional PI and PID controllers except for the peak overshoot (274.216rpm) for Adaptive PID, (253.249rpm) for PID, and (251.016rpm) for PI. The drawback of this study is that the current controller is not mentioned. And it says adaptive PID controller is better but the overshoot is high though it could affect the operation of the motor. Additionally, an adaptive PID controller is a linear system controller which needs the exact modeling of PMSM.

Field-oriented control and space vector pulse width modulation-based speed control of PMSM drive with sliding mode controller is developed in literature [24]. In this study the disturbance rejection ability of SMC and PID controllers in the speed loop was tested by suddenly varying the load torque from 2N.m to 4N.m Then the result shows that the PID controller's performance is degraded and faced an obvious speed drop when there is a disturbance. However, SMC has better disturbance rejection ability than PID controller [24]. In this work, the chattering phenomenon is not mentioned even if chattering is an issue that will affect the control system.

In the same manner, the closed-loop speed control of PMSM was developed using an adaptive fuzzy-PID controller and compared with the classical PI controller in [25]. It is shown that the control with adaptive fuzzy logic PID controller outperforms the PI controller [25]. The FLC is used because of its ability to perform fuzzy reasoning. The control accuracy increases as the number of fuzzy rules increases. The control algorithm, on the other hand, can be complicated [23]. The main drawback is that there is no current regulator in the system and the starting current might be high which will damage the system.

The authors in [26] proposed a robust fractional-order sliding mode controller for the speed control of PMSM drive. The proposed method's performance and robustness were tested for nonlinear load torque disturbance, and the simulation result demonstrates the effectiveness of the proposed algorithm. In this literature, the simulation is performed under a reference speed of 1000rpm. A step disturbance of 5N.m is applied for a while and the result is compared with the conventional SMC. The result shows that the proposed FOSMC controller has a smaller deviation under the addition of disturbance for a small period of time. In this literature, the authors didn't take the effect of the chattering phenomenon into account.

A novel SMC with nonlinear fractional-order PID sliding surface based on a novel extended state observer for the speed regulator of a surface-mounted PMSM was proposed in the literature [27]. On the basis of the sliding surface with the novel nonlinear state error feedback control law, a nonlinear fractional-order PID sliding mode controller was designed. And the improvement of the dynamic performance is proved using simulation. The problem with this controller is the existence of chattering.

In literature [28] a non-linear and robust sliding mode controller was presented. This paper adopted nonlinear control and high order sliding mode control theory to PMSM control, achieving robust control for a PMSM despite internal parameter uncertainties and unknown external load variations. In this work, the position of the motor is controlled using high order sliding mode controller and it has good performance results. The drawback of this study is that the authors use input/output feedback linearization which increases the complexity of the system unnecessarily.

In the above reviewed literatures different gaps are discussed. There are different gaps in the above reviewed literatures, and the main the gaps are less chattering elimination ability, usage of sensors to measure the speed of the motor, computational complexity, less disturbance rejection abilities (less robust) etc. In this study, a robust and chattering-free higher-order sliding mode controller is implemented to a nonlinear PMSM drive model. This controller has good dynamic performance, good disturbance rejection and chattering suppression abilities. In addition to this, sensorless control using an algorithm known as Extended State Observer is implemented to avoid the usage of mechanical sensors.

CHAPTER 3

MATERIALS AND METHODS

3.1. Chapter Overview

In this chapter the data collection and analysis, mathematical modeling of the vehicle dynamics and permanent magnet synchronous motor (PMSM), and the mathematical modelling of SVPWM based inverter is implemented. Besides the overall block diagram of the system is explained.

3.2. Materials

In this thesis work, different software's are used. Such as MATLAB, MathType Equation, and Microsoft office. MATLAB is the computing software that consists of technical toolboxes and Simulink. Microsoft office is used for editing the thesis documentation. MathType is used for writing mathematical formulas and equations in Microsoft offices word and PowerPoint presentation tools.

3.3. Methods

The general procedures followed throughout this research are shown in Figure 3.1. different literatures related to PMSM motor as well as different control techniques used in PMSM drive are reviewed.

The components like PMSM drive, SVPWM, and the three-wheeler Bajaj are mathematically modeled and the speed controller, as well as the current controllers for PMSM drive, are designed and implemented in MATLAB/Simulink. Then the result of the speed controller is compared with different related controllers. Finally, relevant conclusions and recommendations are given based on the result.

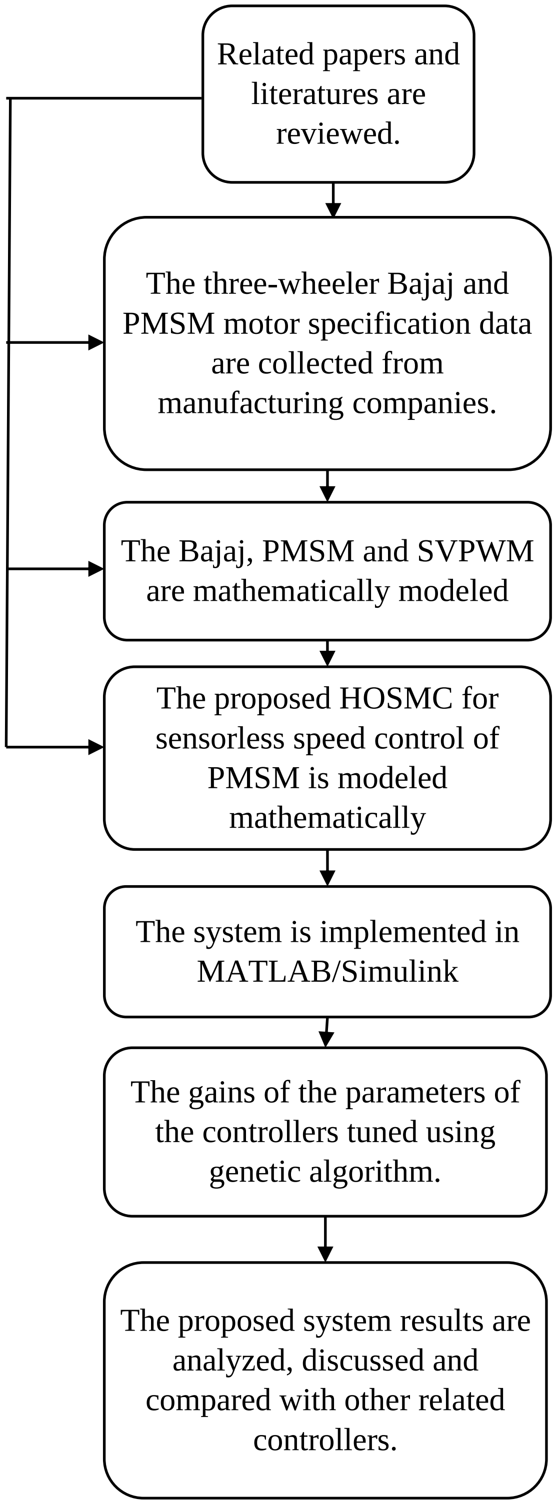

Figure 3.1. Block diagram of a methodology of the system.

3.4. System Block Diagram and Its Description

Vector control is control of the phase and amplitude of the motors' stator voltage/current vectors at the same time. The motor torque is dependent upon the stator currents i_d and i_q. It is possible to control motor torque indirectly by controlling currents i_d and i_q. The current i_d

is for excitation. Hence, we use i_d =0 for the control strategy. Torque can be obtained only by the quadrature current i_q. So, by making the direct current i_d = 0, we are achieving maximum torque. If we control the q axis current i_q, it shows that the torque of the motor is controlled through i_q.

The Vector-Control Technique is used to achieve high control quality for Permanent - magnet synchronous motors. These algorithms allow you to control the motor's rotational speed as well as its torque/current. The type of vector control used in this study is field-oriented control. The block diagram of field-oriented control of the PMSM motor is shown in Figure 3.2 below.

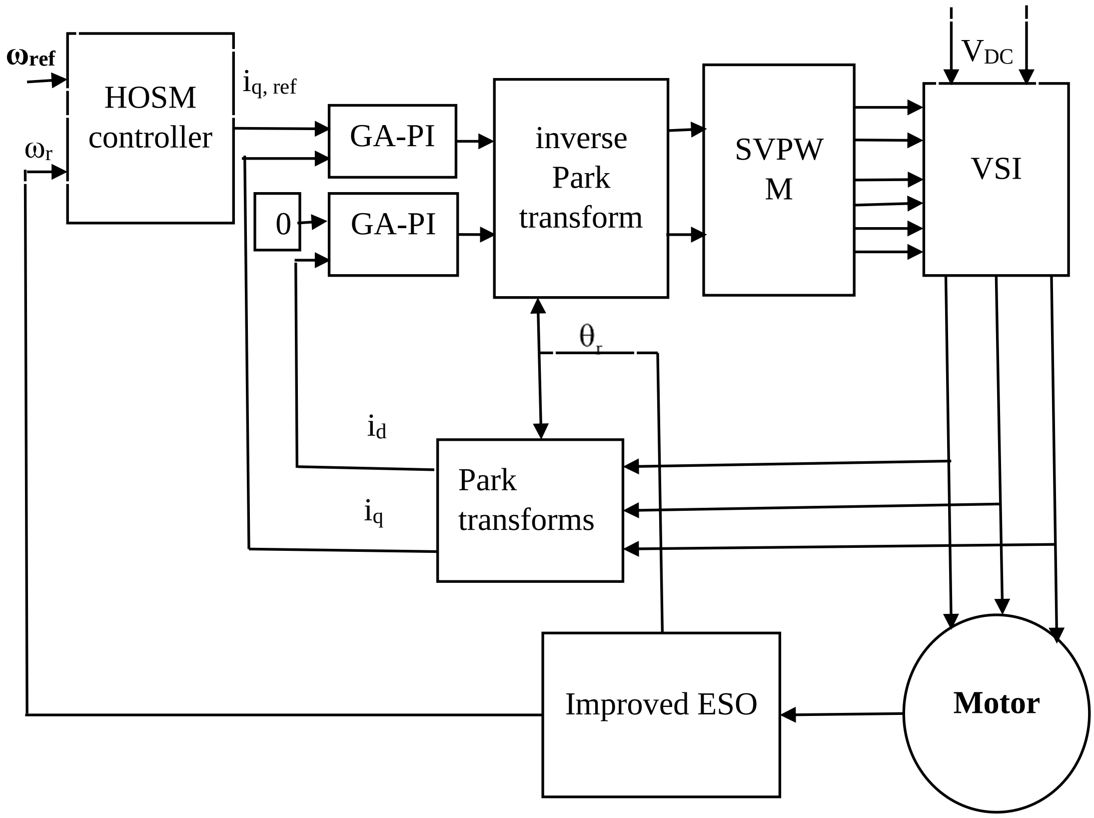

Figure 3.2. Block diagram of the overall control system of permanent magnet synchronous motor (PMSM).

3.5. Dynamics of the Three-Wheeler Bajaj

The electric drive system of vehicles contains the traction motor, battery, inverter, and mechanical transmission systems like a gearbox. This drive line of electric vehicles also contains a control system to control the torque/current of the traction motor and the speed/position of its rotor. The block diagram of the drive system is shown in Figure 3.3. In the diagram, the line with the double arrow head is the electrical connections and the lines with no arrow head are the mechanical connections of the system. The double arrow is to show that energy flows in both directions from the motor to the battery and from the battery to the motor.

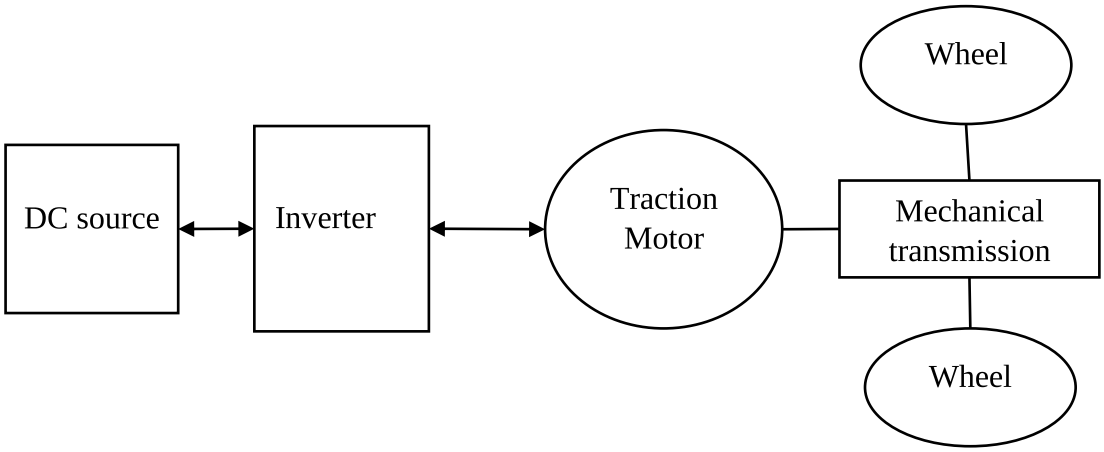

Figure 3.3. Electric drive system of vehicles.

3.5.1. Forces and Power Acted on the 3-wheeler Bajaj

The basics of vehicle design are based on newton's second law of motion. This law states that, the acceleration of a body is directly proportional to the net force applied to it. So, the body moves in the direction of the applied net force when the force applied on it is different from zero. Many forces act on a vehicle, and the net force provided by the traction motor governs the motion in the desired direction according to Newton's second law. This force generated by the motor is used in order to overcome the resisting forces due to gravity, air, and tire resistance. The acceleration of the vehicle depends on:

- The power generated by the motor
- Types of the road
- The aerodynamics of the vehicle
- The vehicles total mass

When the Bajaj motion, it faces a resistive force that opposes its movement. So, the driving force should overcome these forces. The resistive forces are:

- Rolling resistance force
- Aerodynamic drag force
- Uphill resistance/gradient force

When the road conditions like inclination angle and surface of the road change the motor encounter disturbance. So, the controller used should overcome such kind of problems. Figure 3.4 shows the forces acted on a three-wheeler Bajaj.

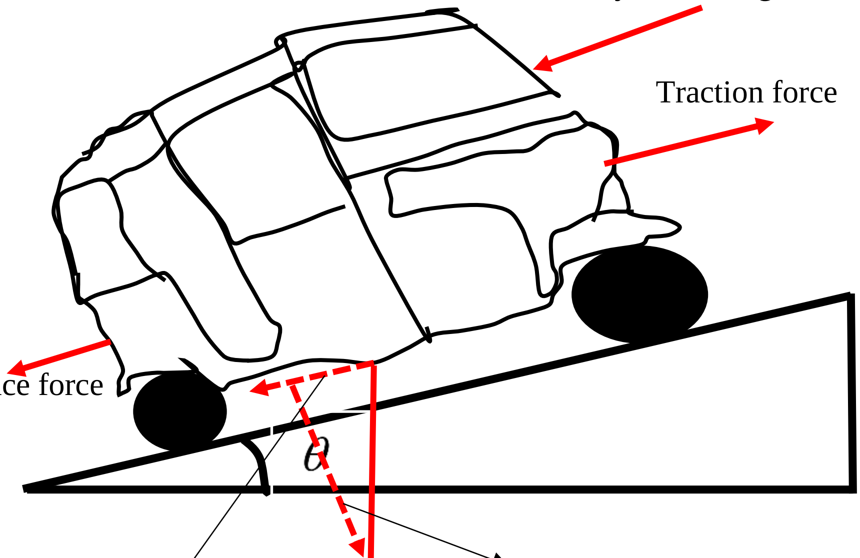

Figure 3.4. forces acting on a moving 3-wheeler Bajaj.

3.5.1.1. Rolling Resistance Force

The rolling resistance on the tires of a moving vehicle is basically contributed by a process called hysteresis. Hysteresis is basically the energy that is lost when the tire rolls through its footprint. This force is a conservative force that is proportional to the platform weight and angle of inclination.

$$F_r = M \times g \times C_r \times \cos(\alpha) \qquad (3.1)$$

$$F_r = 680Kg \times 9.81m/s^2 \times 0.01 \times \cos(11.30) = 65.415N \qquad (3.2).$$

where M is the mass of the Bajaj and cargo (Kg), g is the acceleration due to gravity (m/s^2), C_r is the rolling coefficient, and α is the angle of inclination/gradient angle (rad).

Then the power required to overcome the rolling resistance force is:

$$\mathrm{P_r} = F_r \times V = F_r \times speed(m/s) = 65.415 \times \frac{65000m}{3600\sec} = 1.181kW \qquad (3.3)$$

Rolling resistance coefficients for different types of surfaces are described in Table 3.1.

Table 3.1. Coefficient of friction for different road surfaces [27].

Surface type	Friction coefficient (C_r)
Concrete (good/fair/poor)	0.010/0.015/0.020
Asphalt (good/fair/poor)	0.012/0.017/0.022
Macadam (good/fair/poor)	0.015/0.022/0.037
Snow (2 inch/ 4 inch)	0.025/0.037
Dirt (smooth/sandy)	0.025/0.037
Mud (firm/medium/soft)	0.037/0.090/0.150
Grass (firm/soft)	0.055/0.075
Sand (firm/soft/dune)	0.060/0.150/0.300
Ice	0.1

3.5.1.2. Aerodynamic Drag Force

A car moving at a specific speed in a specific direction faces a resistive force that opposes its movement. This force is caused by aerodynamic drag. Aerodynamic drag is mainly caused by: shape drag and skin drag.

Shape drag is caused by the shape of the vehicle. When the vehicle moves in the forward direction it shoves the air which is in its front. But the air will not immediately move away from it. This produces high air pressure in the vehicles front. Besides, the air behind the vehicle cannot momentarily fill the space cleared out by the forward movement of the vehicle. Because of this, two zones of air pressure are made around the moving vehicle. The high-pressure zone within the front of the vehicle restricts its movement by pushing backward and the low-pressure zone at the back of the vehicle pulls the vehicle backward.

The air near to the vehicle moves nearly at the speed of the vehicle whereas the air away from it remains static. Because of these layers (the layer of the air moving at the speed of the vehicle and the layer of the air which is not moving), the molecules move at various speed ranges. The speed variation between two air molecules causes friction. This causes the other aerodynamic drag type which is known as the skin effect.

The aerodynamic drag force is proportional to the square of the difference between velocity of the Bajaj and velocity of the wind, and frontal area of the vehicle. Which then can be expressed as:

$$F_a = \frac{1}{2}(\rho \times A \times C_d \times (V - V_o)^2) \tag{3.4}$$

Then the power needed to overcome the force caused by aerodynamic drag is given as:

$$P_a = F_a \times V(speed) \tag{3.5}$$

where ρ is the density of air, A is the frontal area of Bajaj (m^2), C_d is the drag coefficient and V is the speed of the vehicle (m/s) and V_o is the speed of the wind. This force is less than the rest of the resistive forces. The speed of the air is a little less than the speed of the vehicle. The power is considered to be a maximum of 1.5kW.

3.5.1.3. Uphill Resistance (Grading) Force

In the upward or downward movement of a vehicle, its weight produces a type of a force that's continuously directed to down the grade. This force restricts its forward movement, i.e., the grade climbing. However, while the vehicle is moving downward, this force helps the vehicles forward movement. This force can be given as:

$$F_g = M \times g \times \sin(\alpha) \tag{3.6}$$

$$F_g = 680kg \times 9.81m/s^2 \times \sin(11.30) = 1{,}307.12N \tag{3.7}$$

where M is the mass of the vehicle and cargo (kg), g is the acceleration due to gravity (m/s^2), and α is gradient angle (rad). In some literatures, rolling resistance and grading resistance are summed up and known as road resistance forces.

The power needed to overcome this force at half of the speed assumed can be calculated as:

$$P_g = F_g \times V(speed) = 1307.12N \times \frac{32500m}{3600\sec} = 11{,}800.73W = 11.8kW \tag{3.8}$$

The speed is halved because when the vehicle moves uphill more torque is needed. So, the speed has to be reduced.

Finally, the total resistive force that opposes the motion of the vehicle is the sum of all the above forces.

$$F_t = F_r + F_a + F_g \tag{3.9}$$

$$F_t = (M \times g \times C_r \times \cos(\alpha)) + (0.5 \times \rho \times A \times C_d \times V^2) + (M \times g \times \sin(\alpha)) \tag{3.10}$$

Then the total maximum power can be calculated as:

$$P_{t(\max)} = F_t \times V(speed) \tag{3.11}$$

Or simply,

$$P_{t(\max)} = \mathrm{P_r} + P_a + P_g = 1.181kW + 1.5kW + 11.8kW = 14.481kW \tag{3.12}$$

This power is to balance the resistive forces acting on the vehicle. But there are losses due to different factors. So, it has to be considered when calculating the power that is needed to drive the vehicle.

The total driving power can be expressed as follows:

$$P_{t(driving)} = P_{t(\max)} + losses \tag{3.13}$$

Then,

$$\eta = \frac{P_{t(\max)}}{P_{t(driving)}} \Rightarrow P_{t(driving)} = \frac{P_{t(\max)}}{\eta} \tag{3.14}$$

$$P_{t(driving)} = \frac{14.481kW}{0.95} = 15.2432kW \approx 16kW \tag{3.15}$$

where, η is gear transmission efficiency.

3.5.2. Electric Bajaj (3-wheeler) Specifications

The specifications of the three-wheeler Bajaj are taken from a literature and manufacturing companies. Based on the gasoline Bajaj specifications from the manufacturing company, the specifications of electric Bajaj (3-wheeler) are given in the Table 3.2. The gross weight of the Bajaj is the sum of the mass of the vehicle, the average weight of the cargo, the people, and the weight of the battery that can be used as a DC source.

Table 3.2. Electric Bajaj specifications [L1], [29].

Parameter	Value [unit]
Gross weight	680 [kg]
Peak power	16 [kW]
Rated power	8 [kW]
Maximum torque	56 [Nm]
Rated torque	22 [Nm]
Rated speed	1500 [rpm]
Maximum speed	65 [km]
Maximum gradient angle	11.3 [degrees]
Seat capacity	4 persons including the driver

3.5.5. Selection of Traction Motor

The combustion engine that is used in traditional vehicles is replaced by a traction motor in electric vehicles. the first and foremost component to be selected in electric vehicles is the traction motor which must produce the appropriate power, torque required, and other characteristics required by the vehicle.

In literature [30], [5], and [L1] the performance of different motor drives for electric vehicles is compared and concluded that PMSM drive is a better choice for this purpose because it suppresses all other motor types in its efficiency (due to the absence of field windings) and power density. The main drawback of PMSM drive is its cost but now a days neodymium-iron-boron (NdFeB) magnets have become available in the market at a reasonable price [5]. The decreasing cost of permanent magnet materials, as well as the trend of increasing efficiency in permanent magnet and brushless DC motors, make them increasingly appealing for EV applications [30].

BLDC motor is the most competitive type of motor with PMSM for electric vehicle application. This motor is used for traction purpose in Bajaj RE electric rickshaw vehicles. PMSM drive is the AC counterpart of BLDC motor and there is no major difference in their control system except the nature of the current (sinusoidal for PMSM and trapezoidal for BLDC) and the commutation mechanism (through a six-step process which will result in torque ripple for BLDC and continuous in case of PMSM).

BLDC motors are long-lasting, relatively efficient, and inexpensive. They have the ability to work at high speeds and they are electronically controllable. Because of the above-mentioned characteristics, BLDC is ideal to be used as traction motor for vehicles. However, PMSM have all of the characteristics of BLDC motors with the added benefits of being less noisy and are more efficient [L1]. Because of all the above factors, PMSM is selected as a traction motor for the three-wheeler electric Bajaj in this study. The parameter specifications of the PMSM are shown in Table 3.3.

Table 3.3. parameter specifications of PMSM used in this thesis [L2] [L4].

Parameters	Value [unit]
Number of poles	4
Efficiency	93.5 [%]
Control input voltage	144 [V]
Rated motor current	60.5[A]
Rated motor power	8 [kw]
Rated torque	22 [Nm]
Rated speed	1500 [rpm]
Armature phase winding resistance (Rs)	0.675 [mΩ]
L_d	0.375 [mH]
L_q	0.675 [mH]
Flux (λ_m)	0.0008 [Wb]
Inertia (J)	0.4 [Kg.m^2]
Damping coefficient (B)	0.0008

In PMSM drives the permanent magnet can be inserted in various ways. Based on the way of placing the permanent magnet on the rotor, PMSM can be classified as surface-mounted permanent magnet synchronous motor (SPMSM) and interior permanent magnet synchronous motor (IPMSM). SPMSM has a surface-mounted permanent magnet rotor (mounted on the outer periphery of rotor laminations). This positioning gives the highest airgap flux since it is in direct contact with the airgap. The drawback of these motor types is their lower structural integrity and mechanical robustness as they are not tightly fitted into the rotor laminations. This motor has equal inductances in quadrature and direct axis, $L_d = L_q$.

IPMSM drives have a permanent magnet mounted inside the rotor. Its construction is mechanically robust. In IPMSM, the inductance of the quadrature axis is greater than the direct axis of the motor. This motor is selected for this study because of the following advantages.

- Field weakening ability.
- Under-excited functioning for many load conditions.
- Robust construction.
- Permanent magnet demagnetization elimination.

3.6. Dynamic Modeling of PMSM Drive

In this study, the three-phase star-connected PMSM drive is used as a traction motor for a 3-wheeler electric Bajaj. In order to use PMSM for 3-wheeler electric Bajaj, its precise model is required. PMSM can be represented in several frame of references. These includes three-phase a-b-c reference frame, stationary (α-β) reference frame, and rotating (d-q) reference frame. The control technique used in this study is field-oriented control which mainly depends on the d-q frame of reference. This technique is described in the following section.

3.6.1. The proposed Field Oriented Control

The vector control (FOC) is applied in order to regulate the magnitude as well as the phase of the stator current and voltage. It is depending on transformation of the three-phase time varying and speed-depending system into a two-phase (d-q) steady system which makes the structure alike with the control of DC motor. This control technique requires information of the rotor position. Similar to separately excited DC motors, FOC looks for recreating these orthogonal elements in AC machines to regulate the torque producing current (aligned with the q-axis) separately from the magnetic flux producing current (lined up with the d-axis) [31].

In order to design the mathematical model of PMSM drive the following assumptions are considered in the d-q reference frame:

- The induced EMF is sinusoidal.
- Eddy currents and hysteresis losses are neglected.
- All winds have equal stator resistances.
- Assumption of rotor flux at a fixed point.

- The motors' core loss is neglected
- The motor currents are symmetrical three-phase sine wave function
- Saturation is neglected
- There are no field current dynamics

In field-oriented control, different reference frame transformations are used which are described in the following section [31].

3.6.1.1. Different Reference Frame Transformations

For dynamic modeling of PMSM, different reference frame transformations are used. The transformation that transforms three-phase (a, b, c) components to two-phase (d, q) components are known as park transform and the reverse is called inverse park transform. The technique that transforms the three-phase quantities into two-phase (α, β) quantities is called Clarke transformation. The transformation matrix that takes stator voltages, currents, and fluxes from (a, b, c) to (α, β) coordinates, i.e., the Clarke transform, is given as K_s, and the transformation matrix that takes variables from (α, β) to (d, q) coordinates, i.e., the Park transform, is given as K_r.

Clarke transformation and inverse Clarke transformation: using this, the components in the a-b-c reference frame are transformed into (α, β) stationary reference frames. In this study, this transformation is applied in the design of SVPWM. The transformation is as shown below [32].

$$f_{\alpha\beta} = K_s f_{abcs} \tag{3.28}$$

$$K_s = \frac{2}{3}\begin{bmatrix} 1 & -1/2 & -1/2 \\ 0 & \sqrt{3}/2 & -\sqrt{3}/2 \end{bmatrix} \tag{3.29}$$

where the vector f can represent voltage, current, or flux vectors, the subscript s refers to stator variables. Assuming a balanced three-phase circuit, i. e., $f_a + f_b + f_c = 0$,

$$\begin{aligned} f_\alpha &= f_a \\ f_\beta &= \frac{2}{\sqrt{3}} f_b + \frac{1}{\sqrt{3}} f_a \end{aligned} \tag{3.30}$$

For example, let's take f as voltage (V). Then

$$V_\alpha = V_a$$
$$V_\beta = \frac{2}{\sqrt{3}}V_b + \frac{1}{\sqrt{3}}V_a \quad (3.31)$$

The inverse Clarke transform that takes stator voltages, currents, and fluxes from (α, β) to (a, b, c) coordinates, can easily be derived as:

$$f_a = f_\alpha$$
$$f_b = -\frac{1}{2} f_\alpha + \frac{\sqrt{3}}{2} f_\beta \quad (3.32)$$
$$f_c = -\frac{1}{2} f_\alpha - \frac{\sqrt{3}}{2} f_\beta$$

Which is the same as to

$$V_a = V_\alpha$$
$$V_b = -\frac{1}{2}V_\alpha + \frac{\sqrt{3}}{2}V_\beta \quad (3.33)$$
$$V_c = -\frac{1}{2}V_\alpha - \frac{\sqrt{3}}{2}V_\beta$$

Park and inverse Park transformations: The transformation that transforms variables from (α, β) coordinate to (d, q) coordinates, is called Park transform, the transformation matrix used is K_r.

The formula for park transformation is given as [32]:

$$f_{dq} = K_r f_{\alpha\beta} \quad (3.34)$$

$$K_r = \begin{bmatrix} \cos(\theta r) & \sin(\theta r) \\ -\sin(\theta r) & \cos(\theta r) \end{bmatrix} \quad (3.35)$$

where:

$$f_d = f_\alpha \cos(\theta_r) + f_\beta \sin(\theta_r)$$
$$f_q = -f_\alpha \sin(\theta_r) + f_\beta \cos(\theta_r) \quad (3.36)$$

Let, f is voltage (V). then

$$V_d = V_\alpha \cos(\theta_r) + V_\beta \sin(\theta_r)$$
$$V_q = -V_\alpha \sin(\theta_r) + V_\beta \cos(\theta_r) \quad (3.37)$$

Then the inverse park transform can easily be performed as:

$$f_\alpha = f_d \cos(\theta_r) - f_q \sin(\theta_r)$$
$$f_\beta = f_d \sin(\theta_r) + f_q \cos(\theta_r) \quad (3.38)$$

Then the inverse transform of the voltage from d-q to α-β can be given as:

$$V_\alpha = V_d \cos(\theta_r) - V_q \sin(\theta_r)$$
$$V_\beta = V_d \sin(\theta_r) + V_q \cos(\theta_r) \quad (3.39)$$

a-b-c to d-q and d-q to a-b-c transformation: For modelling of permanent magnet synchronous motor, a-b-c to d-q and d-q to a-b-c transformations are used.

The equations to convert a-b-c to d-q blocks are given below [33].

$$V_d = -\frac{2}{3}\left[V_a \sin(\theta) + V_b \sin(\theta - \frac{2\pi}{3}) + V_c \sin(\theta + \frac{2\pi}{3})\right]$$
$$V_q = \frac{2}{3}\left[V_a \cos(\theta) + V_b \cos(\theta - \frac{2\pi}{3}) + V_c \cos(\theta + \frac{2\pi}{3})\right] \quad (3.40)$$

And the equations to convert d-q to a-b-c blocks are given as follows:

$$V_a = V_q \cos(\theta) - V_d \sin(\theta)$$
$$V_b = V_q \cos(\theta - \frac{2\pi}{3}) + V_d \sin(\theta - \frac{2\pi}{3}) \quad (3.41)$$
$$V_c = V_q \cos(\theta + \frac{2\pi}{3}) + V_d \sin(\theta + \frac{2\pi}{3})$$

To convert the currents from d-q to a-b-c or from a-b-c to d-q reference frame the above equation can be used by substituting current (i) in place of voltage (V).

3.6.1.2. Model Equations of PMSM in (a, b, c) Frame of Reference

In (a, b, c) reference frame the voltage equation of the motor can be expressed as [13]:

$$V_{abc} = R' i_{abc} + \frac{\partial \lambda_{abc}}{\partial t} \quad (3.20)$$

where R is stator resistance, λ_{abc} are stator flux linkages in a-b-c phases, i_{abc} is the three-phase currents, and V_{abc} the three-phase stator voltages.

$$(f_{abc})^T = [f_a, f_b, f_c] \quad (3.21),$$

f can represent V, I, or λ.

$$R' = \begin{bmatrix} R & 0 & 0 \\ 0 & R & 0 \\ 0 & 0 & R \end{bmatrix} \tag{3.22}$$

The flux linkage equation may be written as:

$$\lambda_{abc} = L \times \begin{bmatrix} i_a \\ i_b \\ i_c \end{bmatrix} + \lambda_m \begin{bmatrix} \sin(\theta) \\ \sin(\theta - \frac{2\pi}{3}) \\ \sin(\theta + \frac{2\pi}{3}) \end{bmatrix} \tag{3.23}$$

From Equation (3.11):

$$\begin{aligned} \lambda_a &= Li_a + \lambda_m \sin(\theta) \\ \lambda_b &= Li_b + \lambda_m \sin(\theta - \frac{2\pi}{3}) \\ \lambda_c &= Li_c + \lambda_m \sin(\theta + \frac{2\pi}{3}) \end{aligned} \tag{3.24}$$

Now, substitute (3.22) and (3.24) into (3.20) as follows.

$$\begin{aligned} V_a &= Ri_a + L\frac{di_a}{dt} + E_a, \qquad \mathrm{E_a} = \omega\lambda_\mathrm{m}\sin(\theta) \\ V_b &= Ri_b + L\frac{di_b}{dt} + E_b, \qquad \mathrm{E_b} = \omega\lambda_\mathrm{m}\sin(\theta - \frac{2\pi}{3}) \\ V_c &= Ri_c + L\frac{di_c}{dt} + E_c, \qquad \mathrm{E_a} = \omega\lambda_\mathrm{m}\sin(\theta + \frac{2\pi}{3}) \end{aligned} \tag{3.25}$$

where L is inductance, λ_m is flux linkage, E is back EMF in the respective phases

The electromagnetic torque then becomes [13]:

$$T_e = (E_a i_a + E_b i_b + E_c i_c)/\omega \tag{3.26}$$

Then it can be written as:

$$T_e = P/2\lambda_m\left[\left(i_a - 1/2\, i_b - 1/2\, i_c\right)sin(\theta) - \sqrt{3}/2(ib - ic)cos(\theta)\right] \tag{3.27}$$

where p is the number of poles

3.6.1.3. Model Equations of the Motor in (α, β) Reference Frame

The voltages in the α-β reference frame can be given as [13]:

$$V_\alpha = Ri_\alpha + L\frac{di_\alpha}{dt} - \omega_r \lambda_m \sin(\theta) \tag{3.42}$$

$$V_\beta = Ri_\beta + L\frac{di_\beta}{dt} - \omega_r \lambda_m \cos(\theta) \tag{3.43}$$

The currents i_α and i_β can be derived from equations (3.42) and (3.43).

Electromagnetic torque in α-β reference frame can be expressed as:

$$T_e = P/2\lambda_m \left[-i_\alpha \, sin(\theta) + i_\beta \, cos(\theta) \right] \tag{3.44}$$

3.6.1.4. Model Equations of the Motor in (d, q) Reference Frame

The d-q axis mathematical model is commonly used in FOC of PMSM. It can be used to analyze not only the steady-state operating characteristics of permanent magnet synchronous motors but also the transient performance of the motor. Finally, the model of the motor in a rotary time-invariant reference frame can be given as follows. The voltage equations in the d-q reference frame are [13]:

$$V_d = Ri_d + \frac{d\lambda_d}{dt} - \omega_r \lambda_q \tag{3.45}$$

$$V_q = Ri_q + \frac{d\lambda_q}{dt} + \omega_r \lambda_d \tag{3.46}$$

where: R is stator resistance, L_d and L_q are d and q-axis inductance values, i_d *and* i_q are d and q-axis currents, similarly V_d and V_q are d and q-axis voltages respectively and λ_d and λ_q are the d and q-axis flux linkages given as:

$$\lambda_d = L_d i_d + \lambda_m \qquad \text{and} \qquad \lambda_q = L_q i_q$$

When the value of λ_d and λ_q are substituted in the above equation and rearranged, the following equations are obtained.

$$\begin{aligned} V_d &= Ri_d - \omega_r L_q i_q + \frac{d}{dt}(L_d i_d + \lambda_m) \\ V_q &= Ri_q + \omega_r (L_d i_d + \lambda_m) + L_q \frac{di_q}{dt} \end{aligned} \tag{3.47}$$

From equations (3.47) we can get the following differential equations of currents.

$$\frac{di_d}{dt} = -\frac{R}{L_d} i_d + \omega_r \frac{L_q}{L_d} i_q + \frac{V_d}{L_d} \tag{3.48}$$

$$\frac{di_q}{dt} = -\frac{R}{L_q} i_q - \omega_r \frac{L_d}{L_q} i_d - \omega_r \frac{\lambda_m}{L_q} + \frac{V_q}{L_q} \tag{3.49}$$

Electromagnetic torque is given by:

$$T_e = \frac{3}{2}(\frac{P}{2})(\lambda_m i_q - \lambda_q i_d) \tag{3.50}$$

In order to produce maximum torque, avoid reluctance effects, and reduce torque ripple, an optimum operation is attained using vector control, which makes sure that the space vector stator-current contains only a quadrature component by pushing the d-axis current towards zero. Therefore, the torque equation becomes [32]:

$$T_e = \frac{3P}{4} \lambda_m i_q \tag{3.51}$$

So, the torque can be regulated by the quadrature (q-axis) current only.

And for all reference frame the electromechanical torque equation can be expressed as:

$$J \frac{d\omega_r}{dt} = T_e - B\omega_r - T_L \tag{3.52}$$

where ω_m is the mechanical speed of the rotor which can be given as:

$$\omega_m = \omega_r (\frac{2}{P}) \tag{3.53}$$

Then,

$$J * \frac{d\omega_r}{dt} = T_e - B * \omega_r - T_L \qquad \Rightarrow \qquad \frac{d\omega_r}{dt} = \frac{1}{J}(T_e - B\omega_r - T_L) \tag{3.54}$$

$$\frac{d\omega_r}{dt} = (\frac{3P}{4J} \lambda_m i_q - \frac{B}{J} \omega_r - T_L) \qquad \Rightarrow \qquad \frac{d\omega_r}{dt} = \frac{3P}{4J} \lambda_m i_q - \frac{B}{J} \omega_r - \frac{T_L}{J} \tag{3.55}$$

Based on the above equations, the state equation of PMSM can be expressed as:

$$\begin{bmatrix} \frac{di_d}{dt} \\ \frac{di_q}{dt} \\ \frac{d\omega_r}{dt} \\ \frac{d\theta_r}{dt} \end{bmatrix} = \begin{bmatrix} -\frac{R}{L_d} i_d + \frac{L_q}{L_d} \omega_r i_q + \frac{V_d}{L_d} \\ -\frac{R}{L_q} i_q - \frac{L_d}{L_q} \omega_r i_d - \frac{\lambda_m}{L_q} \omega_r + \frac{V_q}{L_q} \\ \frac{3P}{4J} \lambda_m i_q - \frac{B}{J} \omega_r - \frac{T_L}{J} \\ \omega_r \end{bmatrix} \tag{3.56}$$

V_d, V_q, i_d& i_q are d-axis and q-axis voltage and current components.

From the above equation, it can be seen that PMSM is a multi-variable, coupled, and nonlinear system. Taking i_d, i_q, ω_r, θ_r as state vector V_d, V_q as input vector and i_d, i_q as output vector, the input-output state-space representation of the system becomes:

$$\begin{bmatrix} \frac{di_d}{dt} \\ \frac{di_q}{dt} \\ \frac{d\omega_r}{dt} \\ \frac{d\theta_r}{dt} \end{bmatrix} = \begin{bmatrix} -\frac{R}{L_d} & \frac{L_q}{L_d}\omega_r & 0 & 0 \\ -\frac{L_d}{L_q}\omega_r & -\frac{R}{L_q} & -\frac{\lambda_m}{L_q} & 0 \\ 0 & \frac{3P}{4J}\lambda_m & -\frac{B}{J} & 0 \\ 0 & 0 & 1 & 0 \end{bmatrix} \begin{bmatrix} i_d \\ i_q \\ \omega_r \\ \theta_r \end{bmatrix} + \begin{bmatrix} \frac{1}{L_d} & 0 \\ 0 & \frac{1}{L_q} \\ 0 & 0 \\ 0 & 0 \end{bmatrix} \begin{bmatrix} V_d \\ V_q \end{bmatrix} + \begin{bmatrix} 0 \\ 0 \\ -\frac{T_L}{J} \\ 0 \end{bmatrix} \tag{3.57}$$

$$\begin{bmatrix} i_d \\ i_q \end{bmatrix} = \begin{bmatrix} 1 & 0 & 0 & 0 \\ 0 & 1 & 0 & 0 \end{bmatrix} * \begin{bmatrix} i_d \\ i_q \\ \omega_r \\ \theta_r \end{bmatrix} \tag{3.58}$$

From the above state-space equation of PMSM motor, the A, B, C, and D matrices are given as follows:

$$A = \begin{bmatrix} -\frac{R}{L_d} & \frac{L_q}{L_d}\omega_r & 0 & 0 \\ -\frac{L_d}{L_q}\omega & -\frac{R}{L_q} & -\frac{\lambda_m}{L_q} & 0 \\ 0 & \frac{3P}{4J}\lambda_m & -\frac{B}{J} & 0 \\ 0 & 0 & 1 & 0 \end{bmatrix}, \quad \mathrm{B}=\begin{bmatrix} \frac{1}{L_d} & 0 \\ 0 & \frac{1}{L_q} \\ 0 & 0 \\ 0 & 0 \end{bmatrix}, \quad \mathrm{C}=\begin{bmatrix} 1 & 0 & 0 & 0 \\ 0 & 1 & 0 & 0 \end{bmatrix} \quad \text{and} \quad \mathrm{D}=0$$

3.7. Control System of PMSM Drive

In the control of PMSM drive using field-oriented control technique the position/speed information of the motor is crucial. Depending on the way of getting rotor speed information, control of PMSM drive can be categorized into sensor-based and senor-less control.

In the sensor-based control technique, the position/speed is measured using a mechanical sensor and used as feedback to the system. However, this control technique has many disadvantages like increasing weight, volume, and connection parts to the system since it needs space on the shaft of the rotor. It also has noise problems, gives the additional cost, and reduces the systems reliability. In the sensor less control technique, the position/speed of the rotor is estimated using algorithms. It overcomes the disadvantages of the sensor-based control with higher efficiency, lesser cost, faster response, and more reliability. Due to the advantages mentioned above, sensor-less control is implemented in this thesis work using Extended State Observer to estimate the rotor speed of the motor.

3.7.1. DC Source

EVs operate under variable speed so variable frequency input for its traction motor is required. However, DC sources can't produce variable frequency signal by itself. So, the dc source from the battery is used in conjunction with a three-phase voltage source inverter.

3.7.2. Voltage Source Inverter (VSI) and Its Control

PMSM Drives used in vehicles work at variable speed. So as to achieve the variable speed of the motor, variable frequency stator voltage should be given to the stator of the motor. However, the power source that can be used in vehicles is the DC source which doesn't have a variable frequency. In this case, voltage source inverters are required to produce a variable frequency three-phase voltage. This can be accomplished by controlling the semiconductor devices used in the three-phase voltage source using six gate signals generated by the space vector pulse width modulation technique which is discussed in the next section.

3.7.2.1. Selection of Power Semiconductor Devices

There are different choices of power semiconductor devices available for the design of inverters. This includes MOSFETs, BJTs, IGBTs, etc. The bipolar transistor was the only power transistor till the MOSFET emerged in the 1970s [34]. It has relatively slow turn-off characteristics and they need a high base current in order to turn on. In addition, they have a negative temperature coefficient which will cause thermal runaway in the system and power loss in the form of heat.

MOSFET is a low voltage device that is mostly available up to 600V and it is a voltage-controlled device and it is surely a device to be chosen for devices with voltages below 250V [34]. Currently, MOSFET and IGBT are competent semiconductor devices. But, IGBT has a collective characteristic of BJT and MOSFET. The gate behavior of IGBT and MOSFET is similar and is easy to turn on and off. The rating of IGBT is in thousands of volts (>1000V). However, voltage levels below 1000V are available and have better performance, but its cost is very high for low voltage applications. The voltage rating of the PMSM in this study is 144V. Due to these, metal oxide semiconductor field-effect transistor (MOSFET) is selected for the design of the three-phase inverter because it has the appropriate ratings that will fit with the PMSM drive used in this study.

3.7.3. Space Vector Pulse Width Modulation (SVPWM)

In the control of PMSM drive, SVPWM has grown in popularity as a pulse width modulation technique for three-phase voltage-source inverters. When compared to a conventional sinusoidal PWM inverter, the SVPWM inverter provides a 15% increase in dc-link voltage usage and lower output harmonic distortions [35], [36]. Additionally, this type of inverters helps in producing high torque at high speeds and are highly efficient. The diagram of the 3-phase (VSI) is given in the following Figure 3.5.

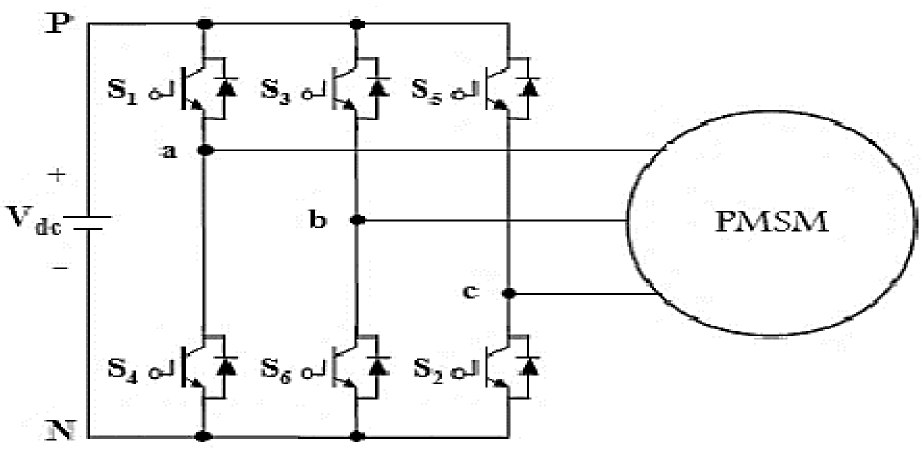

Figure 3.5. Three-phase VSI bridge circuit for PMSM [35].

The voltages Va, Vb, and Vc are the three-phase sinusoidal voltages given to the motor and V_{dc} is the dc input voltage given to the inverter. The switches from s1 to s6 are the six power transistors which control and shapes the output voltage by switching signals. When the transistors in the upper portion are turned on, the complementary lower transistors are switched off. The operation of SVPWM is based on eight switch combinations. Based on this there are eight different voltage vectors of VSI, these are V_0(000), V_1(100), V_2(110), V_3(010), V_4(011), V_5(001), V_6(101), and V_7(111). The switching states (000) and (111) didn't allow a current to pass to the motor. Hence, the line-to-line voltage is zero (also called null vectors). The rest of the switching states induce voltages to be given to the motor [36]. Let, the upper switches of the inverter are represented as $(a\ b\ c)^T$ and the DC link voltage is Vdc, then the three-phase voltages can be calculated as:

$$\begin{bmatrix} V_{an} \\ V_{bn} \\ V_{cn} \end{bmatrix} = \frac{V_{dc}}{3} \begin{bmatrix} 2 & -1 & -1 \\ -1 & 2 & -1 \\ -1 & -1 & 2 \end{bmatrix} \begin{bmatrix} a \\ b \\ c \end{bmatrix} \tag{3.60}$$

The maximum achievable peak voltage using the SVPWM strategy can be given as:

$$V_{svpwm} = \frac{V_{dc}}{2} \tag{3.61}$$

Voltage space vectors for a three-phase VSI are given in Figure 3.6. The six voltage vectors V_1-V_6 are the operating states that make states in the α-β frame of reference and split up the plane into six sectors: every sector having an angle of 60 degrees.

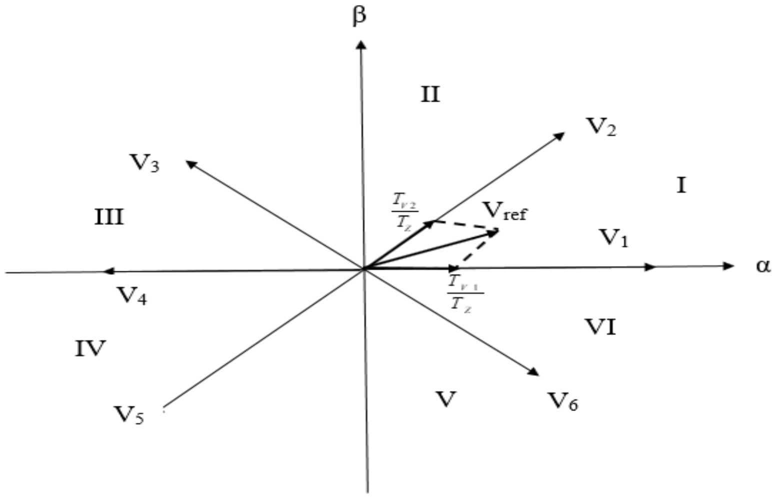

Figure 3.6. voltage space vectors for a three-phase VSI for PMSM [37].

3.7.3.1. Operating Principle of SVPWM

When SVPWM is applied to motor control, it provides energy through a succession of pulses rather than a continuously varying (analog signal). It controls the power delivered to the motor by enlarging or reducing the pulse width of the signal. In this scheme the three-phase inverter is fed with a fixed DC voltage and it is possible to get a controlled ac voltage by regulating the on and off of the inverter switches using SVPWM.

SVPWM uses two signals for its operation. These signals are the controlled signal and carrier signals. By comparing these two signals the rectangular waveform switching signal will be generated. The d-q currents are controlled and the resulting signal which is the d-q voltages are changed into α-β voltages to be used as input of the SVPWM. Then three-phase voltages are generated using the SVPWM technique to be compared with the carrier signal.

If the amplitude of the voltage signal is greater than that of the carrier signal the switching signal will be one and the switch will be on otherwise it will be off. The triangular wave carrier signal given in figure 3.7 is generated by the carrier signal generator using a switching frequency of 5kHz.

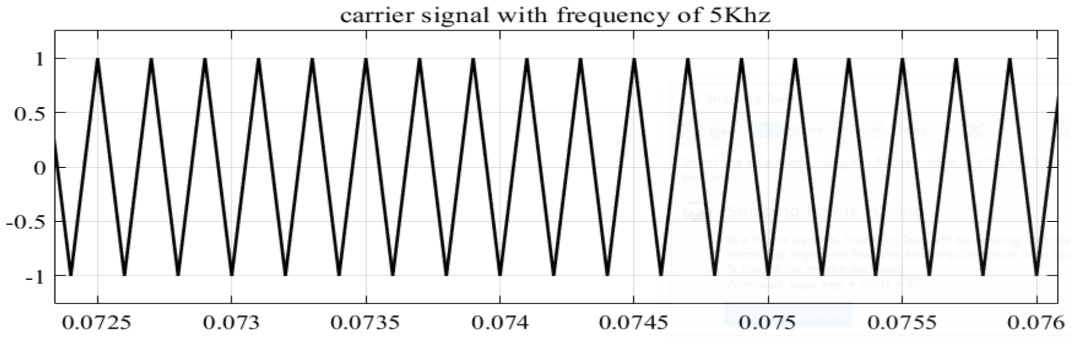

Figure 3.7. The carrier signal output waveform.

The design of the SVPWM is implemented using the following steps:

Step 1: determine V_α, V_β and angle (α)

In SVPWM, α-β frame is used rather than a-b-c reference frame and Clarke transformation is implemented. So, V_α and V_β are used as inputs which can be given as:

$$\begin{bmatrix} V_\alpha \\ V_\beta \end{bmatrix} = \frac{2}{3} \cdot \begin{bmatrix} 1 & -\frac{1}{2} & -\frac{1}{2} \\ 0 & \frac{\sqrt{3}}{2} & -\frac{\sqrt{3}}{2} \end{bmatrix} \cdot \begin{bmatrix} V_{an} \\ V_{bn} \\ V_{cn} \end{bmatrix} \tag{3.62}$$

The α, β values of SVPWM are used to compute the reference voltage $\vec{V}_{ref}$ as follows,

$$\left|\bar{V}_{ref}\right| = \frac{2}{3}.a.\sqrt{V_\alpha^2 + V_\beta^2} \tag{3.63}$$

where, a is the modulation index.

The next step to design SVPWM is to find an angle α, which is given as follows.

$$\alpha = tan^{-1}\left(\frac{V_\beta}{V_\alpha}\right) \tag{3.64}$$

Step 2: determine time durations T_1, T_2 and T_0

The time duration T_1, T_2 and T_0 are the switching times can be determined as:

Switching time for sector 1 can be determined as follows,

$$\int_0^{T_z} \overline{V}_{ref} = \int_0^{T_1} \overline{V}_1 dt + \int_{T_1}^{T_1+T_2} \overline{V}_2 dt + \int_{T_1+T_2}^{T_z} \overline{V}_0 dt \tag{3.65}$$

$$\therefore T_z \cdot \overline{V}_{ref} = (T_1 \cdot \overline{V}_1 + T_2 \cdot \overline{V}_2) \tag{3.66}$$

Then the average voltage for sector 1 and the switching times can be given as:

$$T_z \cdot \left|\overline{V}_{ref}\right| \cdot \begin{bmatrix} cos(\alpha) \\ sin(\beta) \end{bmatrix} = T_1 \cdot \frac{2}{3} \cdot V_{dc} \cdot \begin{bmatrix} 1 \\ 0 \end{bmatrix} + T_2 \cdot \frac{2}{3} \cdot V_{dc} \cdot \begin{bmatrix} cos(\pi/3) \\ sin(\pi/3) \end{bmatrix} \tag{3.67}$$

$$\begin{aligned} T_1 &= T_z \cdot a \cdot \frac{sin(\frac{\pi}{3} - \alpha)}{sin(\frac{\pi}{3})} \\ T_2 &= T_z \cdot a \cdot \frac{sin(\alpha)}{sin(\frac{\pi}{3})} \\ T_0 &= T_z - (T_1 + T_2) \end{aligned} \tag{3.68}$$

where $a = \frac{\left|\overline{V}_{ref}\right|}{\frac{2}{3} V_{dc}}$ is modulation index, T_1, T_2 are switching time durations of vectors V_1, V_2 respectively, T_0 is the time of the zero vector and T_z is the time for which one sector is applied. For any given sector, the switching time duration can be given as:

$$\begin{aligned} T_n &= \frac{\sqrt{3} \cdot T_z \cdot \left|\overline{V}_{ref}\right|}{V_{dc}} \left(sin\left(\frac{\pi}{3} - \alpha + \frac{n-1}{3}\pi \right) \right) \\ &= \frac{\sqrt{3} \cdot T_z \cdot \left|\overline{V}_{ref}\right|}{V_{dc}} \left(sin\frac{n}{3}\pi - \alpha \right) \\ &= \frac{\sqrt{3} \cdot T_z \cdot \left|\overline{V}_{ref}\right|}{V_{dc}} \left(sin\frac{n}{3}\pi \cdot cos\,\alpha - cos\frac{n}{3}\pi \cdot sin\,\alpha \right) \end{aligned} \tag{3.69}$$

$$\begin{aligned} T_{n+1} &= \frac{\sqrt{3} \cdot T_z \cdot \left|\overline{V}_{ref}\right|}{V_{dc}} \left(sin\left(\alpha - \frac{n-1}{3}\pi \right) \right) \\ &= \frac{\sqrt{3} \cdot T_z \cdot \left|\overline{V}_{ref}\right|}{V_{dc}} \left(-cos\,\alpha \cdot sin\frac{n-1}{3}\pi + sin\,\alpha \cdot cos\frac{n-1}{3}\pi \right) \end{aligned} \tag{3.70}$$

$$T_0 = T_z - (T_n + T_{n+1}), \tag{3.71}$$

Where, n is the sector number (1 to 6), and $0 \le \alpha \le 60$.

Step 3: determine the switching time of every sector.

The switching time of every sector, for both the upper and lower switches are discussed in the following Table 3.4. In switching of the transistors, when the upper switch is on the corresponding lower switches turn off.

Table 3.4. Switching time for each sector [38].

Sector number (n)	Upper switches (S_1, S_3, S_5)	Lower switches (S_2, S_4, S_6)
1	$S_1 = T_1 + T_2 + T_0/2$ $S_3 = T_2 + T_0/2$ $S_5 = T_0/2$	$S_4 = T_0/2$ $S_6 = T_1 + T_0/2$ $S_2 = T_1 + T_2 + T_0/2$
2	$S_1 = T_1 + T_0/2$ $S_3 = T_1 + T_2 + T_0/2$ $S_5 = T_0/2$	$S_4 = T_2 + T_0/2$ $S_6 = T_0/2$ $S_2 = T_1 + T_2 + T_0/2$
3	$S_1 = T_0/2$ $S_3 = T_1 + T_2 + T_0/2$ $S_5 = T_2 + T_0/2$	$S_4 = T_1 + T_2 + T_0/2$ $S_6 = T_0/2$ $S_2 = T_1 + T_0/2$
4	$S_1 = T_0/2$ $S_3 = T_1 + T_0/2$ $S_5 = T_1 + T_2 + T_0/2$	$S_4 = T_1 + T_2 + T_0/2$ $S_6 = T_2 + T_0/2$ $S_2 = T_0/2$
5	$S_1 = T_2 + T_0/2$ $S_3 = T_0/2$ $S_5 = T_1 + T_2 + T_0/2$	$S_4 = T_1 + T_0/2$ $S_6 = T_1 + T_2 + T_0/2$ $S_2 = T_0/2$
6	$S_1 = T_1 + T_2 + T_0/2$ $S_3 = T_0/2$ $S_5 = T_1 + T_0/2$	$S_4 = T_0/2$ $S_6 = T_1 + T_2 + T_0/2$ $S_2 = T_2 + T_0/2$

CHAPTER 4

CONTROLLER DESIGN FOR PMSM DRIVE

The control of PMSM drive in this thesis work contains two control loops, the inner and the outer loop. The out one is to control the speed of the motor in which HOSMC is used with ESO. The inner loop is to controls the d-q currents, id, and iq and indirectly the electromagnetic torque which mainly depends on the quadrature current (iq). in this loop, the GA-PI controller is applied.

The major issue in designing the control system of motors for electric vehicles is to design a controller to stabilize the speed of the motor at the desired level under different internal and external disturbances, load variation, and for various speed ranges. Different controllers are available to control the speed of the PMSM drive. PI controller is the simplest of all control techniques which might work properly under less internal and external disturbance conditions. However, in systems like electric vehicles, better controllers with better dynamic performance are required which will deal with such nonlinear systems as chattering-free SMC.

4.1. Speed Controller Design

In this chapter, the theoretical and mathematical design of different speed controllers is discussed and compared with the proposed chattering free high order sliding mode controller with ESO.

4.1.1. PI Controller

This controller is the simplest control method but it is highly affected by internal and external parameter variations. The controllers' time-domain equation can be given as [23]:

$$u(t) = K_p [e(t) + \frac{1}{T_i} \int e(t)dt] \tag{4.1}$$

where K_p and T_i are the proportional gain and the integral time respectively and K_{ic} is the integral gain given by: $K_i = \frac{K_p}{T_i}$. And in the frequency domain, the PI controller can be expressed as:

$$U(s) = (K_p + \frac{K_i}{s})E(s) \tag{4.2}$$

4.1.2. Review on Conventional Sliding Mode Controller (SMC)

Sliding mode controller (SMC) is a robust, non-linear type of controller which is insensitive to internal parameter variations and external disturbances compared to other non-linear and linear controllers. High-performance permanent magnet motors need their speed controller to have fast response, good tracking ability, smaller overshoot, and a strong capability to reject disturbance. Previously linear controllers like PI controllers were used to control the speed of this motor. But the performance of such a controller is not satisfactory due to its poor tracking ability and lack of robustness. So, a non-linear and robust controller which is a sliding mode controller is used in this study.

This controller is robust even if there are internal parameter variations and load variations. Although, it has its own disadvantage, that is the chattering phenomenon which occurs because of the high frequency switching near the sliding surface of the system by discontinuous control law in SMC design. To enhance the performance of traditional SMC in terms of ability to track and ability to reject disturbance, as well as to suppress chattering phenomenon, various SMC enhancement methods have been proposed. Sliding surface design modification, reaching law methods, higher-order sliding mode controller (HOSMC), and composite SMC designs, for example, when combined with artificial intelligence or disturbance compensation techniques, are examples of these methods [22]. In the following section the modeling of conventional SMC, SMC with exponential reaching law, linear as well as nonlinear FOSMC, and the proposed chattering free HOSMC with ESO is discussed.

There are two steps in designing sliding mode controllers. The first step is choosing an appropriate sliding surface. The next step is designing of the control input so as to force the system trajectory to the sliding surface, which makes sure the system satisfies the sliding mode reaching condition which is described as [22]:

$$s\dot{s} < 0 \tag{4.3}$$

where, s is the sliding surface.

Mathematical Model of Conventional SMC: This controller is the basic sliding mode control type, which has high robustness and very simple to design. In this controller, there is only one parameter that has to be adjusted that is why it is simple. It can be designed easily as follows.

The sliding surface of conventional SMC is the difference between the setpoint and actual output [22].

$$s = \omega^* - \omega_r \tag{4.4}$$

where, s is the sliding surface, ω^* is the speed setpoint, and ω_r is the output of the rotor speed of the motor. Figure 4.1 implies the sliding surface of a conventional SMC controller with a reference speed of 100rad/s. It is visible that chattering is produced when the control objective of this controller is fulfilled (i.e., $s(t) = 0$).

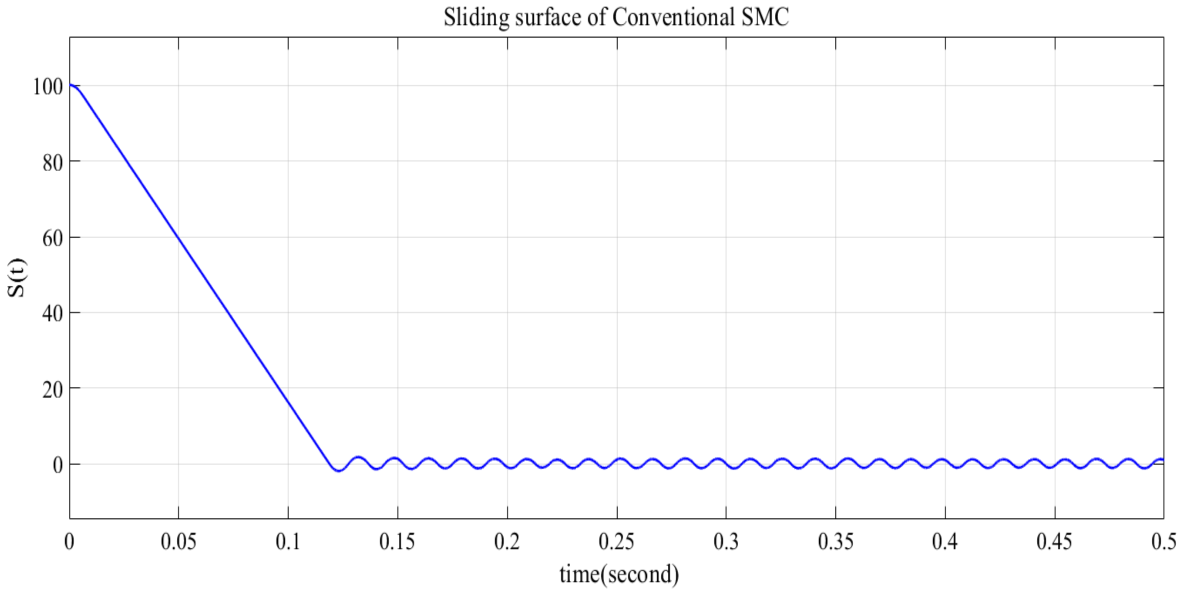

Figure 4.1. The sliding surface of conventional SMC.

Then by using constant rate reaching law the reaching law can be designed as:

$$\dot{s} = K_s \, sgn(s) \tag{4.5}$$

where K_s is a positive number and $sgn(s)$ is defined as follows [39]:

$$sgn(s) = \begin{cases} 1 & for\ s > 0 \\ -1 & for\ s < 0 \\ 0 & if\ s = 0 \end{cases} \tag{4.6}$$

In this control law, if K_s is too small the reaching time for the system would be too long. If K_s is too high there will be too much chattering in the system. So, when selecting this gain there has to be a compromise between the two.

Now derivate the sliding surface and equate it with the reaching law as follows.

$$\dot{s} = -\dot{\omega}_r = -(\frac{3P}{4J}\lambda_m i_q - \frac{B}{J}\omega_r - \frac{T_L}{J}) \tag{4.7}$$

Then equate (4.5) and (4.7) to get the control input i_q

$$-(\frac{3P}{4J}\lambda_m i_q - \frac{B}{J}\omega_r - \frac{T_L}{J}) = K_s sgn(s) \tag{4.8}$$

The control input i_q becomes

$$i_q = \frac{4J}{3P\lambda_m}(\frac{B}{J}\omega + \frac{T_L}{J} + K_s sgn(s)) \tag{4.9}$$

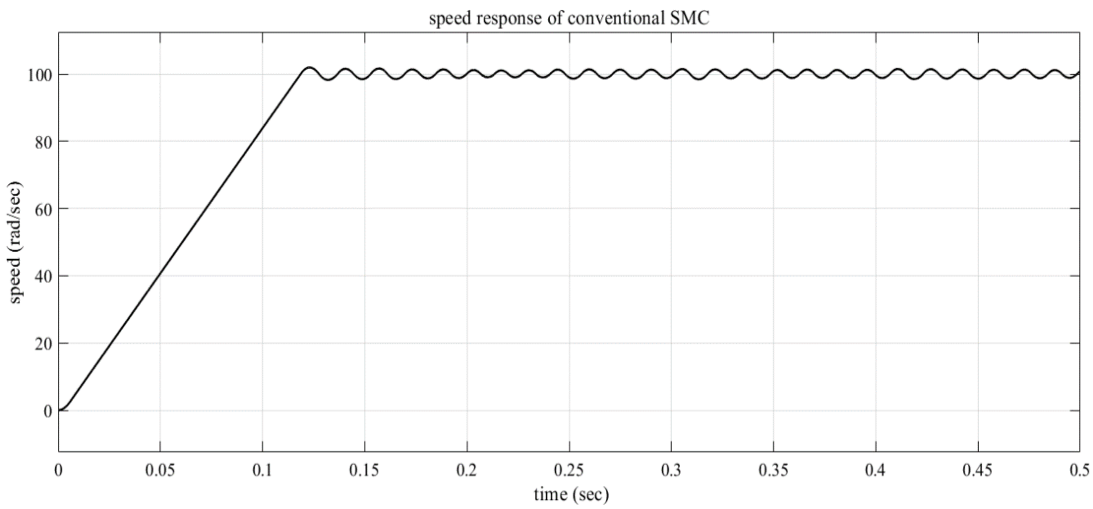

Figure 4.2. Speed response of conventional SMC with $K_s = 1200$.

This controller produces too much chattering, this chattering in the system will result in a reduction of the control accuracy which might end up in high power and heat losses in electrical power circuits and wear in the mechanical moving parts of the motor. Figure 4.2 shows the speed response of conventional SMC with a reference speed of 100rad/s and value of $K_s = 1200$.

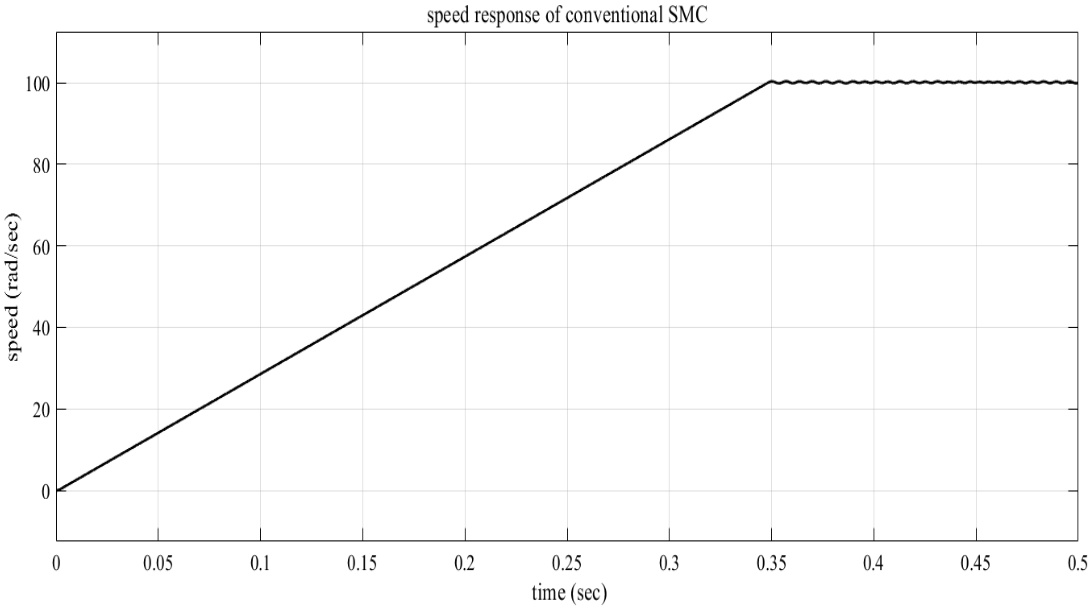

Figure 4.3. Speed response of conventional SMC with $K_s = 400$.

As described above the chattering is dependent on the value of K_s. Figure 4.3 shows the speed response of this controller with $K_s = 400$. The chattering is minimized but the reaching time is higher. The reaching time in this graph is at $t = 0.35$ while at $K_s = 1200$, the reaching time is 0.122. which shows that the reaching time is about 3 times higher but with reduced chattering.

4.1.3. Review on Mathematical Modelling of SMC with Exponential Reaching Law

Some researchers used this type of controller to suppress the chattering phenomenon. It can be designed as follows: The typical sliding surface for the system under SMC can be chosen as:

$$S = ce + \dot{e} \tag{4.10}$$

An exponential reaching law is used for the system, this law constrains the switching variable to reach the switching manifold s at a constant rate K_s. it can be designed as follows [40].

$$\dot{s} = -K_s sgn(s) - Ws \tag{4.11}$$

where, c, Ks and W are positive numbers.

The advantage of this reaching law is its simplicity and ability to suppress the chattering in the speed response.

$\dot{s} = -Ws$ is an exponential term of the reaching law in which its solution can be defined as, $s = s(0)e^{-W(t)}$. Clearly, by adding the proportional rate term $-Ws$, the state is forced to approach the switching manifolds faster when s is large.

$sgn(s)$, is a signum function defined in Equation (4.6):

Now derivate the sliding surface given at Equation (4.10) as follows,

$$\dot{s} = c\dot{e} + \ddot{e} \tag{4.12}$$

But,

$$e = \omega^* - \omega_r. \quad \text{then} \quad \dot{e} = -\dot{\omega}_r \tag{4.13}$$

$$\dot{e} = -\dot{\omega}_r = -\left(\frac{3P}{4J}\lambda_m i_q - \frac{B}{J}\omega_r - \frac{T_L}{J}\right) \tag{4.14}$$

$$\ddot{e} = -\ddot{\omega}_r = -\frac{3P}{4J}\lambda_m \dot{i}q + \frac{B}{J}\dot{\omega}_r \tag{4.15}$$

Now, in order to find the control input, equate the derivative of the sliding surface s and the control law.

$$\dot{s} = -K_s sgn(s) - Ws = c\dot{e} + \ddot{e} \tag{4.16}$$

$$-K_s sgn(s) - Ws = c\dot{e} - \frac{3P}{4J}\lambda_m \dot{i}_q + \frac{B}{J}\dot{\omega}_r \tag{4.17}$$

From this equation the control input i_q is given here:

$$i_q = \frac{4J}{3P\lambda_m}\int\left(c\dot{e} + \frac{B}{J}\dot{\omega}_r + K_s sgn(s) + Ws\right)dt \tag{4.18}$$

The sliding surface of this controller is implied in Figure 4.4 and it is visible that there is a lot of chattering when the system arrives at the sliding surface. But in the speed response of the controller (SMC-ERL), the chattering is reduced as shown in Figure 4.5.

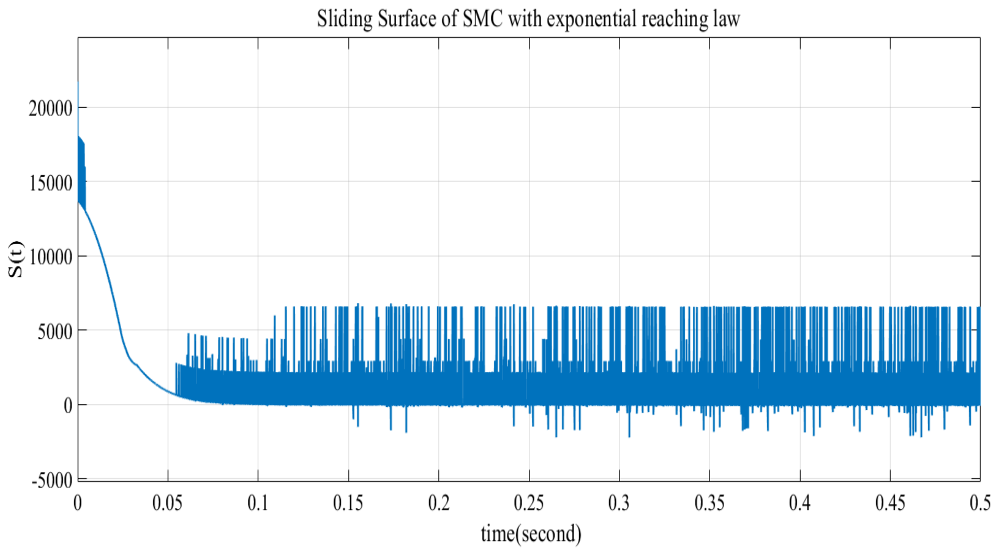

Figure 4.4. The sliding surface of exponential reaching law SMC.

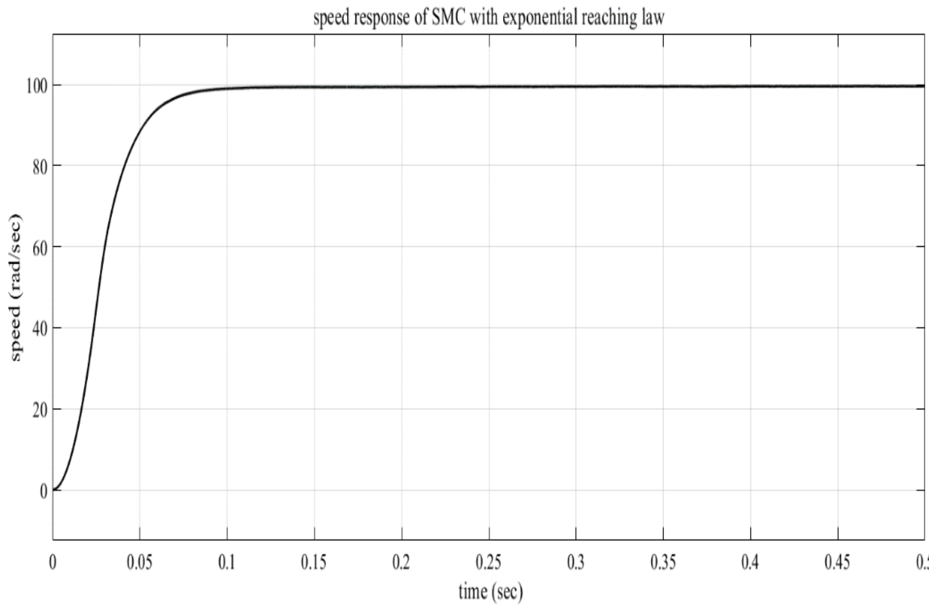

Figure 4.5. Speed response of SMC- ERL.

4.1.4. Review on Fractional-Order Sliding Mode Controller (FOSMC)

The other extension of the SMC which is the FOSMC controller is discussed in the following section. To use the robustness and simplicity of the sliding mode controller, its drawback is the existence of the chattering in the system and it has to be eliminated or it has to be reduced significantly. FOSMC is a composite controller which contains fractional order PID which is used for sliding surface design.

FOSMC uses fractional-order calculus to design the sliding surface of the system. This controller gives extra robustness, accuracy, chattering reduction, and an additional degree of freedom for the system for the sliding mode controller [41]. But when compared to the proposed second-order sliding mode controller this controller is inferior in its chattering reduction.

Fractional Calculus Theory and Definition: The basic operator of fractional calculus is denoted as ${}_aD_t^r$, where a is the lower limit and t is the upper limit of the operation, r is the order of operation. r is generally, $r \in R$ but r could also be a complex number [42]. The operator can be defined as follows:

$$ {}_aD_t^r = \begin{cases} \dfrac{d^r}{dt^r} & \text{for, r>0.} \\ 1 & \text{for, r=0.} \\ \int (d\tau)^{-r} & \text{for r<0.} \end{cases} \tag{4.19} $$

There are three basically used definitions for the general fractional-order differential-integral namely the Grunwald-Letnikov definition, the Riemann-Liouville, and the Caputo definitions for $n-1<r<n$. Riemann-Liouville definition of fractional calculus for differentiation and integration is also formulated in form of Laplace transformation for $n-1<r<n$ and $s \equiv j\omega$ which is the Laplace transform variable, since this method is commonly used in engineering problems solving [8], [43].

The Grunwald-Letnikov definition is defined as:

$$ {}_aD_t^r f(t) = \lim_{h\to 0} h^{-r} \sum_{j=0}^{\left[\frac{t-a}{h}\right]} (-1)^j \binom{r}{j} f(t-jh) \tag{4.20} $$

The Riemann-Liouville definition is given as:

$$ {}_aD_t^r f(t) = \frac{1}{\Gamma(n-r)} \frac{d^n}{dt^n} \int_a^t \frac{f(\tau)}{(t-\tau)^{r-n+1}} d\tau \tag{4.21} $$

Finally, the last definition which is the Caputo definition is given as.

$$ {}_aD_t^r f(t) = \frac{1}{\Gamma(n-r)} \int_a^t \frac{f^n(\tau)}{(t-\tau)^{r-n+1}} d\tau \tag{4.22} $$

The Reimann-Liouville definition of fractional order operation in the form of Laplace transformation is given as follows:

$$ \int_0^\infty e^{-st} \, {}_aD_t^r f(t) = s^r F(s) - \sum_{k=0}^{n-1} s^k \, {}_0D_t^{r-k-1} f(t)t = 0 \tag{4.23} $$

where $\Gamma(.)$ is gamma function, and referring to it is expressed as:

$$\Gamma(x) = \int_{0}^{\infty} t^{x-1} e^{-t} dt \tag{4.24}$$

where the real part of $R(x) > 0$.

The fractional derivatives and integrals have the following rules.

$$\frac{d^n}{dt^n}({}_{t0}D_t^{\alpha} f(t)) = {}_{t0}D_t^{\alpha+n} f(t) \tag{4.25}$$

$$\frac{d^n}{dt^n}({}_{t0}D_t^{\beta} f(t)) = {}_{t0}D_t^{\beta+n} f(t) \tag{4.26}$$

Design of linear fractional order SMC for speed control of PMSM: Similar to the conventional SMC controller FOSMC controller uses two steps in its design. The first one is to design a suitable sliding surface and the design of the control input. FOSMC controller can be designed as follows: the sliding surface is based on fractional-order PID ($PI^{\alpha}D^{\beta}$) and is designed as follows [26]:

$$s_{FOPID}(t) = k_p e(t) + k_i({}_0D_t^{-\alpha} e(t)) + k_d({}_0D_t^{\beta} e(t)) \tag{4.27}$$

where, ${}_0D_t^{-\alpha}e(t)$ is fractional order integration and ${}_0D_t^{\beta}e(t)$ is fractional order differentiation, and k_p, k_i *and* k_d are the proportional, integral, and differential gains of the PID controller respectively. Then the ranges of the parameters are given as: $0 < \alpha, \beta < 1$, $k_p, k_i, k_d > 0$. Figure 4.6 shows the block diagram of the sliding surface of FOPID.

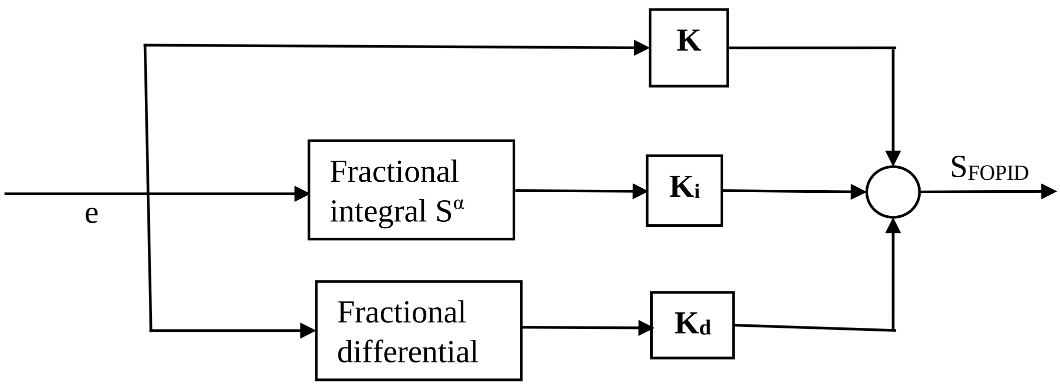

Figure 4.6. Block diagram of FOPID sliding surface.

The sliding surface of the linear FOSMC result in the Figure 4.7 shows that the control objective which is making the sliding surface of the system converges to zero within limited time period is accomplished.

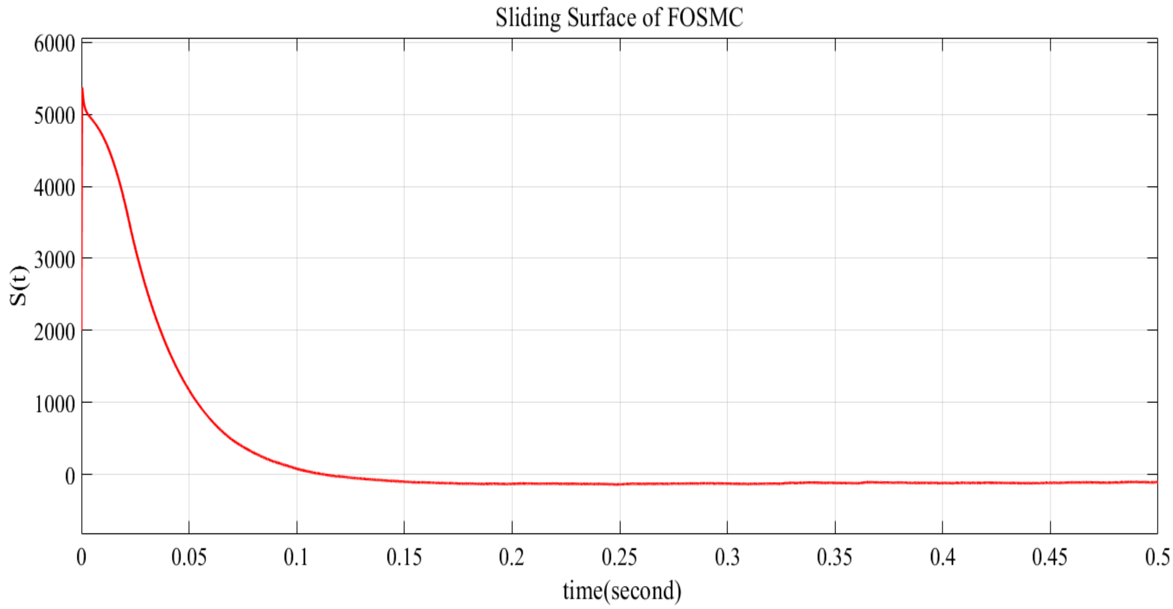

Figure 4.7. The sliding surface of FOSMC.

The control law of the FOSMC controller based on the conventional exponential reaching law is given as [26]:

$$\dot{s}_{FOPID}(t) = -Ws_{FOPID}(t) - K_s sign(s_{FOPID}(t)) \tag{4.28}$$

where $W, K_s \in R^+$.

Now, derivate the sliding surface given at equation (4.27).

$$\dot{S}_{FOPID}(t) = k_p\dot{e}(t) + k_i({}_0D_t^{1-\alpha}e(t)) + k_d({}_0D_t^{\beta+1}e(t)) \tag{4.29}$$

But the error signal between the reference and the actual speed of the motor is given as:

$$e(t) = \omega^* - \omega_r \quad \text{then} \quad \dot{e}(t) = \dot{\omega}^* - \dot{\omega}_r \tag{4.30}$$.

But the derivative of rotor speed ($\dot{\omega}_r$) is given by:

$$\frac{d\omega_r}{dt} = \frac{3P}{4J}\lambda_m i_q - \frac{B}{J}\omega_r - \frac{T_L}{J} \tag{4.31}$$

Then substitute Equation (4.31) into Equation (4.30).

$$\dot{e}(t) = \dot{\omega}^* - (\frac{3}{2J} * (\frac{P}{2})^2 \lambda_m i_q - \frac{B}{J}\omega_r - \frac{P}{2} * \frac{T_L}{J}) \tag{4.32}$$

Now, using Equations, (4.29) and (4.32), the sliding surface of the system becomes:

$$\dot{S}_{FOPID}(t) = k_p(\dot{\omega}^* - (\frac{3P}{4J}\lambda_m i_q - \frac{B}{J}\omega_r - \frac{T_L}{J})) + k_i({}_0D_t^{1-\alpha}e(t)) + k_d({}_0D_t^{\beta+1}e(t)) \tag{4.33}$$

From (4.28) and (4.33) the control input can be calculated as follows.

$$\begin{aligned} -Ws_{FOPID}(t) - K_s sign(s_{FOPID}(t)) = k_p(\dot{\omega}^*(t) - (\frac{3P}{4J}\lambda_m i_q(t) - \frac{B}{J}\omega_r(t) - \frac{T_L}{J})) + k_i({}_0D_t^{1-\alpha}e(t)) \\ + k_d({}_0D_t^{\beta+1}e(t)) \end{aligned} \tag{4.34}$$

Then,

$$\begin{aligned} k_p(\frac{3P}{4J}\lambda_m i_q(t)) = k_p(\dot{\omega}^* + \frac{B}{J}\omega_r(t) + \frac{T_L}{J})) + k_i({}_0D_t^{1-\alpha}e(t)) + k_d({}_0D_t^{\beta+1}e(t)) + Ws_{FOPID}(t) \\ + K_s sign(s_{FOPID}(t)) \end{aligned} \tag{4.35}$$

Finally, the control input i_q based on linear fractional order PID (LFOPID) and the exponential reaching law is:

$$\begin{aligned} i_q = \frac{1}{k_p(\frac{3P}{4J}\lambda_m)} k_p(\dot{\omega}^* + \frac{B}{J}\omega_r + \frac{T_L}{J})) + k_i({}_0D_t^{1-\alpha}e(t)) + k_d({}_0D_t^{\beta+1}e(t)) + Ws_{FOPID}(t) \\ + K_s sign(s_{FOPID}(t)) \end{aligned} \tag{4.36}$$

But,

$$Ws_{FOPID}(t) = WK_p e(t) + WK_i\, {}_0D_t^{-\alpha} e(t) + WK_d\, {}_0D_t^{\beta} e(t) \tag{4.37}$$

Now substitute Equation (4.37) into (4.36).

$$\begin{aligned} i_q = \frac{1}{k_p(\frac{3P}{4J}\lambda_m)}(k_p(\dot{\omega}^* + \frac{B}{J}\omega_r + \frac{T_L}{J}) + k_{i0}D_t^{1-\alpha}e(t) + k_{d0}D_t^{\beta+1}e(t) + WK_p e(t) \\ + WK_i\, {}_0D_t^{-\alpha} e(t) + WK_d\, {}_0D_t^{\beta} e(t) + K_s sign(s_{FOPID}(t))) \end{aligned} \tag{4.38}$$

Let,

$$\Phi(t) = \dot{\omega}^* + \frac{B}{J}\omega_r + \frac{T_L}{J} \tag{4.39}$$.

Then, the control input can be written as:

$$i_q = \frac{1}{k_p(\frac{3P}{4J}\lambda_m)}(k_p\Phi(t) + k_{i0}D_t^{1-\alpha}e(t) + k_{d0}D_t^{\beta+1}e(t) + WK_pe(t) + WK_{i\,0}D_t^{-\alpha}e(t)$$

$$+WK_{d\,0}D_t^{\beta}e(t) + K_s sign(s_{FOPID}(t))) \quad (4.40)$$

Stability Analysis: The fractional sliding manifold needs to satisfy the reaching condition to ensure the convergence of the system state to the manifold for any initial condition. For this purpose, the Lyapunov stability theorem is used, where the Lyapunov function candidate is selected to be a function of state dynamics and it must be positive definite. It is chosen as, $V = \frac{1}{2}S^2_{FOPID}$ for any initial conditions, $t_0 \neq 0$. According to the Lyapunov stability theorem, if $V > 0$ (positive definite), and $\dot{V} < 0$ (negative definite), then the closed-loop is asymptotically stable.

The reaching condition of the system will be satisfied when the derivative of the Lyapunov candidate with respect to time is less than zero (i.e., $\dot{V} < 0$). But $\dot{V} = S_{FOPID}.\dot{S}_{FOPID} < 0$ holds.

So,

$$\dot{V} = s_{FOPID}.\dot{s}_{FOPID} = s_{FOPID}(-Ws_{FOPID} - K_s sign(s_{FOPID})) \quad (4.41)$$

$$\dot{V} = -Ws^2_{FOPID} - K_s\left|s_{FOPID}\right| \quad (4.42)$$

But, W, $K_s > 0$. In this case, $\dot{V} < 0$ or it is negative definite. So, the Lyapunov stability condition is satisfied for values of W, $K_s > 0$. The system $s_{FOPID}\dot{s}_{FOPID} < 0$ implies that the system is globally stable, and s and $\dot{s}$ will be forced to zero in a definite period.

Design of nonlinear fractional-order sliding mode controller (NFOSMC): To enhance the robustness, the static and dynamic performance of the FOPID-SMC controller a new nonlinear FOPID sliding surface is designed [27]. This sliding surface is basically depending on FOPID by combining it with nonlinear state error feedback control law (NSEF). The key for the traditional NLSF is the nonlinear function $fal(.)$. The sliding surface of the FOPID controller based on nonlinear state error feedback control law (NSEF) can be developed as [27]:

$$s(t) = K_pe(t) + K_iD_t^{-a} fal(x,a,d) + K_dD_t^{b} fal(x,a,d) \quad (4.43)$$

The expression for the nonlinear function $fal(.)$ is given as [27]:

$$fal(x,a,d) = \begin{cases} |x|^a \, sign(x), & |x| > d, \\ \dfrac{x}{d^{1-a}}, & |x| \le d, \end{cases} \tag{4.44}$$

where δ is a filter factor, x is the error signal and a is a nonlinear factor of $fal(.)$. Figure 4.8 shows the block diagram of the NLSEF based FOPID sliding surface.

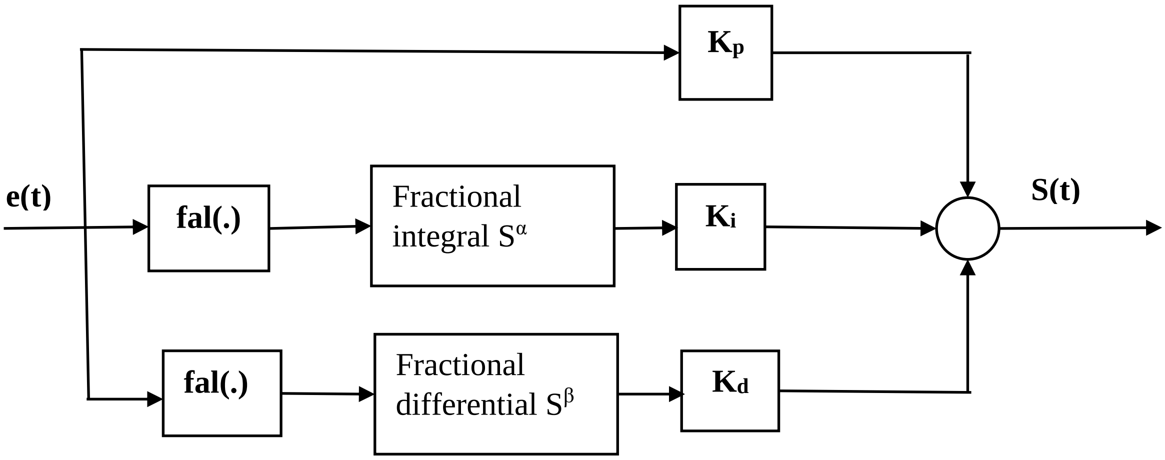

Figure 4.8. Block diagram of NLSEF based FOPID sliding surface.

This nonlinear function $fal(.)$ is continuous, however, it is non-derivable, and it will cause a high-frequency flutter phenomenon to the system. So, a new novel nonlinear function $f_{new}(.)$ is developed. The continuous and derivable function $f_{new}(.)$ is designed as follows [27].

$$f_{new}(x,\alpha,\delta) = \begin{cases} |x|^{\alpha} \, sign(x), & |x| > \delta, \\ R_1 x + R_2 x^2 + R_3 ver\,sin(|x|) sign(x), & |x| \le \delta, \\ \quad ver\,sin(|x|) = 1 - cos(|x|), & \end{cases} \tag{4.45}$$

where $0 < \delta, \alpha < 1$, and R_1, R_2, R_3 are the parameters of the function that needs to be determined [37]. The continuous and derivable conditions of the function can be satisfied by the expressions given as follows:

$$\begin{cases} f_{new}(x,\alpha,\delta) = \delta^{\alpha}, & \text{e}=\delta, \\ f_{new}(x,\alpha,\delta) = -\delta^{\alpha}, & \text{e}=-\delta, \\ \dot{f}_{new}(x,\alpha,\delta) = \alpha\delta^{\alpha-1}, & \text{e}=\pm\delta, \end{cases} \tag{4.46}$$

Then,

$$\begin{cases} R_1\delta + R_2\delta^2 + R_3(1-\cos\delta) = \delta^\alpha \\ \text{-}R_1\delta + R_2\delta^2 - R_3(1-\cos\delta) = -\delta^\alpha \\ R_1\delta + 2R_2\delta + R_3\sin\delta = \alpha\delta^{\alpha-1} \end{cases} \tag{4.47}$$

From this the parameters R_1, R_2, R_3 can be determined as follows:

$$\begin{cases} R_1 = \delta^{\alpha-1}\alpha - \dfrac{(1-\alpha)\delta^\alpha \sin\delta}{1-\cos\delta - \delta\sin\delta}, \\ \mathrm{R}_2 = 0, \\ R_3 = \dfrac{(1-\alpha)\delta^\alpha}{1-\cos\delta-\delta\sin\delta}, \end{cases} \tag{4.48}$$

Then after substituting R_1, R_2, R_3 into $f_{new}(.)$ we get the following nonlinear, derivable and continuous function [27], [41].

$$f_{new}(x,\alpha,\delta) = \begin{cases} |x|^\alpha \, sign(x), & |x| > \delta, \\ \left[\delta^{\alpha-1}\alpha - \dfrac{(1-\alpha)\delta^\alpha \sin\delta}{1-\cos\delta-\delta\sin\delta}\right] x + \dfrac{(1-\alpha)\delta^\alpha}{1-\cos\delta-\delta\sin\delta}(ver\,sin(|x|)sign(x)), & |x| > \delta, \end{cases} \tag{4.49}$$

The characteristics of this function are: it is continuous and derivable which reduces the high-frequency flutter phenomenon, and the value of α influences the nonlinearity degree of $f_{new}(.)$. The function $f_{new}(.)$ exhibits the characteristics of small errors which is $(|e| \le \delta)$ with higher gains $(|f_{new}(x,\alpha,\delta)| > |x|)$. On the other side, large errors $(|e| > \delta)$ correspond to lower gains $(|f_{new}(x,\alpha,\delta)| < |x|)$. In this case, the error signal is forced to attenuate to zero quickly. This function has the characteristics of fast convergence and characteristics of saturating the error signal.

The error signal passes through the nonlinear function $f_{new}(.)$ to form the function $f_{new}(e,\alpha,\delta)$ and this function is applied to the integral and differential term sliding surface design of the FOPID controller and a new NFOPID sliding surface will be obtained [27].

The sliding surface of the NFOPID controller based on the nonlinear function can be designed easily by substituting the nonlinear function $f_{new}(.)$ into the error signal $e(t)$ the integral and the differential part of the conventional FOSMC as shown below [41].

$$s_{NFOPID}(t) = K_p e(t) + K_i D_t^{-\alpha} f_{new}(x,a,\delta) + K_d D_t^{\beta}{}_{new}(x,a,\delta) \tag{4.50}$$

where, k_p, k_i *and* k_d are the gains of the fractional-order PID sliding surface, and $D_t^{-\alpha}$ is the fractional integration, and D_t^{β} is the fractional differentiation. Figure 4.9 shows the block diagram of the sliding surface of NFOPID controller.

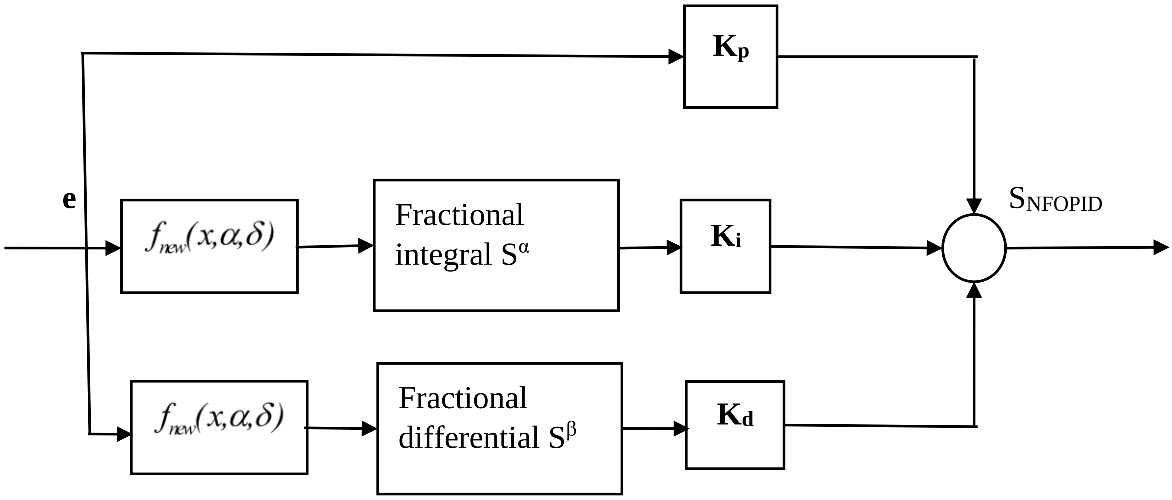

Figure 4. 9. Block diagram of the sliding surface of NFOPID controller.

The exponential reaching law is designed as [36]:

$$\dot{s}_{NFOPID}(t) = -Ks_{NFOPID}(t) - Wsign(s_{NFOPID}(t)) \tag{4.51}$$

where $K > 0$, $W>0$.

Now in order to find the control input of the controller, derivate the sliding surface as:

$$\dot{s}_{NFOPID}(t) = K_p\dot{e}(t) + K_iD_t^{-\alpha+1} f_{new}(x,a,\delta) + K_dD_t^{\beta+1}{}_{new}(x,a,\delta) \tag{4.52}$$

But,

$$\dot{e}(t) = \dot{\omega}^* - (\frac{3P}{4J}\lambda_m i_q - \frac{B}{J}\omega_r - \frac{T_L}{J}) \tag{4.53}$$

Now substitute Equation (4.53) into (4.52):

$$\dot{s}_{NFOPID}(t) = K_p(\dot{\omega}^* - (\frac{3P}{4J}\lambda_m i_q - \frac{B}{J}\omega_r - \frac{T_L}{J})) + K_iD_t^{-\alpha+1} f_{new}(x,a,\delta) + K_dD_t^{\beta+1}{}_{new}(x,a,\delta) \tag{4.54}$$

Then the sliding surface and the new reaching law are equated in order to find the control input as follows:

$$\begin{aligned} -Ws_{NFOPID}(t) - K_s sign(s_{NFOPID}(t)) = {} & K_p\dot{\omega}^* - (\frac{3P}{4J}\lambda_m i_q - \frac{B}{J}\omega_r - \frac{T_L}{J})) \\ & + K_iD_t^{-\alpha+1} f_{new}(x,a,\delta) + K_dD_t^{\beta+1}{}_{new}(x,a,\delta) \end{aligned} \tag{4.55}$$

$$-Ws_{NFOPID}(t)-K_s sign(s_{NFOPID}(t))=K_p(\dot{\omega}^*-\frac{3P}{4J}\lambda_m i_q+\frac{B}{J}\omega_r+\frac{T_L}{J}) + K_i D_t^{-\alpha+1} f_{new}(x,a,\delta)+K_d D_t^{\beta+1}{}_{new}(x,a,\delta) \quad (4.56)$$

Then,

$$K_p\frac{3P}{4J}\lambda_m i_q=K_p(\dot{\omega}^*+\frac{B}{J}\omega_r+\frac{T_L}{J})+K_i D_t^{-\alpha+1} f_{new}(x,a,\delta)+K_d D_t^{\beta+1}{}_{new}(x,a,\delta) + Ws_{NFOPID}(t)+K_s sign(s_{NFOPID}(t)) \quad (4.57)$$

Finally, the control input i_q is:

$$i_q=\frac{1}{K_p(\frac{3P}{4J}\lambda_m)}\begin{pmatrix} K_p\Phi(t)+K_i D_t^{-\alpha+1} f_{new}(x,a,\delta)+K_d D_t^{\beta+1} f_{new}(x,a,\delta) \\ +Ws_{NFOPID}(t)+K_s sign(s_{NFOPID}(t)) \end{pmatrix} \quad (4.58)$$

But,

$$ws_{NFOPID}(t)=WK_p e(t)+WK_i D_t^{-\alpha} f_{new}(x,a,\delta)+WK_d D_t^{\beta}{}_{new}(x,a,\delta), \quad (4.59)$$

So, the control input becomes,

$$i_q=\frac{1}{K_p(\frac{3P}{4J}\lambda_m)}\begin{pmatrix} K_p\Phi(t)+K_i D_t^{-\alpha+1} f_{new}(x,a,\delta) \\ +K_d D_t^{\beta+1} f_{new}(x,a,\delta) \\ +WK_p e(t)+WK_i D_t^{-\alpha} f_{new}(x,a,\delta)+WK_d D_t^{\beta}{}_{new}(x,a,\delta) \\ +K_s sign(s_{NFOPID}(t)) \end{pmatrix} \quad (4.60)$$

The sliding surface of the NFOSMC is shown in Figure 4.10. The figure implies that the sliding surface produces high amount of chattering.

However, when the speed response of this controller is compared with the linear FOSMC, its dynamic performance (like the steady state error) gets better as shown in Figure 4.11. In this case the dynamic performance is improved using NFOSMC. The other problem with fractional order sliding mode controllers is their computational complexity.

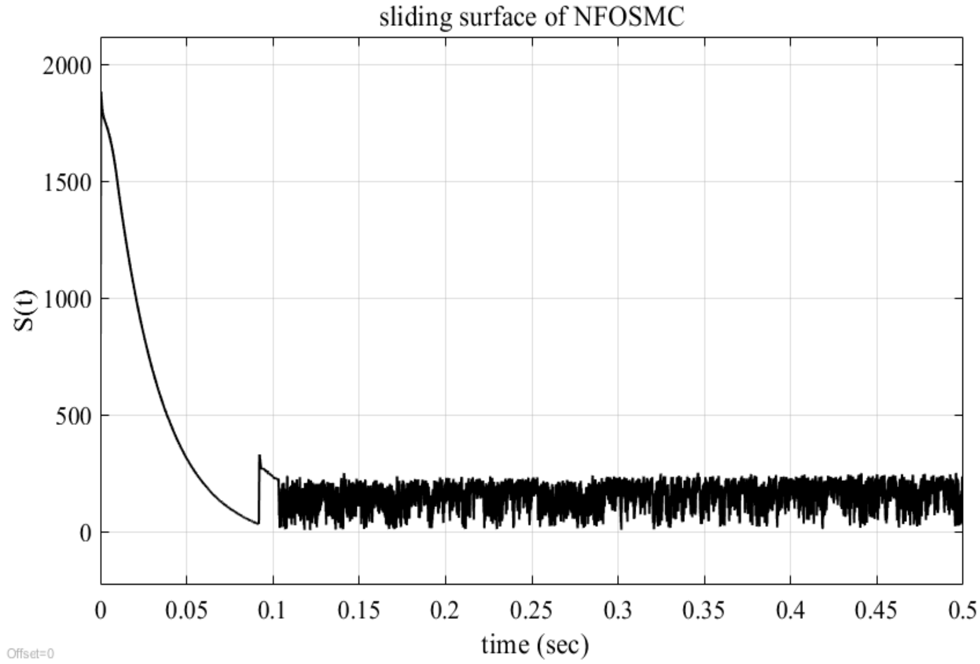

Figure 4.10. The sliding surface of NFOSMC.

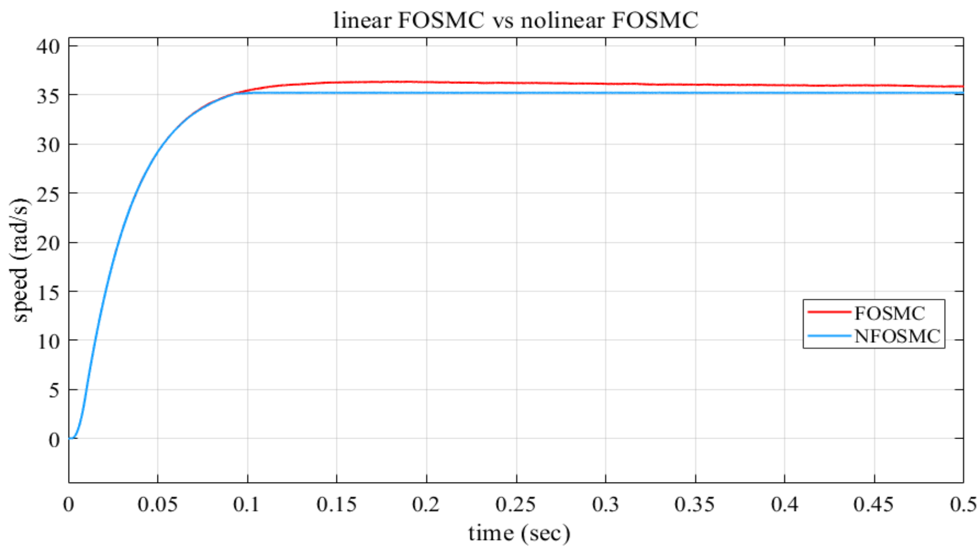

Figure 4.11. Speed result of FOSMC and NFOSMC.

4.1.5. Design of the Proposed High Order Sliding Mode Controller

The proposed speed controller which is high order sliding mode controller with ESO retains not only the conventional first order sliding mode controls' simplicity with robust characteristics, but also suppresses the chattering by transmitting the discontinuous items into high order sliding mode derivatives. The general high order sliding mode control technique which is based on the high order differentiation of the sliding mode variable is designed as follows [44]. Consider the nonlinear system:

$$\dot{x} = f(x) + g(x)u \qquad (4.61)$$
$$y = s(x,t)$$

Where, $x \in R^n$ is a system state variable, t is time, y is output, u is the control input. And $f(x)$, $g(x)$ and $s(x,t)$ are smooth functions. The control objective, in this case, is to make the output function $s = 0$. Differentiate the output function continuously until the control input appears, then we can get every order derivative of s. According to the conception of system relative degree, there are two conditions.

i. Relative degree $r = 1$, if and only if $\partial\dot{s}/\partial u \neq 0$
ii. Relative degree $r \geq 2$, if $\partial s^{(i)}/\partial u = 0$ $(i=1,2,...r-1)$, and $\partial s^{(r)}/\partial u \neq 0$.

In arbitrary order sliding mode control, its core idea is that the discrete function acts on higher-order sliding mode surface making [45]:

$$s(x,t) = \dot{s}(x,t) = \ddot{s}(x,t) = ... = s^{(r-1)}(x,t) = 0 \qquad (4.62)$$

We call the relative degree of the system is r, generally speaking when the control input first occurs in r - order derivative of s, that is $\partial s^{(r)}/\partial u \neq 0$. Then we take the r - order derivative of s for the output system and we can obtain $s, \dot{s}, \ddot{s}, ...s^{(r-1)}$ which are continuous functions for all x and t. However, corresponding discrete control law u acts on $s^{(r)}$. Selecting a new local coordinate, then:

$$y = (y_1, y_2, ...y_r) = (s, \dot{s}, ...s^{(r-1)}) \qquad (4.63)$$

So, we can obtain the following expression [43].

$$s(r) = a(y,t) + b(y,t)u, \quad \text{b(y,t)} \neq 0 \qquad (4.64)$$

From the above equation, the equivalent control can be given as $u = -a(y,t)/b(y,t)$. Where $a(y,t)$ $b(y,t)$ are bounded functions. Let, km, KM and C are positive constants then,

$$0 < km \leq b(y,t) \leq KM \qquad (4.65)$$
$$|a(y,t)| \leq C$$

The control objective in this control technique is to make the variable x follow the reference signal $f(t)$, that is

$$x = f(t) \qquad (4.66)$$

So that, the sliding surface can be designed as

$$s = x - f(t) \tag{4.67}$$

Then derivate the sliding surface s until the control input appears.

Application of HOSM for PMSM drive: The Sliding Mode Control types which are, conventional SMC, SMC based on exponential reaching law, and fractional order SMC are implemented in the above section in order to suppress the chattering effect in the speed control of PMSM. However, those controllers didn't remove the chattering completely. So that, a new technology of SMC which is HOSM is introduced in the following section which effectively eliminates the chattering phenomenon in the speed control of PMSM.

This control method is a robust approach to solve the control problems of nonlinear systems. Robustness properties against several types of disturbance like parameter perturbations and external disturbances can be assured. The main objective in this control technique is to obtain finite convergence with a sliding manifold $s = \dot{s} = \ddot{s} = ... = s^{(r-1)} = 0$ by acting discontinuously on r order derivative of the sliding surface [45].

The rotor angular speed ω_r has to track the reference speed trajectory ω^*. In order to accomplish this control objective, the sliding surface can be designed as follows:

$$s = \omega - \omega^* \tag{4.68}$$

As described above the control objective of every sliding mode controller is to bring the sliding surface s to zero in a limited period of time.

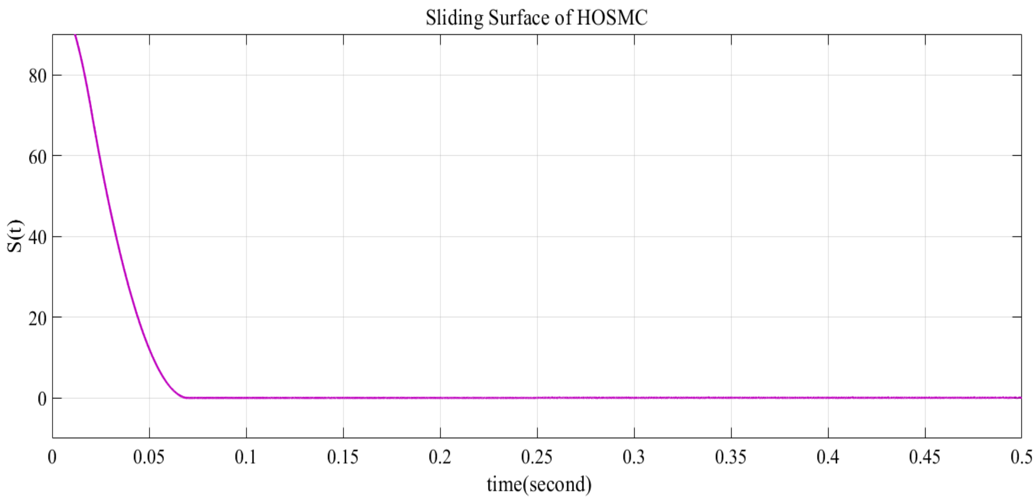

Figure 4.12. The sliding surface of the HOSM controller with reference speed of 100rad/s.

Figure 4.12 shows the sliding surface of HOSM controller with a system simulated for 0.5sec and a command speed of 100 rad/s. As can be seen from the figure, the control objective is accomplished with smaller steady-state error and fast convergence compared to the previously discussed controllers.

Now derivate the sliding surface s as follows:

$$\begin{aligned}\dot{s} &= -\dot{\omega}_r \\ &= -(\frac{3P}{4J}\lambda_m i_q - \frac{B}{J}\omega_r - \frac{T_L}{J})\end{aligned} \tag{4.69}$$

Then the control input second-order sliding mode controller based on the super twisting algorithm is given as follows.

$$i_{qref} = i_{qeq} + i_{qn} \tag{4.70}$$

Where i_{qeq} is the equivalent current component and i_{qn} is the switching component of the control variable or simply we can call it the control law of second-order SMC.

The equivalent current component can be derived from the derivative of the sliding surface as follows:

From the equation, $\dot{s} = -(\frac{3P}{4J}\lambda_m i_q - \frac{B}{J}\omega_r - \frac{T_L}{J})$, the system converges with a finite time and the sliding surface tends to zero.

So that,

$$-(\frac{3P}{4J}\lambda_m i_q - \frac{B}{J}\omega_r - \frac{T_L}{J}) = 0 \tag{4.71}$$

Then derivate Equation (4.71) to get the second-order relative degree of the system as follows:

$$\dot{i}_q = \frac{4J}{3P\lambda_m}(\frac{B}{J}\dot{\omega}_r) \tag{4.72}$$

Which is equal to:

$$i_q = \int \frac{4J}{3P\lambda_m}(\frac{B}{J}\dot{\omega}_r)dt \quad (4.73)$$

The other component i_{qn} or second-order control law is given according to the super twisting algorithm as follows [46], [47], [41].

$$i_{qn} = c_1 |s|^{1/2} sgn(s) + c_2 \int sgn(s)dt \quad (4.74)$$

where $c_1, c_2 > 0$.

Finally, the control input designed using second-order sliding mode controller based on STA is given by,

$$i_{qref} = i_{qeq} + i_{qn} = \int \frac{4J}{3P\lambda_m}(\frac{B}{J}\dot{\omega}_r) + c_1 |s|^{1/2} sgn(s) + c_2 \int sgn(s)dt \quad (4.75)$$

4.2. GA-PI Current Controller

In the closed-loop control of the PMSM drive, the current also needs to track the desired trajectory. There are different available controllers in order to reduce the steady-state error of the d-q current. PI controller is the most frequently used current controller but it is sensitive to the step change of the speed setpoint, parameter variations, and other disturbances. The derivative term (D) in PID controller is better to be ignored, if there is large disturbance in the system. In the case of EVs there is much disturbance due to the frequent load change and the road condition. So, PI controller is used as a current controller in this study because of the above-mentioned reason as well as its simplicity. However, the problem here is that it is difficult to set the appropriate values of the parameters of this controller manually, since it takes much time to select the parameter values. So, to come up with this problem the parameters are tuned using genetic algorithm. In order to get the best performance of the PI current controller, genetic algorithm optimization technique is used in this study. In GA-PI current controller the parameters (K_p, K_i) are tuned using a genetic algorithm.

GA is basically inspired by biological evolutionary algorithms such as inheritance, mutation, etc. it follows the basic principle of evolution which starts from randomly generated individuals and happens in generations. In every generation, the fitness of each individual is evaluated and modified to form a better population. This iteration continues until the maximum generation is reached or the best fit value is achieved.

The objective of every controller is to reduce the error between the actual output and the reference output. In the same manner, the actual outputs of the currents are compared with the reference currents, and the error is given to the GA-PI controller. Finally, the controller tries to minimize the error between the actual output and the setpoint. The GA tuning response of the GA-PI current controller for the quadrature current is shown in Figure 4.13.

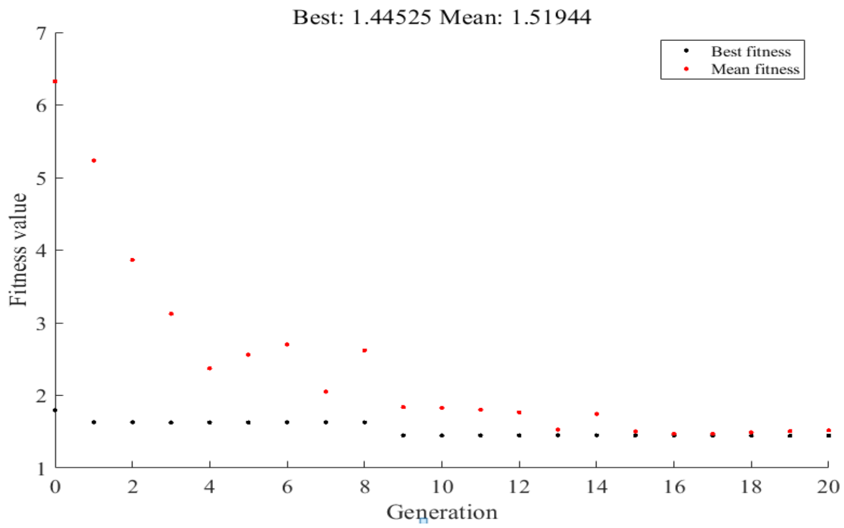

Figure 4.13. GA Tuning response of the quadrature current controller.

Figure 4.14 shows the convergence of the tuning process of the parameters of the PI controller using genetic algorithm.

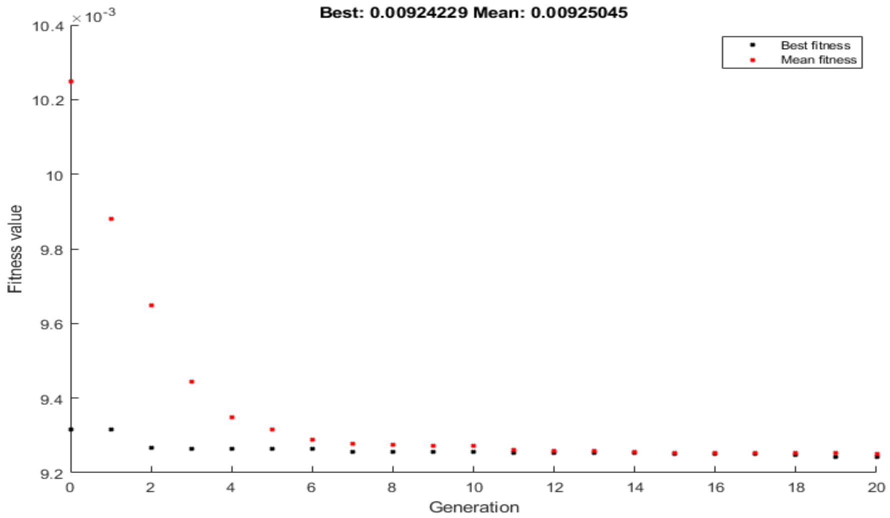

Figure 4. 14. The GA tuning response for the direct current

The objective of GA in the PI current controller is to obtain the values of the controller gains (K_p, K_i) that will best fit with the whole PMSM drive control system. GA is implemented for both d and q current control and the optimized parameter values are obtained as shown in the Table 4.1 below with IAE value 1.4453.

Table 4.1. The GA-PI parameter values

Current controllers	Optimized parameters	Optimized parameter values
PI controller for (i_q)	K_{pq}	482.1467
	K_{iq}	475.1667
PI controller for (i_d)	K_{pd}	489.9670
	K_{pi}	455.7443

In FOC, the reference of the d-axis current is set to zero. However, the q-axis current is generated using the proposed speed controller as shown in the following section.

4.2.1. Reference Current Generation

In the field-oriented control technique, the currents to be controlled are transformed into two-phase d-q currents. The direct current is used only for excitation so we can assume it as zero. So, in this study, the reference current for direct current i_d is set to zero. While the quadrature current i_q is the torque-producing component. The reference signal for this current component is generated by the speed controller. The output signal of the speed controller is taken as the reference input for the PI quadrature current controller.

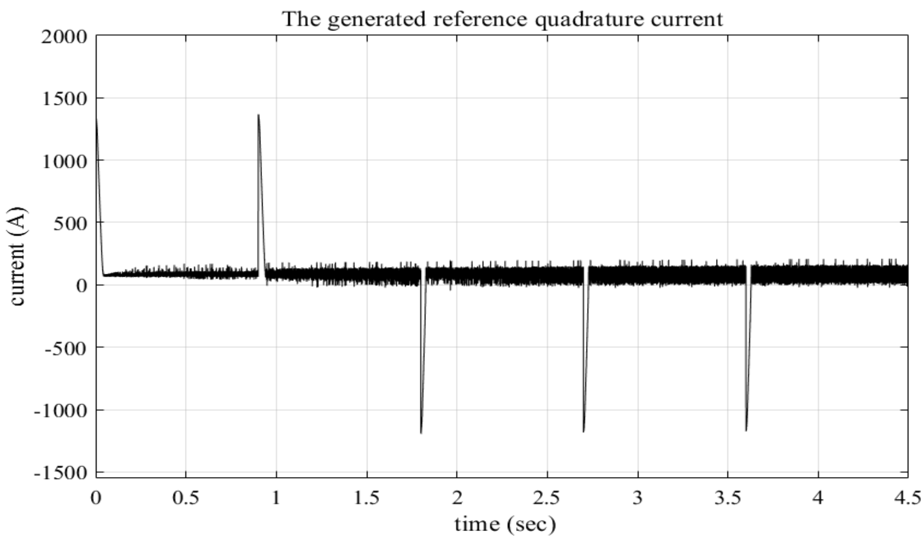

Figure 4.15. The generated quadrature reference current.

In this study, the HOSM controller is used for controlling the speed of the motor so its output is used as a reference signal for the GA-PI current controller. The generated reference signal under a load torque of 20Nm is shown in Figure 4.14.

4.3. Design of Extended State Observer

In the FOC technique, the speed of the motor is used as a feedback signal to be compared with the reference input. Then the error between them is minimized using a speed controller. So, in order to use the speed signal as feedback, it has to be measured first. Sensors can be used for this purpose but it has many disadvantages to the system. To come up with this problem an observer is used for estimation of the rotor speed of the motor and take the place of the sensor. There are different observers available but an Extended state observer (ESO) is used in order to estimate the rotor speed of the motor because of its simplicity. After the rotor speed is estimated, it is applied to the controller. The traditional linear ESO can be designed as follows [37]:

$$\begin{cases} \bar{e} = Z_{21} - \omega_r \\ \dot{Z}_{21} = Z_{22} - \tilde{\beta}_{01}\bar{e}(t) + \tilde{b}_0 i_q \\ \dot{Z}_{22} = -\tilde{\beta}_{02}\bar{e}(t) \end{cases} \quad (4.76).$$

where Z_{21} is the estimated speed of the motor, $\bar{e}$ is the error between the actual rotor speed and the estimated speed, β_{01} and β_{02} are positive parameters and Z_{22} is lumped estimate of load torque and disturbance.

In order to improve the dynamic performance of the observer a nonlinear extended state observer is developed based on a novel nonlinear function. This function is better since it is more continuous and derivable compared to previously available functions and it is effective in reducing the high-frequency flutter phenomenon [41], [48]. Using this technique, the speed of the motor in the control of PMSM drive is extended to a new state. The improved ESO is designed using the nonlinear function $f_{new}(.)$(defined in the previous section in FOSMC) as shown in Equation (4.76).

$$\begin{cases} \bar{e} = Z_{21} - \omega_r, \\ \dot{Z}_{21} = Z_{22} - \beta_{01} f_{new}(\bar{e},\delta,\alpha) + b_0 i_q, \\ \dot{Z}_{22} = -\beta_{02} f_{new}(\bar{e},\delta,\alpha). \end{cases} \quad (4.77)$$

where β_{01} and β_{02} are the positive gain parameters of the nonlinear ESO, b_0 is the compensation factor, and ω_r is the mechanical angular speed of the rotor. After the observer is well designed Z_{21} is the estimated value of the rotor angular speed.

CHAPTER 5

SIMULATION RESULTS AND DISCUSSION

In this chapter the proposed drive control system results of permanent magnet synchronous motor for three-wheeler electric Bajaj are discussed and analyzed. Vehicles operate with a variable speed as well as variable torque and it is affected by different disturbance factors like road condition. In this section, the effect of variable speed, torque variation, and external disturbance are discussed.

The simulation results are compared with different controllers (related works) and the same motor parameters were used throughout this research work. The non-linear model of the PMSM drive is designed and analyzed in MATLAB/Simulink. HOSM controller is implemented for the rotor speed control of the motor. As mentioned in the previous chapters the GA-PI current controller is also used to control the motor d-q current by cascading with the speed controller and its results are discussed in this chapter.

5.1. Results of the Proposed HOSM Controller

In this portion, the simulation results of the proposed chattering-free higher-order sliding mode speed controller are discussed. For this work, the variable setpoint and load torque were considered to study and analyze the effects of different speed and current controllers.

5.1.1. The Proposed HOSM Speed Controller Result

The following Figure 5.1 shows the result of the proposed chattering free sliding mode controller with a variable speed input as a reference. A second-order sliding mode controller based on STA with an extended state observer is used to control the rotor speed of the PMSM drive. Its result shows that the motor’s rotor speed follows the given reference input.

The speed response shows that the result has good dynamic performances with small overshoot (0.4874), no steady-state error (0%), small rise time (0.0222), and fast convergence with a settling time of (0.0356sec).

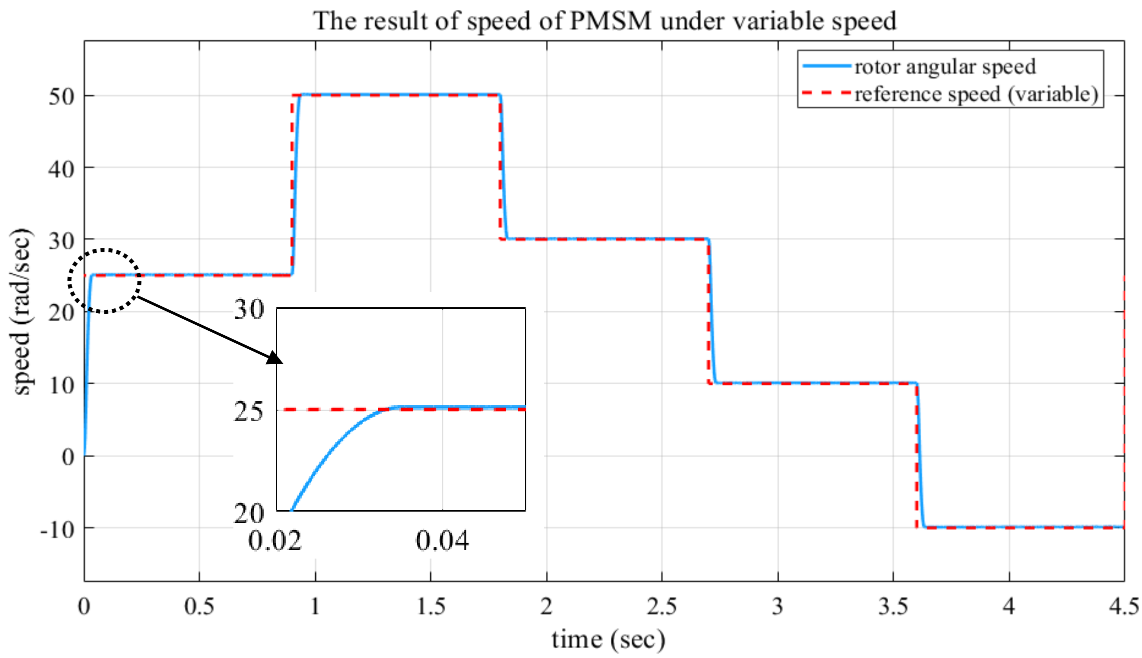

Figure 5.1. The result of the proposed speed controller at variable speed and no-load conditions.

5.1.2. The Three-phase Stator Current Result

Since the PMSM motor has a sinusoidal flux distribution and its three-phase stator current result waveform is given in Figure 5.2. The three-phase stator currents have a 120^{o} phase shift with each other and they are generated from the three-phase inverter. The stator current created in the motor is used to create the magnetic field that makes the rotor of the motor in the direction of field.

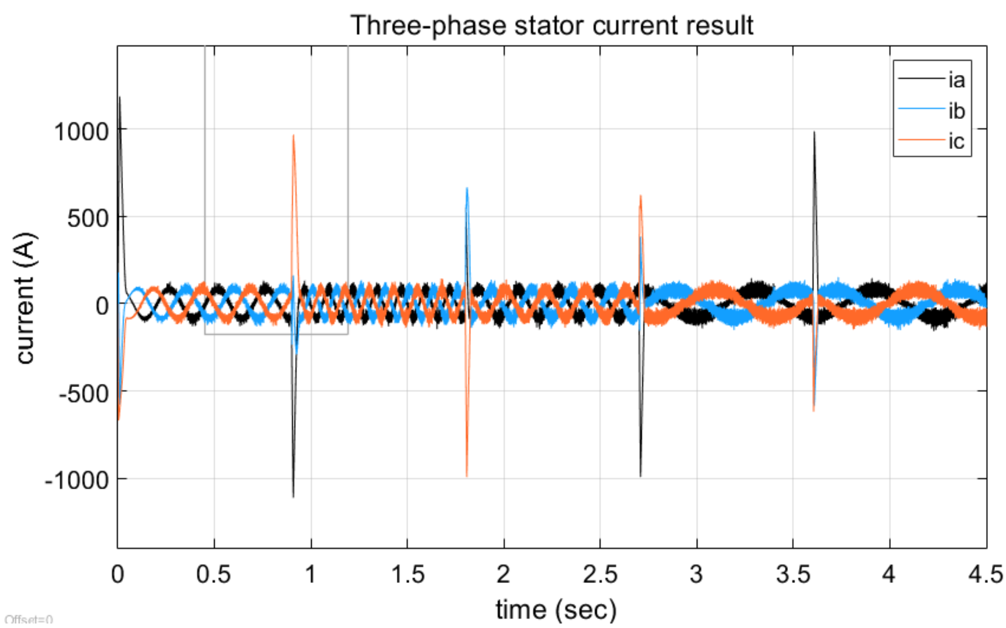

Figure 5.2. The three-phase stator current results under variable speed.

In this work, the SVPWM is implemented to generate the triggering signals for commutating the three-phase inverter in order to get an appropriate current and voltage generation. The frequency of the currents is dependent on the speed of the motor. From 0.9sec to 0.18sec the speed command is 50rad/s which is the highest from the given speed commands, due to this, the frequency of oscillation is higher as shown in the figure below. Figure 5.2 depicts the three-phase stator current results under variable speed.

5.1.3. The d-axis Current Result using GA-PI Controller

The following Figure 5.3. shows the d-axis current result of the motor with a reference (command) current set to zero. GA-PI current controller is implemented and the result shows that the actual direct current of the motor follows the path of the reference current and has a settling time of 0.01sec.

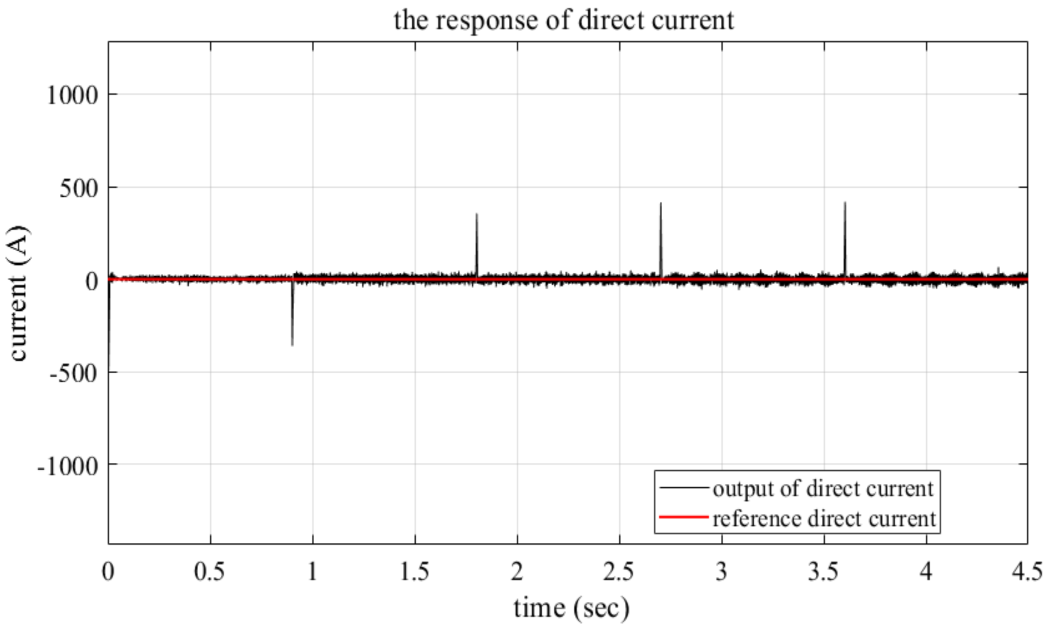

Figure 5.3. The direct current result under variable speed.

5.1.3. The q-axis Current Result using GA-PI Controller

The reference current of the GA-PI current controller is generated using the proposed HOSM controller. The actual quadrature current output signal follows the reference current signal generated by the speed controller. The result is given in Figure 5.4.

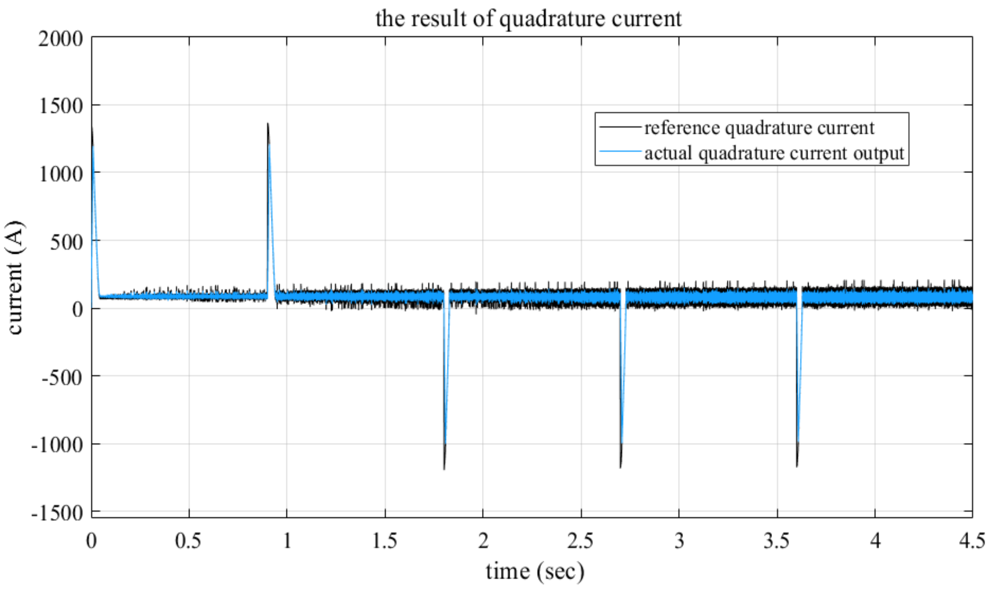

Figure 5.4. The result of the quadrature current under a load of 20Nm.

5.1.4. The Electromagnetic Torque Result of PMSM Drive

The electromagnetic torque is directly proportional to the quadrature current (i_q), and dependent on the load torque.

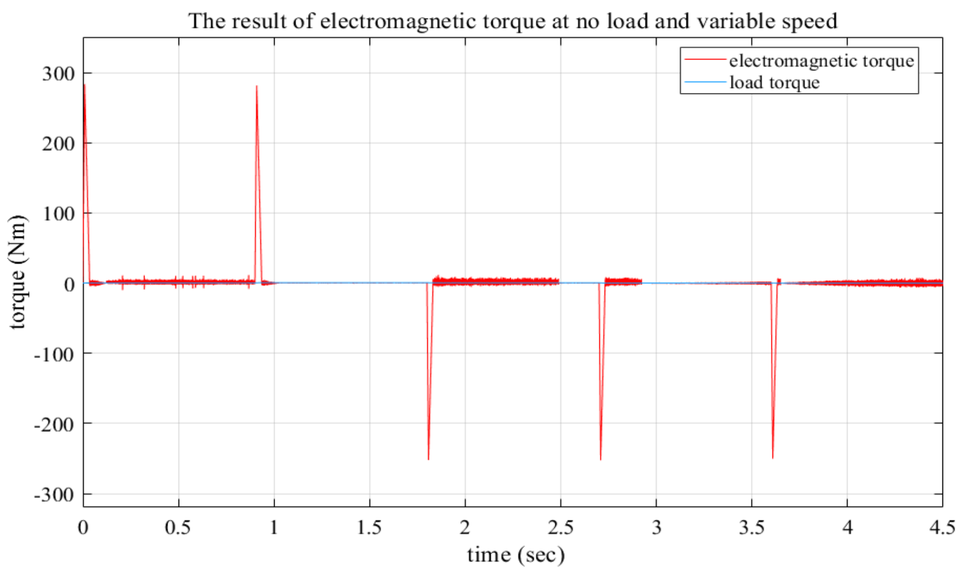

Figure 5.5. Result of Electromagnetic torque for PMSM drive under no-load condition and variable speed

Figures (5.5. and 5.6.) show the response of the electromagnetic torque under variable speed and with no-load as well as load conditions. As shown in the following graphical results, when a variable reference speed is applied, there is an increase in the torque value for a short period of time. Since electromagnetic torque is a constant multiple of the quadrature current, their result follows the same path.

The result of the electromagnetic torque with a load of 20Nm is given in Figure 5.6 below.

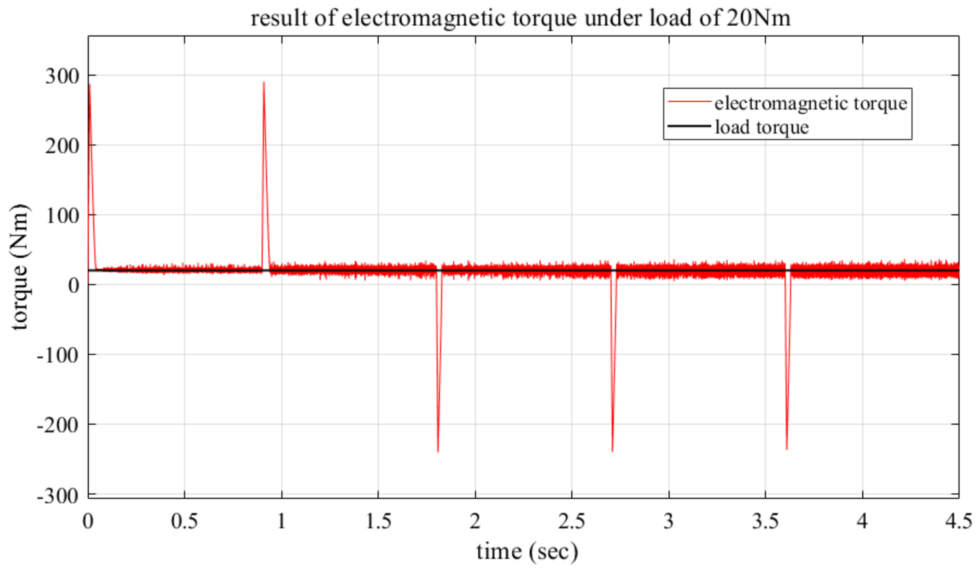

Figure 5.6. Electromagnetic torque result with a load torque of 20Nm.

5.1.5. The Three-Phase Inverter Output Voltage

The three-phase voltage of the PMSM drive is generated through the three-phase inverter and the result is shown in Figure 5.7.

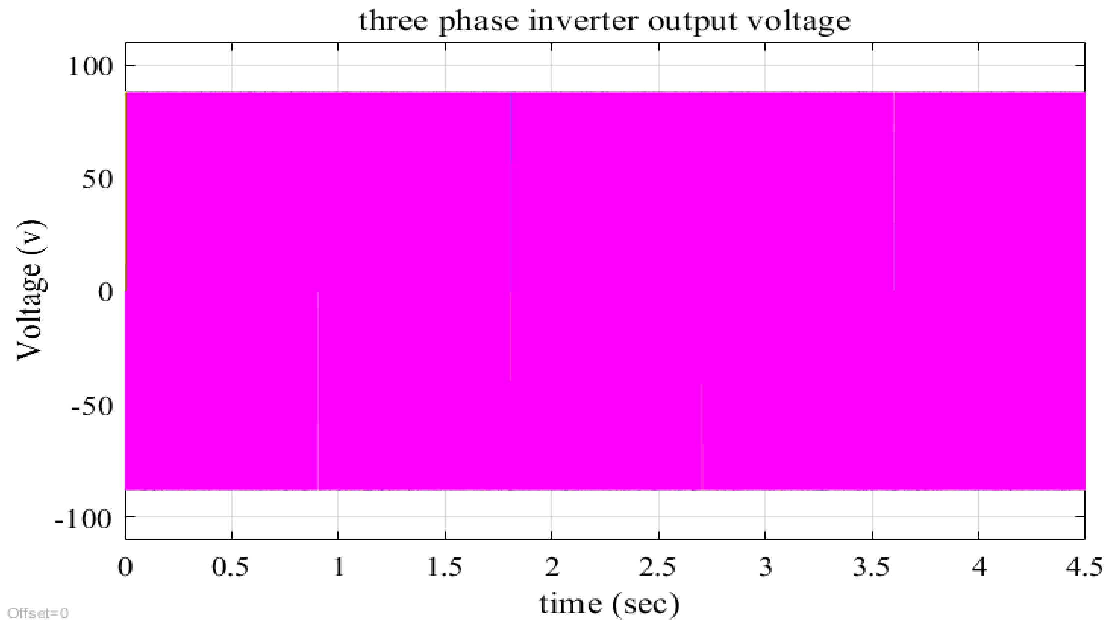

Figure 5.7. Three-phase inverter output voltage.

The signal has a rectangular waveform in which it is controlled based on an SVPWM switching technique. The maximum achievable voltage using SVPWM is half of the DC-link voltage. The DC link voltage used in this simulation is 144v. So, the maximum value of the inverter output voltage is 72v. The zoomed view of Figure 5.7 is shown in Figure 5.8.

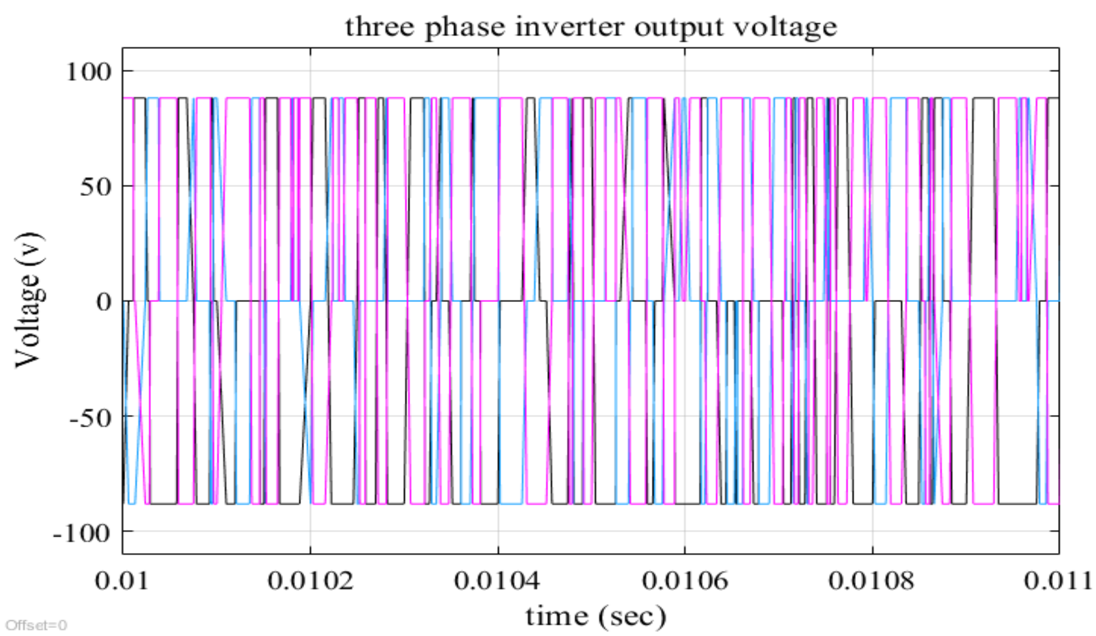

Figure 5.8. Zoomed view of three-phase inverter voltage.

5.1.6. The Result of Speed Observer under Variable Speed and No-load Condition

In the speed control of the PMSM drive, the rotor speed is used as feedback to the controller. For this purpose, sensors have been used to measure the speed of the motor.

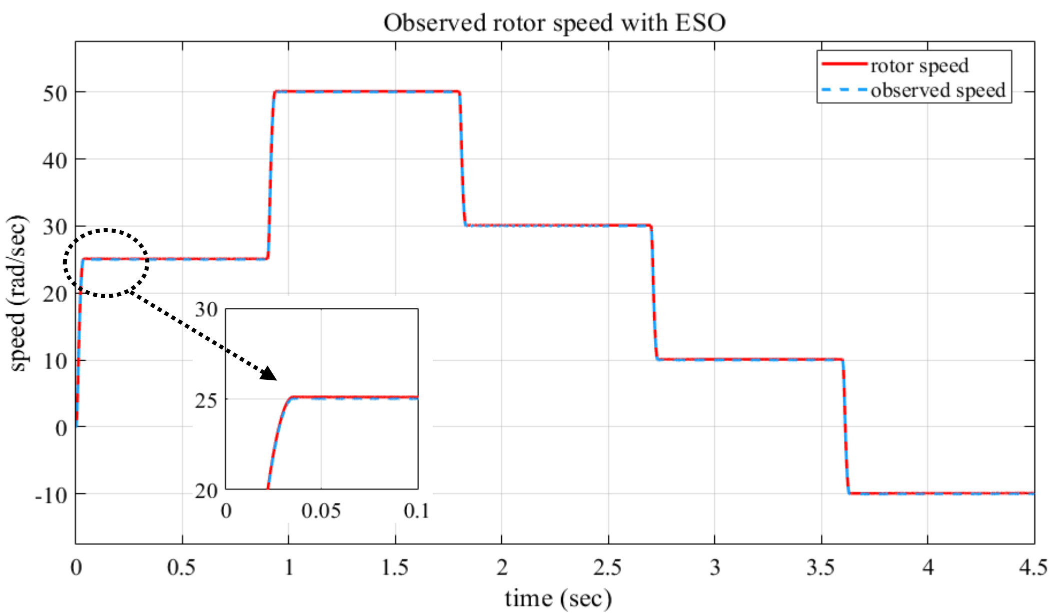

Figure 5. 9. comparison of the actual rotor speed with the observed speed of the motor.

But using sensors have its own disadvantage like, reduced reliability, extra additional cost, and adding complexity to the hardware environment of the three-wheeler Bajaj. For this problem, speed control of sensorless PMSM drive is implemented using extended state observer to replace the usage of speed sensor. Figure 5.9 shows that, the output of the extended state observer follows the path of the actual rotor speed with equal settling time (0.0356sec) and percentage overshoot (0.0049%).

5.1.7. Sliding Surface of The Proposed HOSM Controller Variable Speed

The control objective in sliding mode controllers is to bring the sliding surface to zero in a finite time. Figure 5.10 shows that the control objective is accomplished since the sliding surface of the proposed HOSM controller reaches the origin in a short period of time (0.0356sec) regardless of the speed variation.

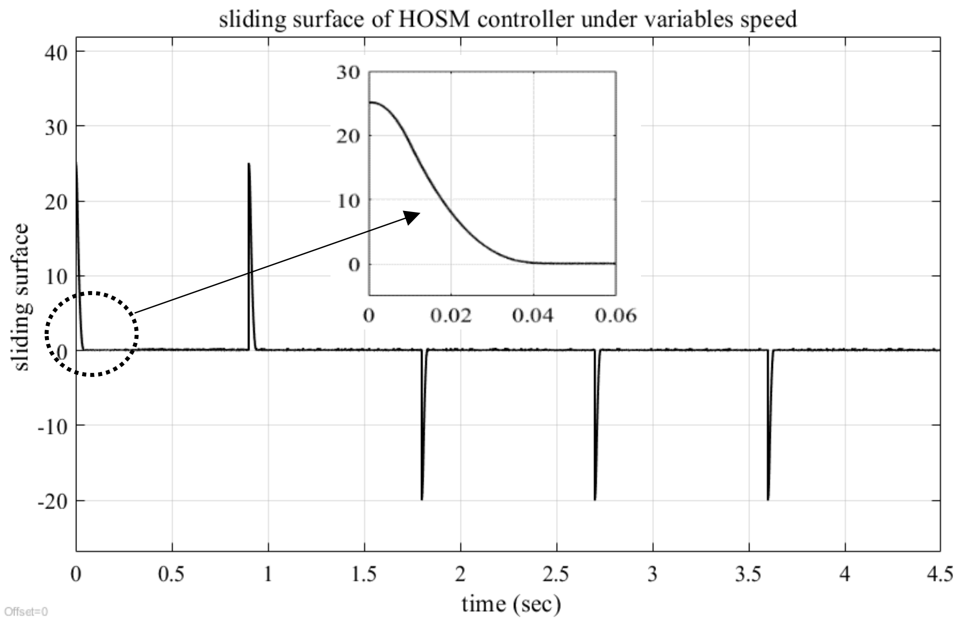

Figure 5.10. The sliding surface of the proposed HOSM controller under variable speed.

5.2 Result of The Motor at Rated Speed Command

The following Figure 5.11 is the rotor speed result of PMSM drive at a rated speed of the motor (157rad/s which is equal to 1500rpm) and it implies that the rotor speed tracks the command speed and converges with setpoint with in 0.1sec.

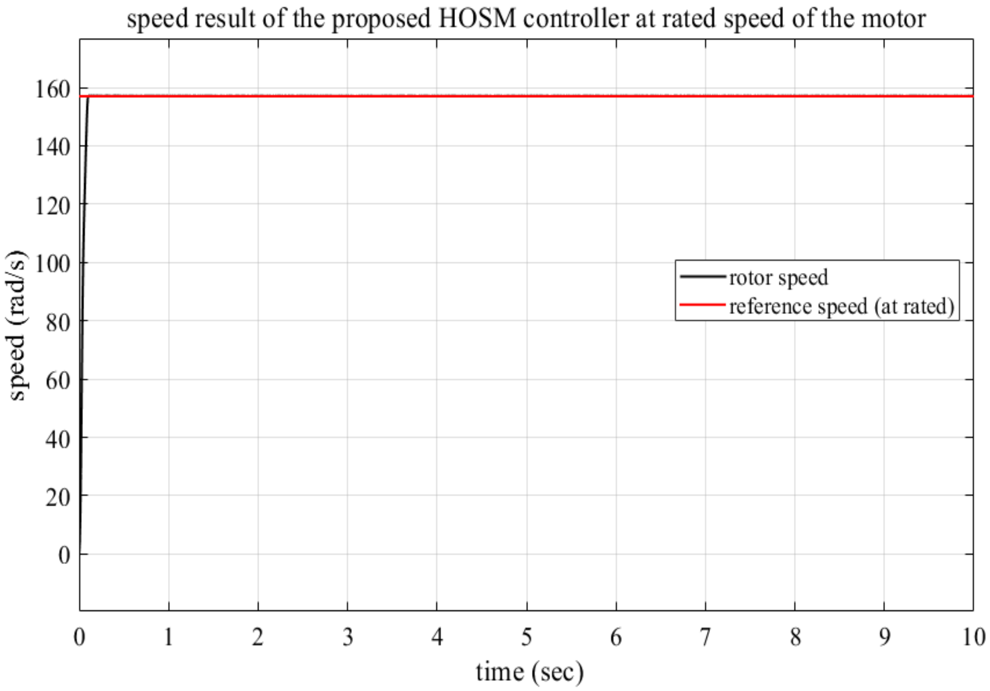

Figure 5.11. Speed response of the motor at rated speed.

5.2.1. speed response of HOSM controller with variable load

The carrying capacity of three-wheeler Bajaj is 4 persons including the driver. The load applied to the vehicle is not constant so the performance of the controller is checked by applying variable torque shown in Figure 5.12 to the system.

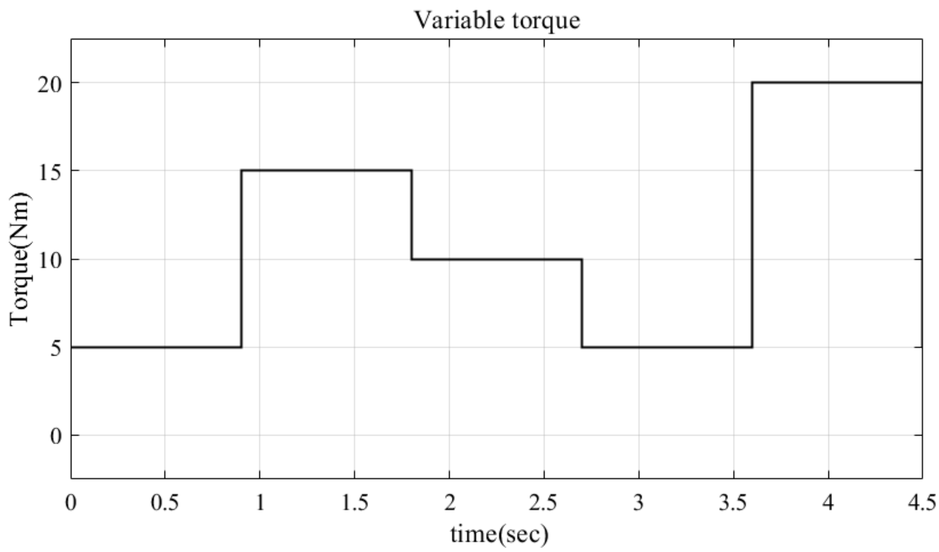

Figure 5.12. A variable load torque added to the system

Since the driver is always on the vehicle the initial load is assumed to be 5Nm from 0 to 0.9sec, then 2 more people are added and the load is 15Nm from 0.9 to 1.8sec. the load torque is varied with a step change of 0.9 seconds. The final load implies that 4 people are loaded on the Bajaj. Based on this the robustness of the controller towards variable load is tested.

The response of the High-order Sliding Mode Controller to the variable load is shown in Figure 5.13 below. By considering the carrying capacity of the Bajaj (four person), four different load torque values are applied to the system. The result implies that, the performance of the controller is not affected with the addition of the variable load to the system. This implies that, the controller is robust towards load variation.

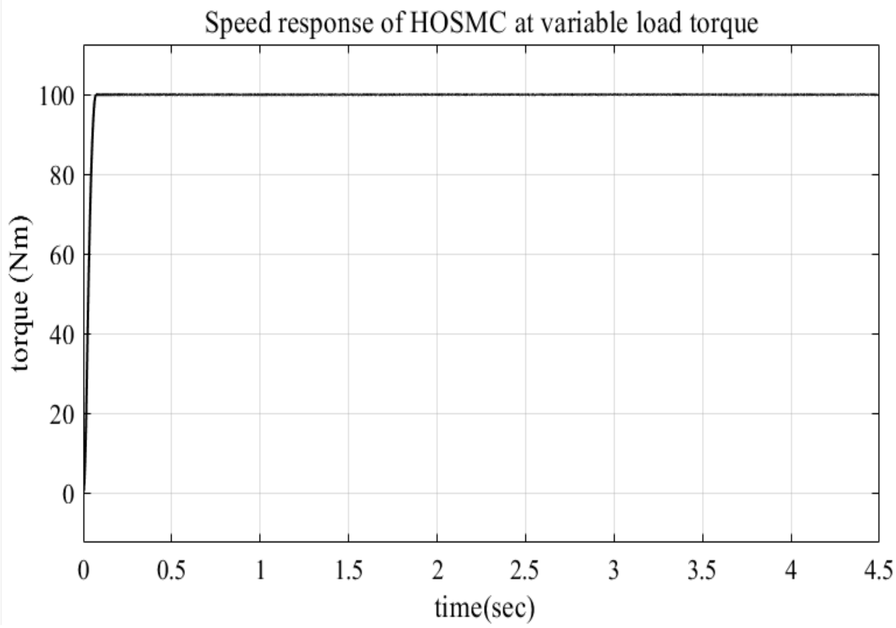

Figure 5.13. The result of HOSMC when variable load torque is applied to the system

5.3. Comparison of Dynamic Performance of Different Controllers

The dynamic performance of different controllers is compared at a constant speed of 100rad/sec, and no-load condition for 5secocnds. The speed response the controllers is shown in Figure 5.14 (for HOSMC, FOSMC, SMC-ERL, and PI controllers) and Figure 5.15 (for SMC controller).

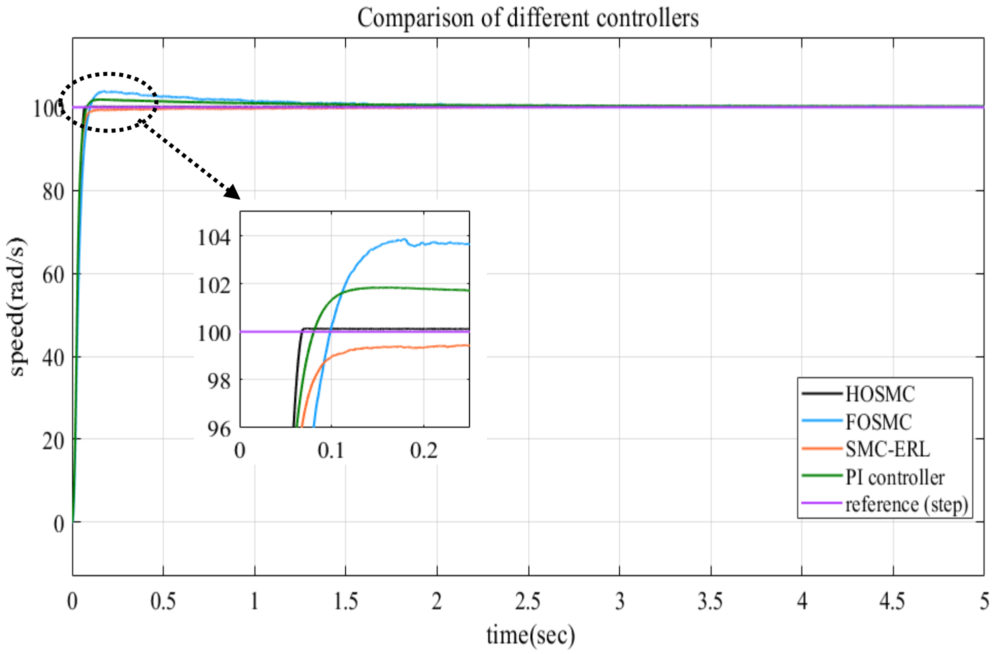

Figure 5.14. The speed result of different controllers

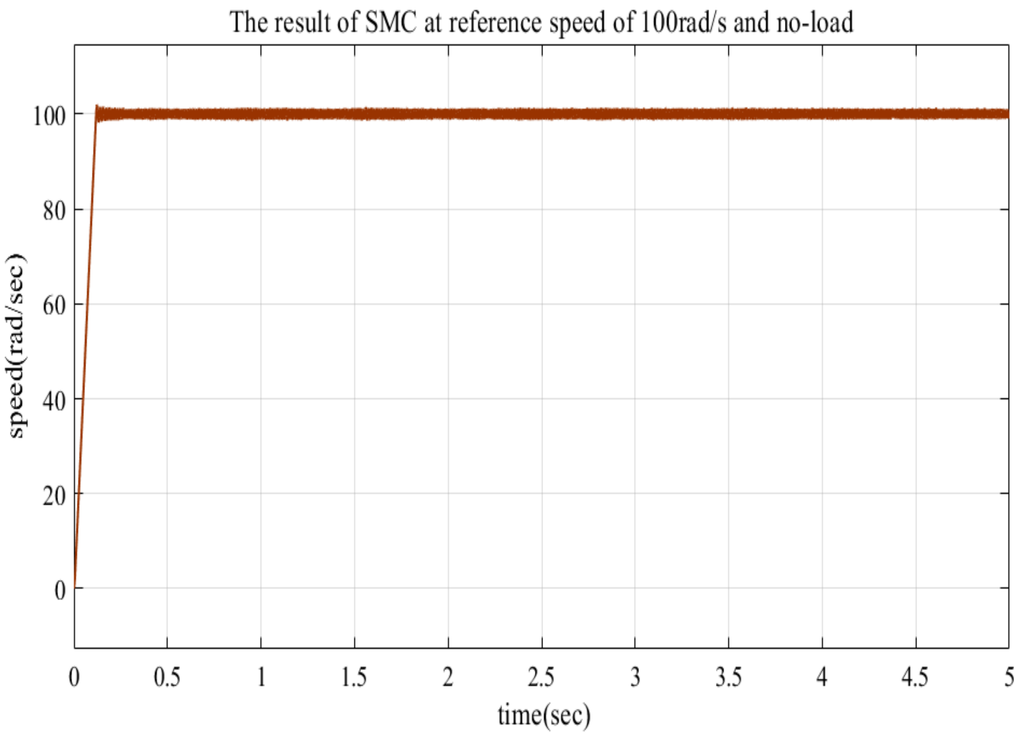

Figure 5.15. The speed response of SMC.

In order to get the dynamic performance of the controllers the step info of all the controllers is taken from the command window and the result is shown in the following Table 5.1. The performance of the controllers is described in graphical as well as tabular form as shown below.

Table 5.1. Dynamic performance comparison of different controllers at constant speed(100rad/s)

HOSMC

```
Command Window
>> stepinfo(out.S1,out.t,100)

ans =

  struct with fields:

         RiseTime: 0.0401
     SettlingTime: 0.0619
      SettlingMin: 90.0100
      SettlingMax: 100.1507
        Overshoot: 0.1507
       Undershoot: 0
             Peak: 100.1507
         PeakTime: 3.0172

fx >>
```

FOSMC

```
Command Window
>> stepinfo(out.S2,out.t,100)

ans =

  struct with fields:

         RiseTime: 0.0520
     SettlingTime: 0.6964
      SettlingMin: 90.0227
      SettlingMax: 103.8707
        Overshoot: 3.8707
       Undershoot: 0
             Peak: 103.8707
         PeakTime: 0.1783

fx >>
```

SMC-ERL

```
Command Window
>> stepinfo(out.S3,out.t,100)

ans =

  struct with fields:

         RiseTime: 0.0407
     SettlingTime: 0.0807
      SettlingMin: 90.0369
      SettlingMax: 100.1030
        Overshoot: 0.1030
       Undershoot: 0
             Peak: 100.1030
         PeakTime: 3.9660

fx >>
```

SMC

```
Command Window
>> stepinfo(out.S4,out.t,100)

ans =

  struct with fields:

         RiseTime: 0.0926
     SettlingTime: 0.1163
      SettlingMin: 90.0121
      SettlingMax: 101.9928
        Overshoot: 1.9928
       Undershoot: 0
             Peak: 101.9928
         PeakTime: 0.1230

fx >>
```

PI controller

```
Command Window
>> stepinfo(out.S5,out.t,100)

ans =

  struct with fields:

         RiseTime: 0.0387
     SettlingTime: 0.0687
      SettlingMin: 90.0342
      SettlingMax: 101.8400
        Overshoot: 1.8400
       Undershoot: 0
             Peak: 101.8400
         PeakTime: 0.1648

fx >>
```

The result shows that the HOSM controller has faster convergence with a smaller settling time (t_s = 0.0619sec), smaller overshoot (0.1030rad/s), and small rise time (0.0401sec). The graphical comparison of these controllers is shown in Figure 5.16.

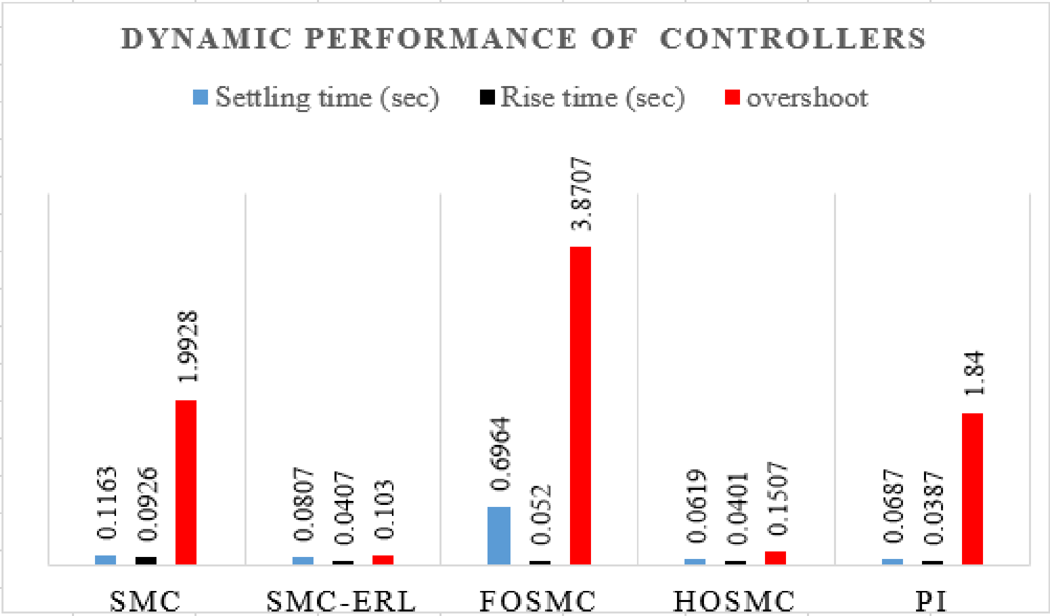

Figure 5.16. Graphical representation of performance of controllers.

The dynamic performance of these controllers is described in tabular form as shown in Table 5.2 below. The result shows that the proposed high order sliding mode controller based on STA has better performance in its settling time (t_s), rise time (t_r), peak time (t_p), peak value (M_p), percentage overshoot ($\%M_p$), and chattering elimination ability.

From those dynamic performances overshoot and settling time are the main ones. Since, the controlled parameter needs to track the desired trajectory (with small overshoot) and converge within a short period of time (small settling time).

Table 5.2. The speed controller's dynamic performance comparison.

Speed controllers	Controller Performance					
	t_s (sec)	t_r (sec)	M_p	t_p (sec)	$\%M_p$	Chattering effect
SMC	0.1163	0.0926	101.9928	0.1230	0.0199	Higher
PI controller	0.0687	0.0387	101.8400	0.1648	0.0184	…
SMC-ERL	0.0807	0.0407	100.1030	0.9660	0.00103	Reduced
FOSMC	0.6964	0.0520	103.8707	0.1783	0.0387	Reduced
HOSMC (proposed)	0.0619	0.0401	100.1507	0.0172	0.0015	Highly suppressed

5.4. The Effect of Chattering on Controllers Under Variable Speed and 20Nm Load Torque

In this section, the chattering phenomenon of different controllers are compared with variable speed given as a reference input at 20Nm load torque.

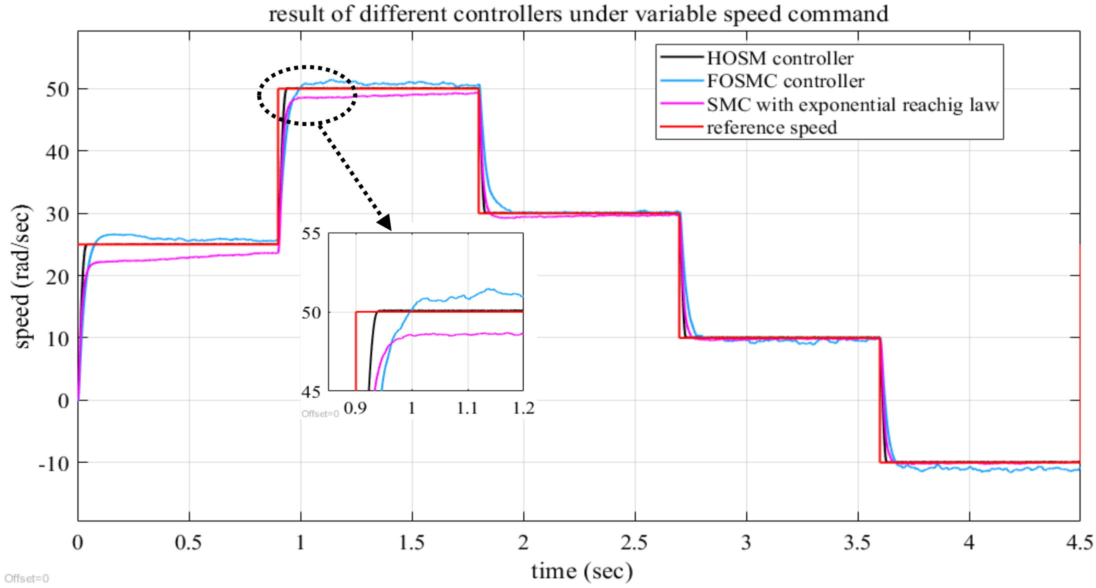

Figure 5.17. The response of different controllers under variable speed and load torque (20Nm).

From the zoomed view of Figure 5.17, chattering is seen at FOSMC and SMC-ERL. However, it is significantly suppressed in the case of the HOSM controller based on super twisting algorithm. HOSM controller tracks the command speed accurately regardless of the given reference value and load torque. In the case of the SMC-ERL, the chattering is reduced compared to SMC, and FOSMC but its robustness is degraded when load torque is applied to the system as discussed in the next section.

Similarly, the speed response of the conventional sliding mode controller is given in Figure 5.18 below. This controller is robust to internal and external disturbance and has good dynamic performance under variable speed and load torque conditions. However, it has too much chattering.

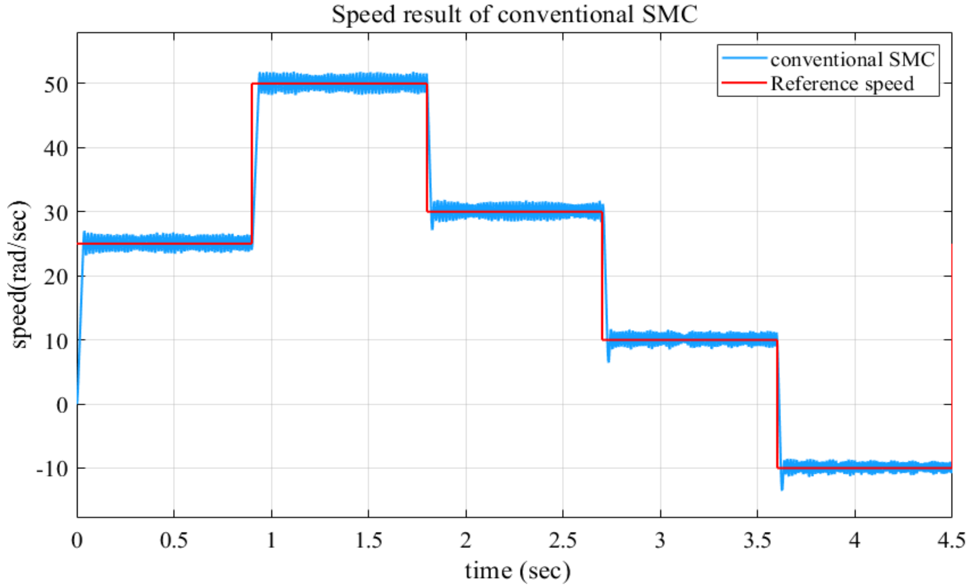

Figure 5.18. Result of conventional SMC under variable speed and load torque (20Nm).

5.5. The Effect of Disturbance on Different Controllers

In this section, the PMSM drive is simulated using different speed controllers using a step reference speed of 100rad/s for 0.5sec. The robustness of these controllers is compared by adding external disturbance to the system.

The controllers implemented in this section include conventional SMC, SMC-ERL, FOSMC, and the proposed chattering free high order sliding mode controller based on super twisting algorithm with ESO. Figure 5.19 shows the response of the controllers without disturbance.

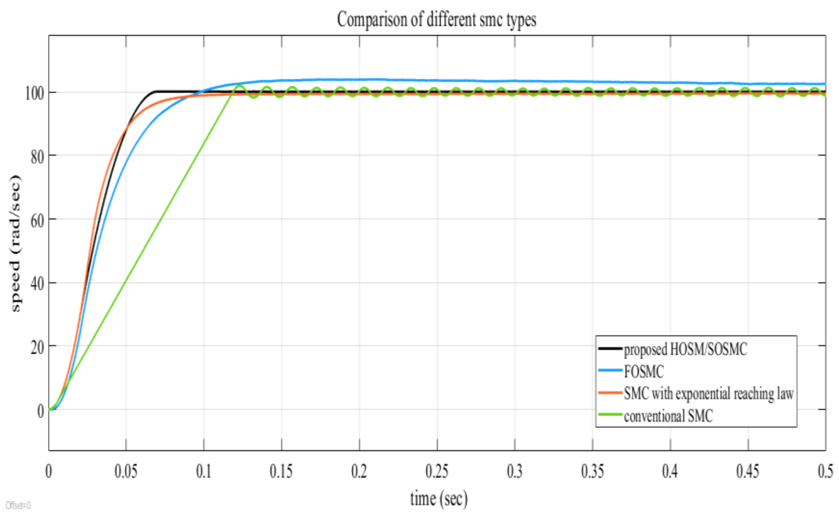

Figure 5.19. Comparison of different SMC controller types at a constant speed and no disturbance.

It is known that disturbance may be either internal or external and maybe both. An internal disturbance may be due to parameter variation in the system because of the operating environment like temperature. An external disturbance may occur due to the variation of the load which depends on the road type and carrying capacity.

Based on this fact the load torque is varied for a short period of time (sudden load change) which will be counted as an external disturbance for the system. the simulation is run for 0.5sec and the load is changed suddenly from 0Nm to 20Nm from 0.35sec to 0.37sec and back to 0Nm at 0.37sec as shown in Figure 5.20.

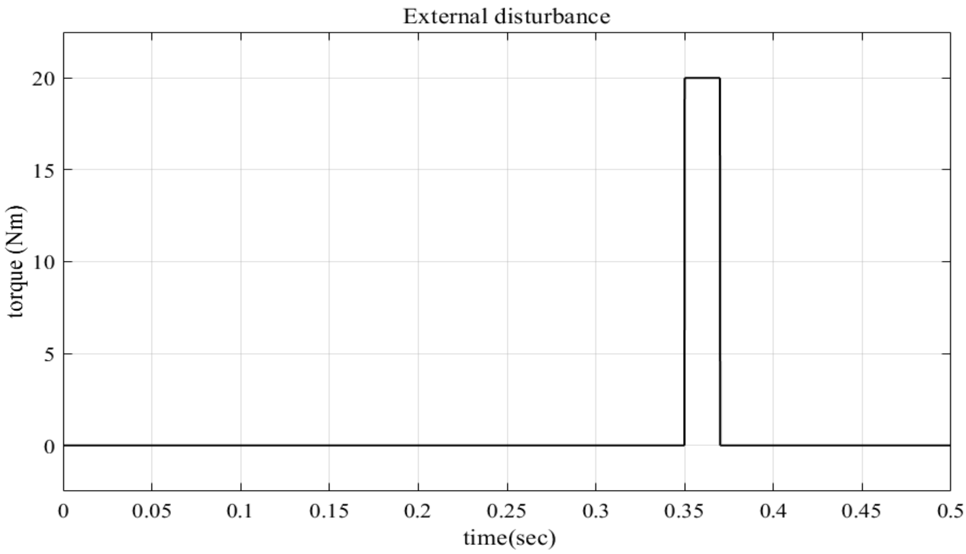

Figure 5.20. Added disturbance to the system

The simulation result shown in Figure 5.21 implies that all the controllers are highly robust since they are not affected by the disturbance. However, there is a little speed fluctuation for SMC with exponential reaching law. In control engineering when we try to improve some dynamic performance of the system, the other will be affected. So, there must be a tradeoff between the two parameters.

In a similar manner, the chattering in conventional SMC is reduced using SMC with ERL but it costs its robustness a little. Even if the SMC controller has high chattering, it shows strong robustness towards external disturbance as shown in the Figure 5.21.

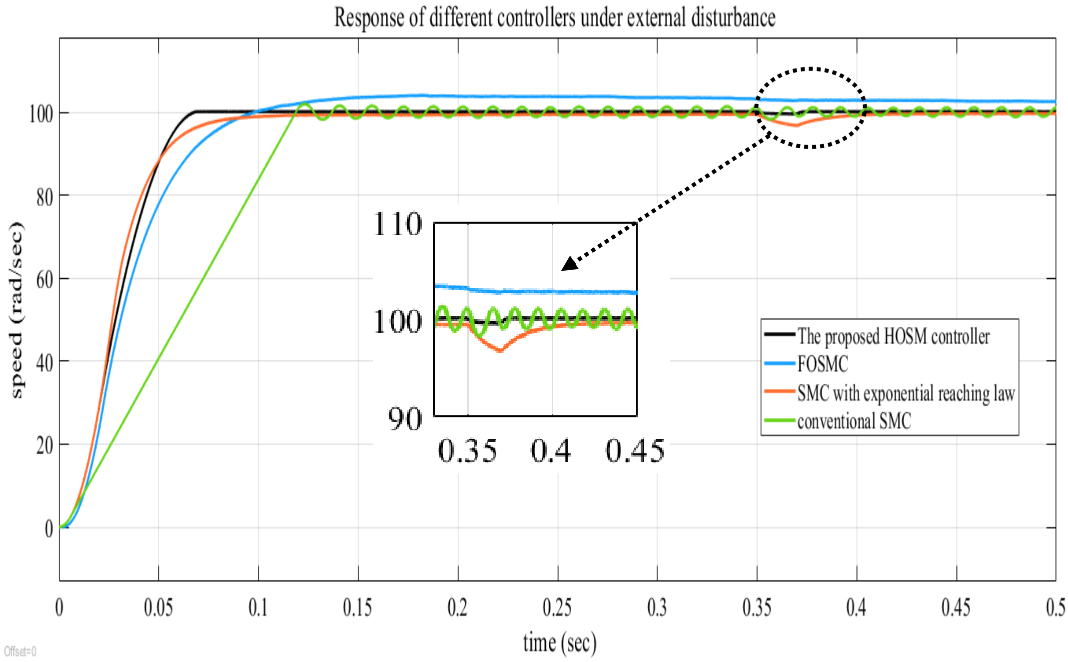

Figure 5.21. Checking robustness of different controllers by adding disturbance to the system.

Then, the proposed HOSM controller is compared with the conventional PI controller. Using the same procedure used in the above section the robustness of these controllers is tested and the simulation result shows that HOSM is more and more robust since the PI controller is highly affected by the sudden load change at the time of $t = 0.36\,sec$ as shown in Figure 5.22.

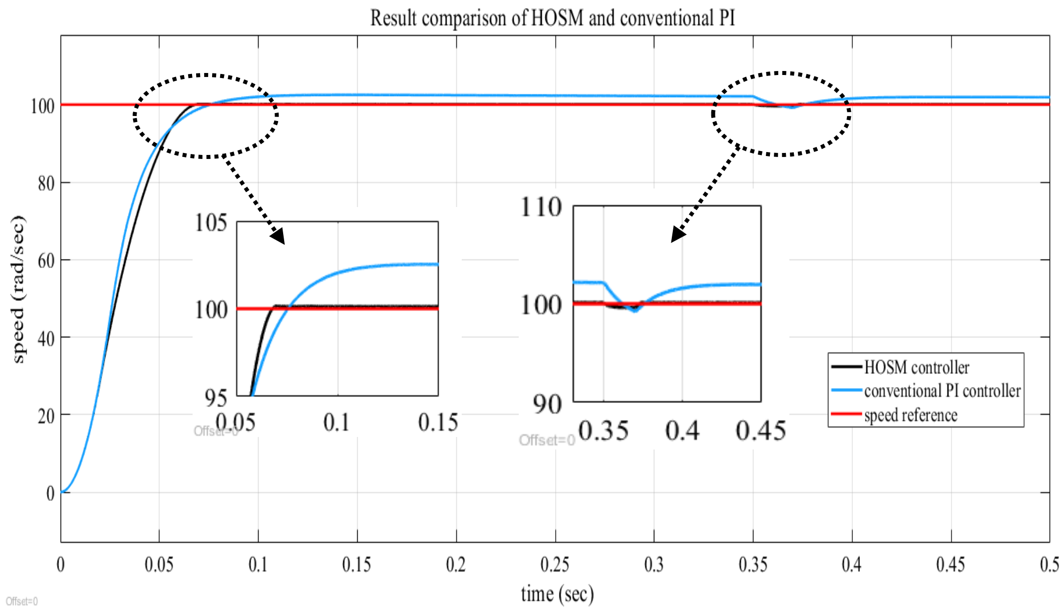

Figure 5.22. Result comparison of conventional PI and the proposed HOSM controller.

The conventional SMC and PI controllers are not recommended to control the speed of traction motor of electric vehicles because the former has high chattering, and the latter is lacking robustness since it is highly affected by external disturbances. FOSMC shows strong robustness towards the external disturbance. However, it has little chattering, and also the convergence is slow. The result of SMC with ERL shows the controller is affected by the addition of external disturbance to the system plus it has little chattering in its speed response.

High order sliding mode controller is the best choice for speed control of the PMSM motor used in three-wheeler electric Bajaj since the controller is robust to internal as well as external disturbances and has good dynamic performance. Besides the chattering phenomenon that exists in conventional sliding mode controller is eliminated using HOSM controller based on super twisting algorithm.

6. CONCLUSIONS AND RECOMMENDATIONS

6.1. Conclusions

The conventional internal combustion engine cars use non-replaceable fossil fuels as a source of energy and emit carbon dioxide to the environment. There is a shortage of fossil fuels in the world and its cost is increasing from time to time. Beyond this, the energy conversion of fossil fuel cars is less efficient. So, internal combustion engine vehicles need to be replaced with emission-free electric vehicles which use a renewable source of energy and have high energy conversion efficiency.

Various motor types are available which can be used for electric vehicles propulsion system. This includes DC motor, PMSM, BLDCM, induction motors (IM), and synchronous reluctance motors. Nowadays AC motors (IM and PMSM), and BLDC motors are popular to be used in electric vehicles. The common requirements of EVs in selecting electric motor includes high efficiency, high power density, high torque at low speed, high power to size ratio, low maintenance cost, less torque ripple. These requirements are best fulfilled with PMSM so this motor is selected to be used as a traction motor in a three-wheeler electric Bajaj.

PMSM motor has been the area of study for many researchers. Different kinds of literature are reviewed related to this thesis work. PMSM is a nonlinear, multivariable coupled system that is sensitive to internal parameter changes, external load disturbance and is affected by unmodeled nonlinear dynamics. To overcome these problems a nonlinear and robust controller which is a sliding mode controller is selected for speed control of the motor.

In this study, the nonlinear Simulink model of the motor is designed and its speed is controlled using a higher-order sliding mode controller based on Super Twisting algorithm with ESO. The field-oriented control technique is implemented in this thesis work. Field-oriented control uses Park and Clarke transformations to convert the three-phase quantities into two-phase quantities. In this control technique, the current of the motor is controlled after it is transformed from a three-phase current to a two-phase d-q current. In this study, the d-q currents are controlled using a GA-PI controller.

In this thesis work, different speed controllers are compared with the proposed high order sliding mode controller. The speed controllers compared includes PI, conventional SMC, SMC with ERL, linear FOSMC, nonlinear FOSMC, and the proposed HOSM controller.

The result of the comparison shows that, the proposed HOSMC outweighs the other controllers in its dynamic performance, high disturbance rejection ability, and chattering elimination ability.

6.2. Recommendations

The speed control of permanent magnet synchronous motor for three-wheeler electric Bajaj is simulated using HOSM controller and the result shows that the controller has good performance. However, this controller can be further improved by incorporating online parameter identification and tuning techniques. In addition to this, due to the cost of materials, and the limited time I had, the system is not proved with experiment. So, it is recommended to make hardware implementation of the system.

References

[1] A. Sheela and M. A. Mohan, “Design of permanent magnet synchronous motor for electric vehicle application using finite element analysis,” *Int. J. Sci. Technol. Res.*, vol. 9, no. 3, pp. 523–527, 2020.

[2] A. Albatayneh, M. N. Assaf, D. Alterman, and M. Jaradat, “Comparison of the Overall Energy Efficiency for Internal Combustion Engine Vehicles and Electric Vehicles,” *Environ. Clim. Technol.*, vol. 24, no. 1, pp. 669–680, 2020, doi: 10.2478/rtuect-2020-0041.

[3] S. Liu, K. Liu, and X. Zhang, “Analysis on Permanent Magnet Synchronous Motor and Its controller for Electric Vehicle,” vol. 166, no. Amcce, pp. 737–742, 2018, doi: 10.2991/amcce-18.2018.128.

[4] X. Liu, H. Chen, J. Zhao, and A. Belahcen, “Research on the Performances and Parameters of Interior PMSM Used for Electric Vehicles,” *IEEE Trans. Ind. Electron.*, vol. 63, no. 6, pp. 3533–3545, 2016, doi: 10.1109/TIE.2016.2524415.

[5] “RESEARCH ARTICLE DESIGN OF PMSM AND ITS APPLICATION Dr . Karunamoorthy , B . and * Dhivyaa , D . Kumaraguru College of Technology , Coimbatore , India,” pp. 2015–2018, 2017.

[6] R. Murmu and A. K. Singh, “Study to Improve the Performance of a PMSM Drive System by Achieving More Precise Speed Tracking and Smooth Torque Response,” vol. 5, no. 11, pp. 955–958, 2016.

[7] H. Yi-geng, “A Dissertation for the Degree of Philosophy Doctor Research of Nonlinear System High Order Sliding Mode Control and its Applications for PMSM,” 2010.

[8] F. M. Zaihidee, S. Mekhilef, and M. Mubin, “Fractional Order SMC for Speed Control of PMSM,” *iEECON 2018 - 6th Int. Electr. Eng. Congr.*, pp. 1–4, 2018, doi: 10.1109/IEECON.2018.8712281.

[9] R. E. Neapolitan and K. Hee Nam, *PMSM Control Methods*. 2019.

[10] M. Zeraoulia *et al.*, “Electric motor drive selection issues for HEV propulsion systems : A comparative study Electric Motor Drive Selection Issues for HEV Propulsion Systems : A Comparative Study,” *Ieee Trans. Veh. Technol.*, vol. 55, no.

6, pp. 1756–1764, 2010.

[11] N. Hashernnia and B. Asaei, “Comparative Study of Using Different Electric,” *Int. Conf. Electr. Mach.*, no. c, pp. 1–5, 2008.

[12] P. Blaha and P. Vaclavek, “Robust control of permanent magnet synchronous motor,” *Int. Conf. Control. Autom. Syst.*, pp. 1317–1322, 2012.

[13] K. Suman and A. T. Mathew, “Speed Control of Permanent Magnet Synchronous Motor Drive System Using PI, PID, SMC and SMC plus PID Controller,” *2018 Int. Conf. Adv. Comput. Commun. Informatics, ICACCI 2018*, pp. 543–549, 2018, doi: 10.1109/ICACCI.2018.8554788.

[14] T. Liu, G. Chen, and S. Li, “Application of vector control technology for PMSM used in electric vehicles,” *Open Autom. Control Syst. J.*, vol. 6, no. 1, pp. 1334–1341, 2015, doi: 10.2174/1874444301406011334.

[15] M. S. Merzoug and F. Naceri, “Comparison of Field-Oriented Control and Direct Torque Control for Permanent Magnet Synchronous Motor (PMSM),” *Int. J. Electr. Comput. Eng.*, vol. 2, no. 9, pp. 1797–1802, 2008, doi: 10.5281/zenodo.1330719.

[16] N. Maleki, “A Detailed Comparison Between FOC and DTC Methods of a Permanent Magnet Synchronous Motor Drive,” *J. Electr. Electron. Eng.*, vol. 3, no. 2, p. 92, 2015, doi: 10.11648/j.jeee.s.2015030201.30.

[17] M. A. W. Begh and Hans-Georg Herzog, “Comparison of Field Oriented Control and Direct Torque Control for PMSM,” *World Acad. Sci. Eng. Technol.*, vol. 21, no. April, pp. 209–304, 2019, doi: 10.13140/RG.2.2.21677.59360/1.

[18] C. Ed-Dahmani, H. Mahmoudi, and M. El Azzaoui, “Direct torque control of permanent magnet synchronous motors in MATLAB/SIMULINK,” *Proc. 2016 Int. Conf. Electr. Inf. Technol. ICEIT 2016*, vol. 0, no. 28, pp. 452–457, 2016, doi: 10.1109/EITech.2016.7519641.

[19] F. V. A. Raj and V. K. Kannan, “Analysis of Different Speed Control Techniques Using PMSM,” vol. 4, no. 10, pp. 11–17, 2016, doi: 10.17148/IJIREEICE.2016.41003.

[20] H. Aygun, M. Gokdag, M. Aktas, and M. Cernat, “A novel sensorless field oriented controller for Permanent Magnet Synchronous Motors,” *IEEE Int. Symp. Ind.*

Electron., no. June, pp. 715–720, 2014, doi: 10.1109/ISIE.2014.6864700.

[21] P. Maji, P. G. KPanda, and P. P. KSaha, "Field Oriented Control of Permanent Magnet Synchronous Motor Using PID Controller," *Int. J. Adv. Res. Electr. Electron. Instrum. Eng.*, vol. 04, no. 02, pp. 632–639, 2015, doi: 10.15662/ijareeie.2015.0402019.

[22] F. M. Zaihidee, S. Mekhilef, and M. Mubin, "Application of Fractional Order Sliding Mode Control for Speed Control of Permanent Magnet Synchronous Motor," *IEEE Access*, vol. 7, pp. 101765–101774, 2019, doi: 10.1109/ACCESS.2019.2931324.

[23] S. Jumana Beegum N and P. Sheenu, "Comparison of Speed control of PMSM with PI, PID& Adaptive PID Controllers Jumana," *Int. Res. J. Eng. Technol.*, pp. 2376–2383, 2016.

[24] Q. Song and C. Jia, "Robust speed controller design for permanent magnet synchronous motor drives based on sliding mode control," *Energy Procedia*, vol. 88, pp. 867–873, 2016, doi: 10.1016/j.egypro.2016.06.102.

[25] V. M. J and V. Sreelekha, "Speed Control of PMSM Drive Using Adaptive Fuzzy Logic Controller," pp. 156–160, 2018.

[26] J. Huang, H. Li, F. Teng, and D. Liu, "Fractional order sliding mode controller for the speed control of a permanent magnet synchronous motor," *Proc. 2012 24th Chinese Control Decis. Conf. CCDC 2012*, pp. 1203–1208, 2012, doi: 10.1109/CCDC.2012.6244192.

[27] P. Gao, G. Zhang, H. Ouyang, and L. Mei, "A Sliding mode control with nonlinear fractional order pid sliding surface for the speed operation of surface-mounted pmsm drives based on an extended state observer," *Math. Probl. Eng.*, vol. 2019, 2019, doi: 10.1155/2019/7130232.

[28] H. Yigeng, S. Laghrouche, L. Weiguo, and A. Miraoui, "Robust High Order Sliding Mode Control of Permanent Magnet Synchronous Motors," *Recent Adv. Robust Control - Theory Appl. Robot. Electromechanics*, no. November, 2011, doi: 10.5772/17808.

[29] T. Hofman, S. G. van der Tas, W. Ooms, E. W. P. van Meijl, and B. M. Laugeman, "Development of a micro-hybrid system for a three-wheeled motor taxi," *World*

Electr. Veh. J., vol. 3, no. 3, pp. 572–580, 2009, doi: 10.3390/wevj3030572.

[30] N. Hashemnia and B. Asaei, "Comparative study of using different electric motors in the electric vehicles," *Proc. 2008 Int. Conf. Electr. Mach. ICEM'08*, no. November, 2008, doi: 10.1109/ICELMACH.2008.4800157.

[31] Y. KIRAN and D. P. S. P. SWAMY, "Field Oriented Control of a Permanent Magnet Synchronous Motor using a DSP," *Int. J. Adv. Res. Electr. Electron. Instrum. Eng.*, vol. 03, no. 10, pp. 12364–12378, 2014, doi: 10.15662/ijareeie.2014.0310008.

[32] M. B. B. Sharifian, T. Herizchi, and K. G. Firouzjah, "Field oriented control of permanent magnet synchronous motor using predictive space vector modulation," *2009 IEEE Symp. Ind. Electron. Appl. ISIEA 2009 - Proc.*, vol. 2, no. Isiea, pp. 574–579, 2009, doi: 10.1109/ISIEA.2009.5356385.

[33] B. Tamene and T. Engineering, "Addis Ababa University Addis Ababa Institute of Technology School of Electrical and Computer Engineering," no. February, 2020.

[34] C. Blake and C. Bull, "IGBT or MOSFET: Choose wisely," *EngineerIT*, vol. 2018, no. April, pp. 37–39, 2018.

[35] A. Maamoun, Y. M. Alsayed, and A. Shaltout, "Space-vector PWM inverter feeding a Permanent-Magnet synchronous motor," *World Acad. Sci. Eng. Technol.*, vol. 65, no. 100, pp. 627–631, 2010, doi: 10.5281/zenodo.1335230.

[36] M. S. Mahammadsoaib and M. P. Sajid, "Vector controlled PMSM drive using SVPWM technique - A MATLAB / simulink implementation," *Int. Conf. Electr. Electron. Signals, Commun. Optim. EESCO 2015*, no. February, 2015, doi: 10.1109/EESCO.2015.7253938.

[37] A. M. Nazlee, N. H. Hamid, F. A. Hussin, and N. B. Z. Ali, "Space Vector PWM for PMSM simulation using Matlab Simulink," *IEEE Asia-Pacific Conf. Circuits Syst. Proceedings, APCCAS*, no. August 2014, pp. 1127–1130, 2010, doi: 10.1109/APCCAS.2010.5774974.

[38] M. M. Gaballah, "Design and Implementation of Space Vector PWM Inverter Based on a Low Cost Microcontroller," *Arab. J. Sci. Eng.*, vol. 38, no. 11, pp. 3059–3070, 2013, doi: 10.1007/s13369-012-0464-2.

[39] D. Q. Zhang and S. K. Panda, "Chattering-free and fast-response sliding mode

controller," pp. 171–177.

[40] N. Bharathi, "Sliding Mode Control for Speed Control of Brushless Dc Motor," *Int. J. Sci. Eng. Res.*, vol. 5, no. 4, pp. 22–27, 2014.

[41] P. Gao, G. Zhang, and X. Lv, "A Novel Compound Nonlinear State Error Feedback Super-Twisting Fractional-Order Sliding Mode Control of PMSM Speed Regulation System Based on Extended State Observer," *Math. Probl. Eng.*, vol. 2020, 2020, doi: 10.1155/2020/1843598.

[42] L. Poletto and F. Frassetto, "Cost-effective plane-grating monochromator design for extreme-ultraviolet application," *Appl. Opt.*, vol. 57, no. 5, p. 1202, 2018, doi: 10.1364/ao.57.001202.

[43] F. M. Zaihidee, S. Mekhilef, and M. Mubin, "Application of Fractional Order Sliding Mode Control for Speed Control of Permanent Magnet Synchronous Motor," *IEEE Access*, vol. 7, pp. 101765–101774, 2019, doi: 10.1109/ACCESS.2019.2931324.

[44] A. Levant, "Higher-order sliding modes, differentiation and output-feedback control," *Int. J. Control*, vol. 76, no. 9–10, pp. 924–941, 2003, doi: 10.1080/0020717031000099029.

[45] S. Laghrouche, F. Plestan, and A. Glumineau, "A higher order sliding mode controller for a class of MIMO nonlinear systems: Application to PM synchronous motor control," *Proc. Am. Control Conf.*, vol. 3, pp. 2592–2597, 2004, doi: 10.1109/ACC.2004.182497.

[46] S. Kamal, A. Chalanga, J. A. Moreno, L. Fridman, and B. Bandyopadhyay, "Higher order super-twisting algorithm," *Proc. IEEE Work. Appl. Comput. Vis.*, no. November, 2014, doi: 10.1109/VSS.2014.6881129.

[47] A. Dendouga, "Conventional and second order sliding mode control of permanent magnet synchronous motor fed by direct matrix converter: Comparative study," *Energies*, vol. 13, no. 19, pp. 7–10, 2020, doi: 10.3390/en13195093.

[48] B. Liu, "Speed control for permanent magnet synchronous motor based on an improved extended state observer," *Adv. Mech. Eng.*, vol. 10, no. 1, pp. 1–12, 2018, doi: 10.1177/1687814017747663.

Reference Links

[L1] https://www.embitel.com/blog/embedded-blog/brushless-dc-motor-vs-pmsm-how-these-motors-and-motor-control-solutions-work.

[L2] http://www.xindaenergy.com/Brushless-permanent-magnet-vehicle--motor-3kw-15kw-p245.html.

[L3] https://www.engineering.com/story/the-many-types-of-ev-motors.

[L4] http://file01.up71.com/File/CorpProductImages/2013/12/08/0_liyuanbattery_7604_20131208065807.png.

[L5] https://www.magneticinnovations.com/faq/difference-ac-motor-dc-motor/

APPENDICES

A MATLAB code for GA-PI current controller.

```
function Tune_Model_PI
clear all
options= optimoptions('ga','PlotFcn',@gaplotbestf);
options.PopulationSize= 30;
options.MaxGenerations= 20;  % Increase value if needed
nvar= 2; % Number of parameters
LB= [400 400]; % Lower bound of tuning parameters
UB= [500 500]; % Upper bound of tuning parameters

[x,fval]= ga(@EvalObj,nvar,[],[],[],[],LB,UB,[],options)

% Updates Kp, Ki and Kd in simulink model workspace for verification
simulink_model= 'Model_PI';
load_system(simulink_model);
gains= get_param(simulink_model,'modelworkspace');
gains.assignin('Kp1', x(1));
gains.assignin('Ki1', x(2));

function obj= EvalObj(x)
% Updates the values of Kp, Ki and Kd in Simulink model workspace
simulink_model= 'Model_PI';
load_system(simulink_model);
gains= get_param(simulink_model,'modelworkspace');
gains.assignin('Kp1', x(1));
gains.assignin('Ki1', x(2));

% Simulates the simulink model to get the outputs
simOut= sim(simulink_model,'SaveOutput','on');

% Retrieves time t and error e
t= simOut.find('t');
e= simOut.find('e');
```

B Simulink model of the entire system

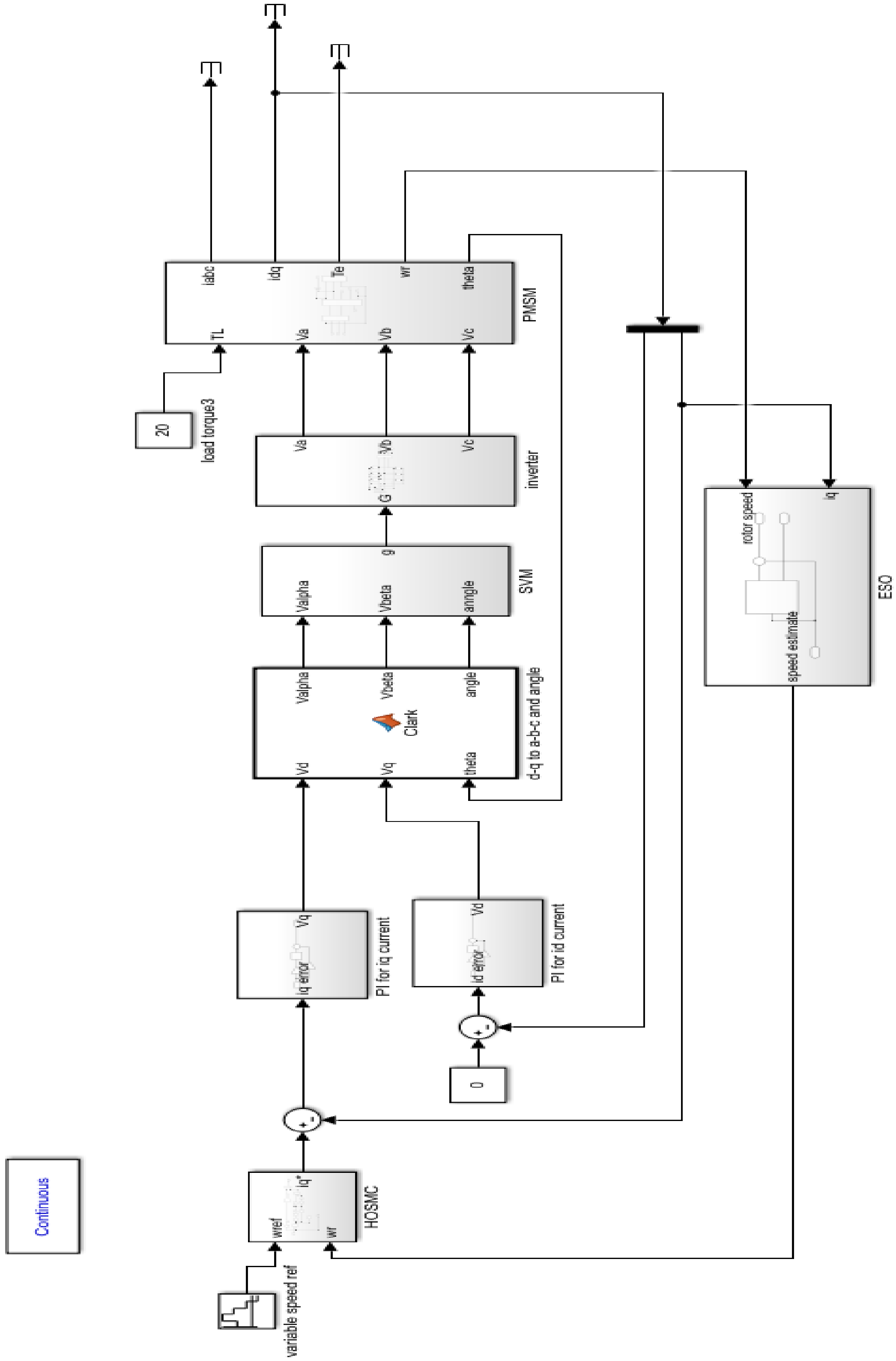

Figure A. 1.The overall Simulink model of the proposed system.

C Simulink model of PMSM motor

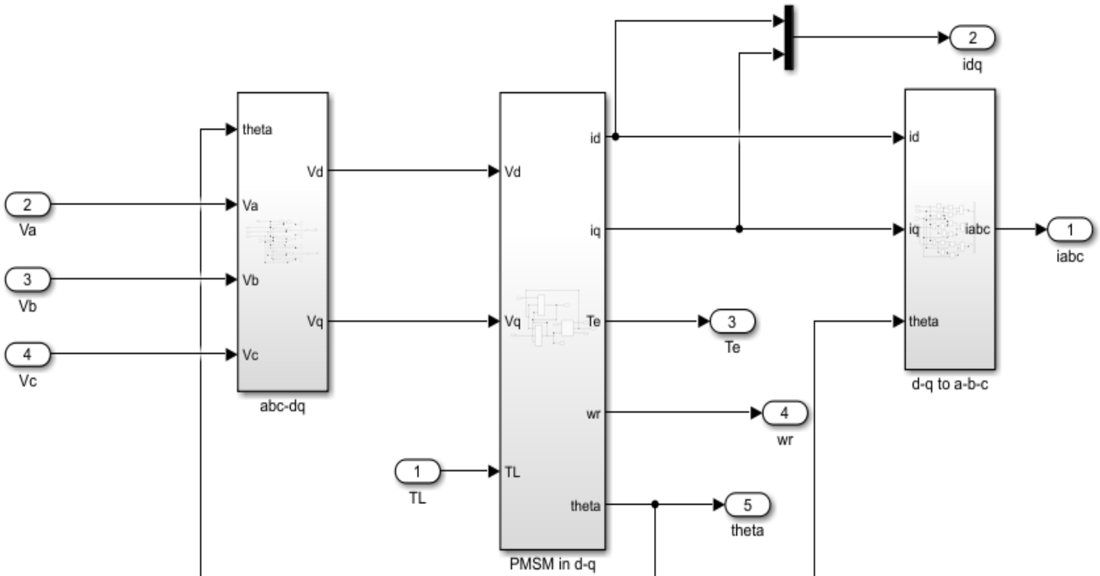

Figure A. 2.PMSM motor Simulink block.

D ABC to D-Q voltage transformation Simulink block

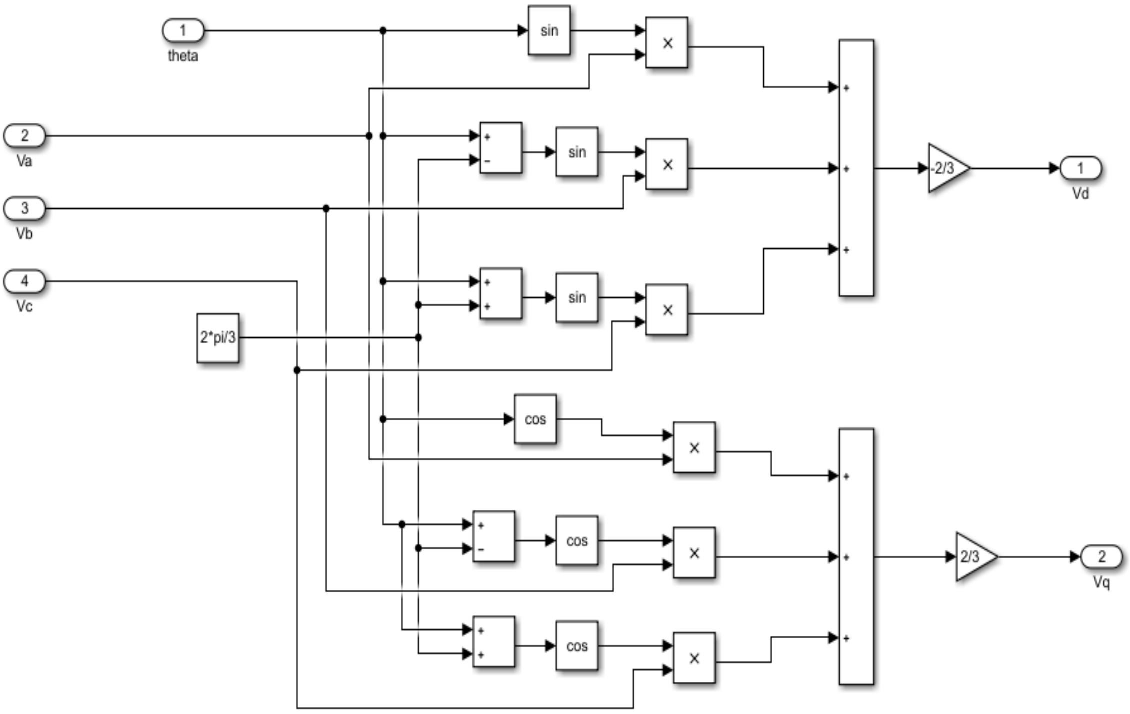

Figure A. 3.a-b-c to d-q transformation

E Electromagnetic torque, speed, position, i_d and i_q calculation for PMSM

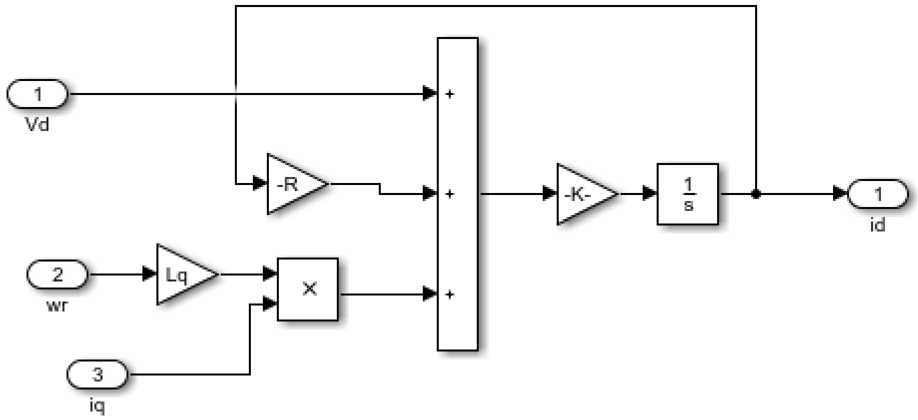

Figure A. 4.Direct current (id) Simulink block (k=1/Ld).

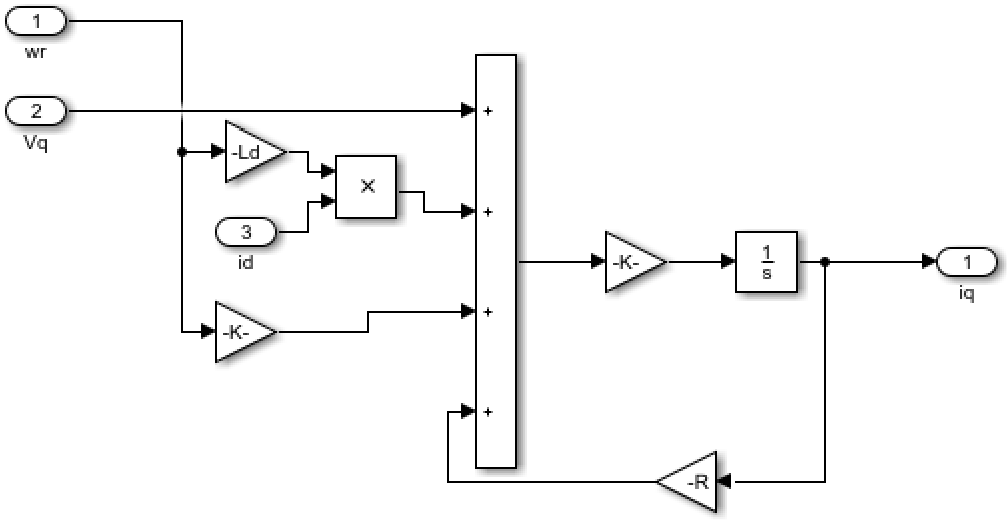

Figure A. 5.Simulink block of quadrature current (k=1/Lq).

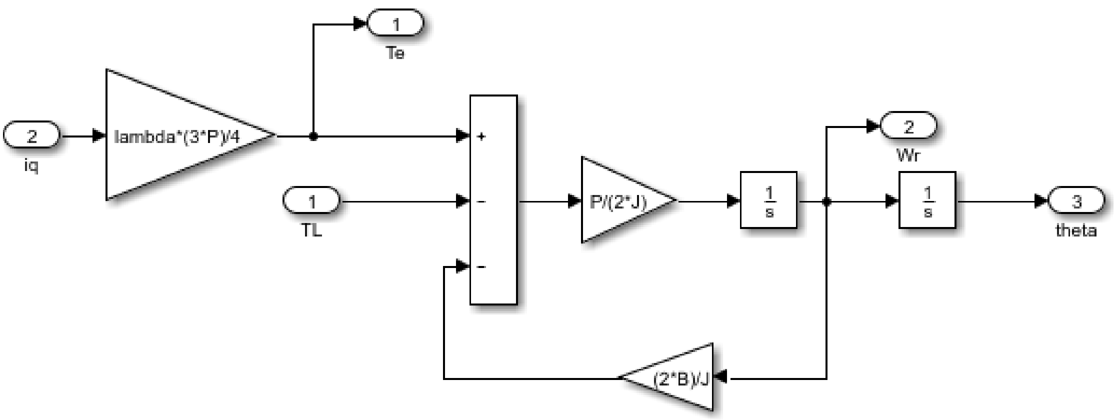

Figure A. 6.Electromagnetic torque, speed and position Simulink model.

F d-q to a-b-c transformation

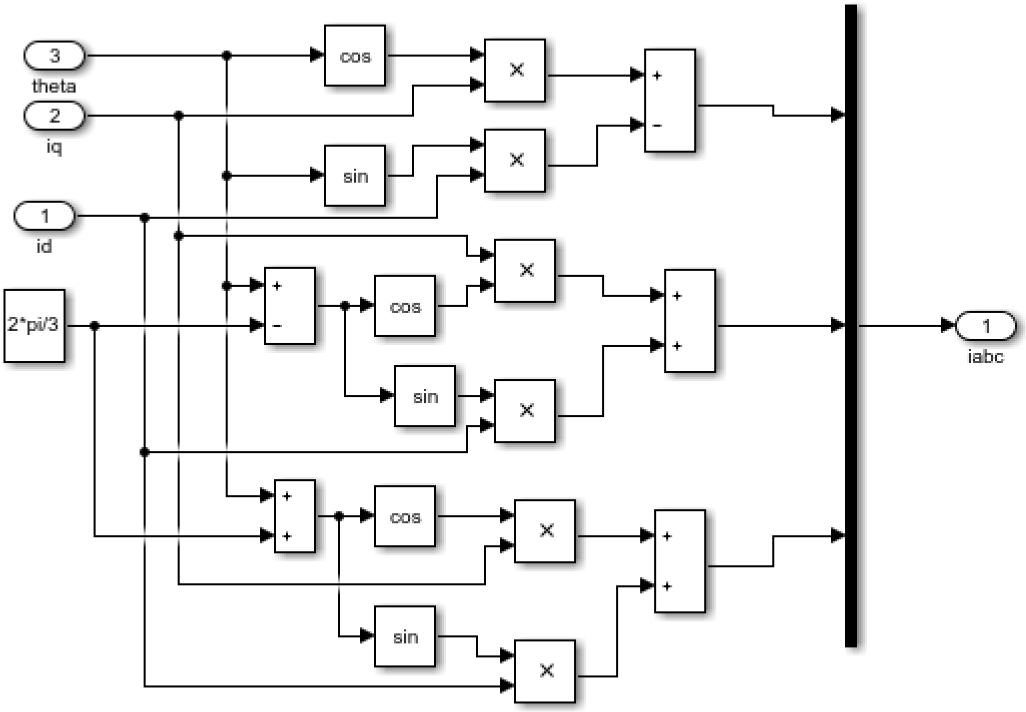

Figure A. 7Simulink block of d-q to a-b-c transformation

Clarke transformation and angle calculation

```
function [Valpha, Vbeta, angle] = Clark(Vd, Vq, theta)
Valpha= Vd*cos(theta)-Vq*sin(theta);
Vbeta= Vd*sin(theta)+Vq*cos(theta);
angle= atan2(Vbeta, Valpha);
```

G Simulink block of SVPWM

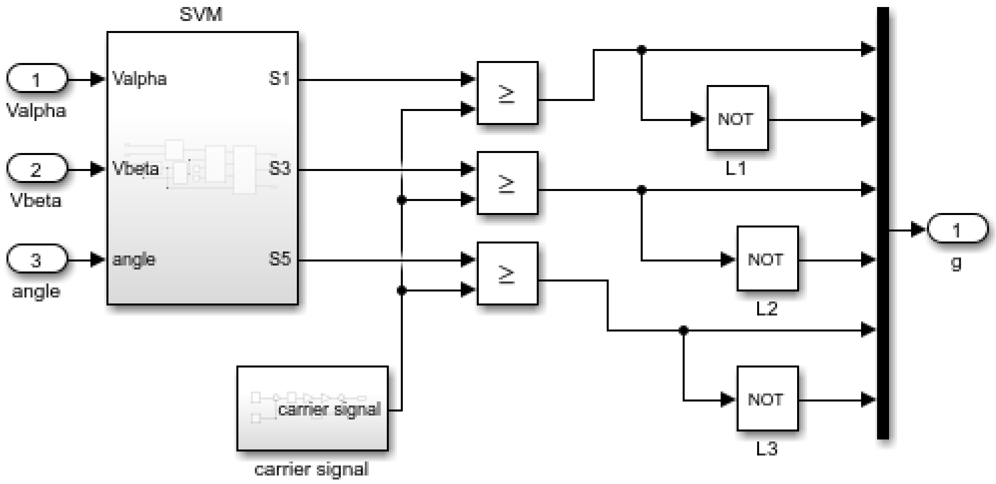

Figure A. 8.Simulink block SVPWM

Carrier signal Simulink block

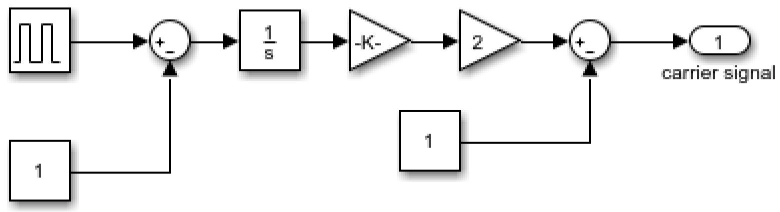

Figure C.1. Simulink block carrier signal

H Internal part of SVM implemented with MATLAB/Simulink

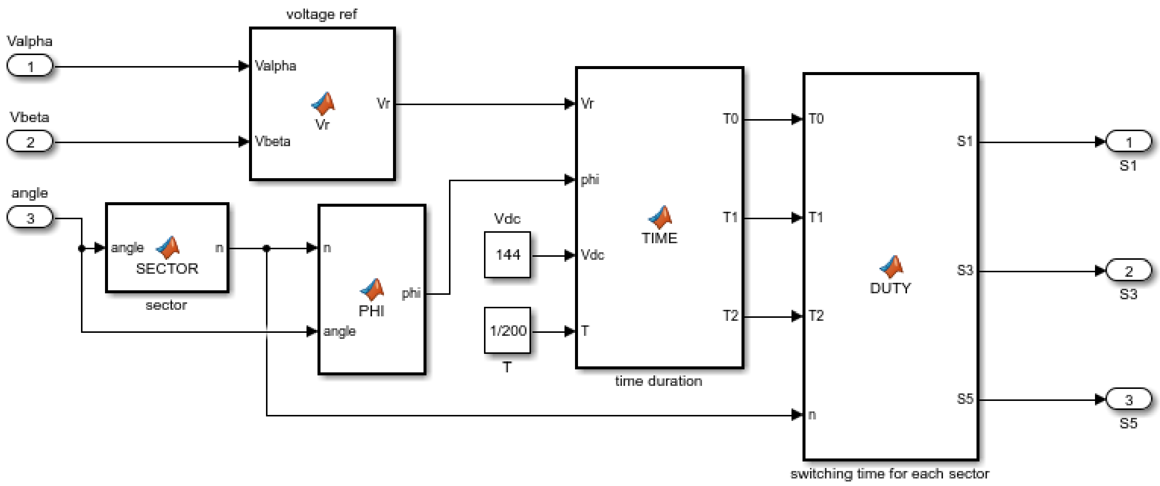

Figure A. 9.internal Simulink blocks of SVPWM implemented with script code.

I Implementation of each Simulink block of the above figure with script

Sector calculation

```
function n = SECTOR(angle)
n=0;
if(angle>0)&&(angle<=pi/3)
    n=1;
end
if(angle>pi/3)&&(angle<=2*pi/3)
    n=2;
end
if(angle>2*pi/3)&&(angle<=pi)
    n=3;
end
if(angle<=0)&&(angle>-1*pi/3)
    n=6;
end
if(angle<=-1*pi/3)&&(angle>-2*pi/3)
    n=5;
end
if(angle<=-2*pi/3)&&(angle>-1*pi)
    n=4;
end
```

V_{ref} calculation

```
function Vr = Vr(Valpha, Vbeta)
Vr=0;
Vr=sqrt(Valpha^2+Vbeta^2);
```

Switching time calculation

```
function [T0, T1, T2] = TIME(Vr,phi,Vdc, T)
a=sqrt(3)*(Vr/Vdc);
T1=T*a*sin(pi/3-phi);
T2=T*a*sin(phi);
T0=T-T1-T2;
```

Switching time for every sector

```
function [S1, S3, S5] = DUTY(T0, T1, T2, n)
S1=0;
S3=0;
S5=0;
if (n==1)
    S1=T1+T2+T0/2;
    S3=T2+T0/2;
```

```
    S5=T0/2;
end
if(n==2)
    S1=T1+T0/2;
    S3=T1+T2+T0/2;
    S5=T0/2;
end
if(n==3)
    S1=T0/2;
    S3=T1+T2+T0/2;
    S5=T2+T0/2;
end
if(n==4)
    S1=T0/2;
    S3=T1+T0/2;
    S5=T1+T2+T0/2;
end
if(n==5)
    S1=T2+T0/2;
    S3=T0/2;
    S5=T1+T2+T0/2;
end
if(n==6)
    S1=T1+T2+T0/2;
    S3=T0/2;
    S5=T1+T0/2;
end
```

J Three-phase inverter Simulink block

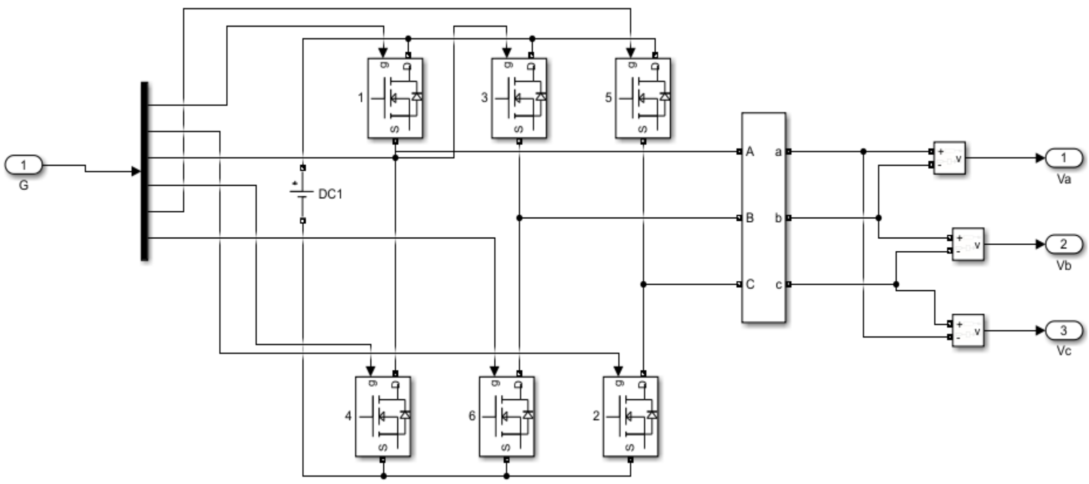

Figure A. 10.Simulink block of three-phase inverter.

K Extended state observer Simulink implementation

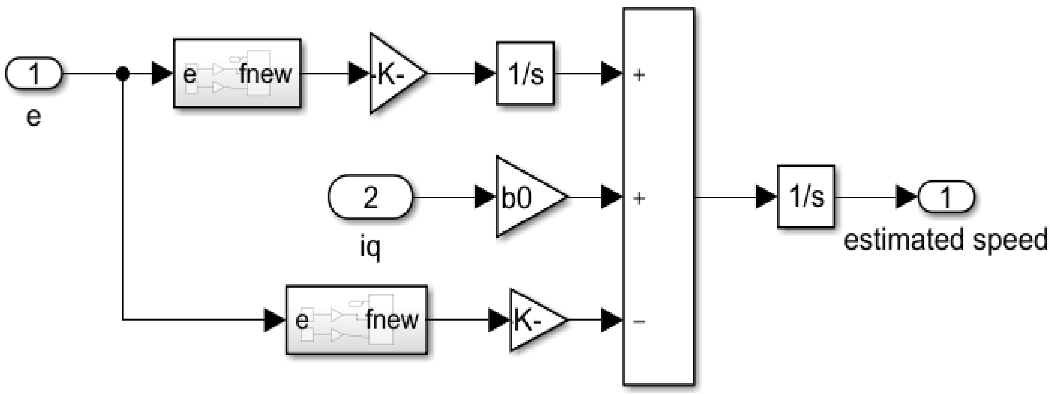

Figure A. 11.Simulink block of ESO

L Dynamic Performance of Different Controllers

Table L.1. Dynamic performance comparison of different controllers at constant speed(100rad/s)

<table>
<tr><th colspan="2">Controllers Result</th></tr>
<tr><td colspan="2">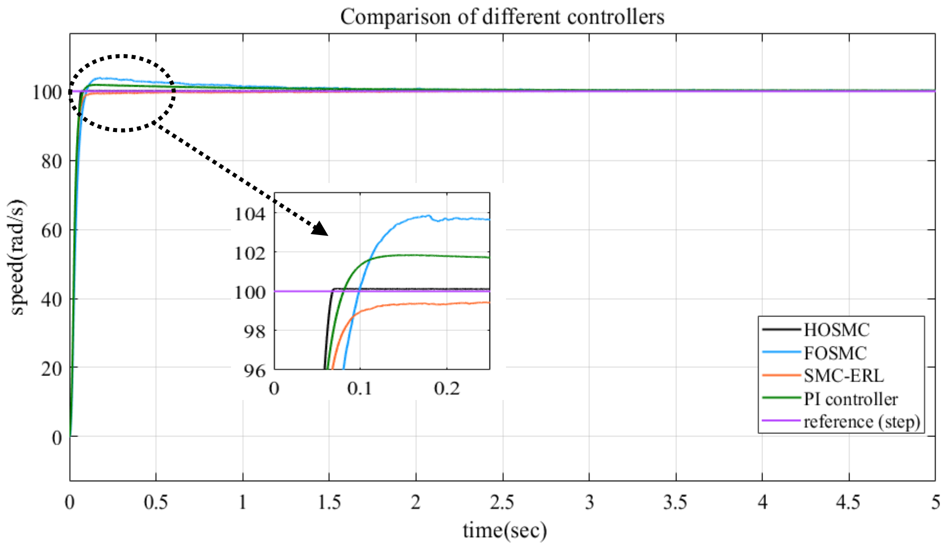
</td></tr>
<tr><th>HOSMC</th><th>FOSMC</th></tr>
<tr><td>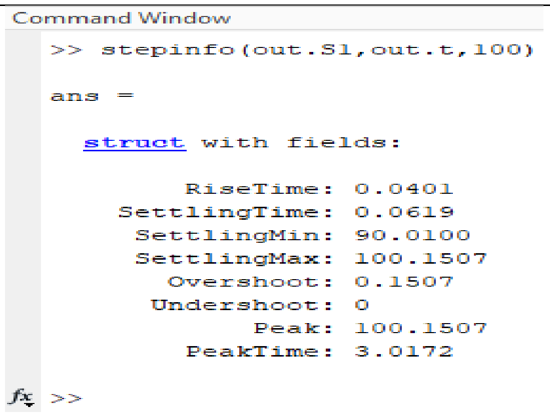
Command Window
>> stepinfo(out.S1,out.t,100)
ans =
struct with fields:
RiseTime: 0.0401
SettlingTime: 0.0619
SettlingMin: 90.0100
SettlingMax: 100.1507
Overshoot: 0.1507
Undershoot: 0
Peak: 100.1507
PeakTime: 3.0172
fx >></td><td>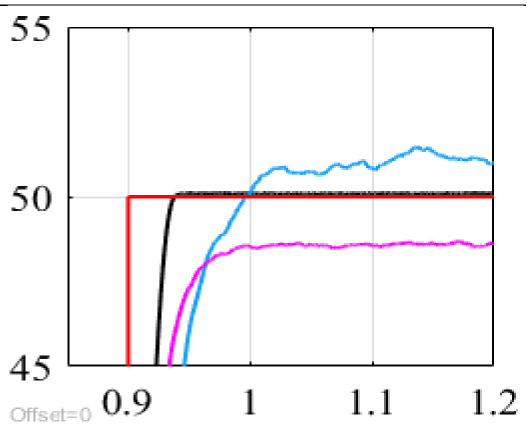
</td></tr>
<tr><th>SMC-ERL</th><th>PI controller</th></tr>
<tr><td>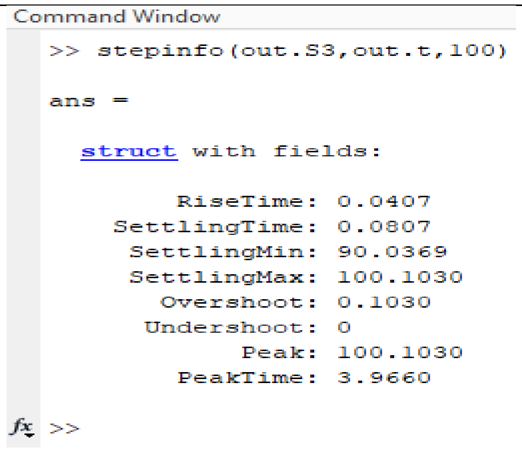
Command Window
>> stepinfo(out.S3,out.t,100)
ans =
struct with fields:
RiseTime: 0.0407
SettlingTime: 0.0807
SettlingMin: 90.0369
SettlingMax: 100.1030
Overshoot: 0.1030
Undershoot: 0
Peak: 100.1030
PeakTime: 3.9660
fx >></td><td>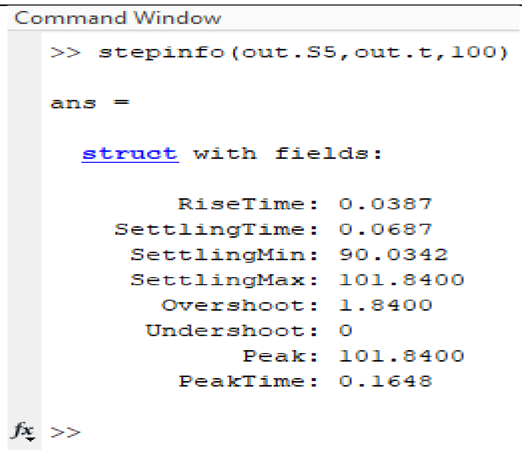
Command Window
>> stepinfo(out.S5,out.t,100)
ans =
struct with fields:
RiseTime: 0.0387
SettlingTime: 0.0687
SettlingMin: 90.0342
SettlingMax: 101.8400
Overshoot: 1.8400
Undershoot: 0
Peak: 101.8400
PeakTime: 0.1648
fx >></td></tr>
</table>

Table L.2. Dynamic performance of SMC at reference sped of 100rad/s

SMC Result
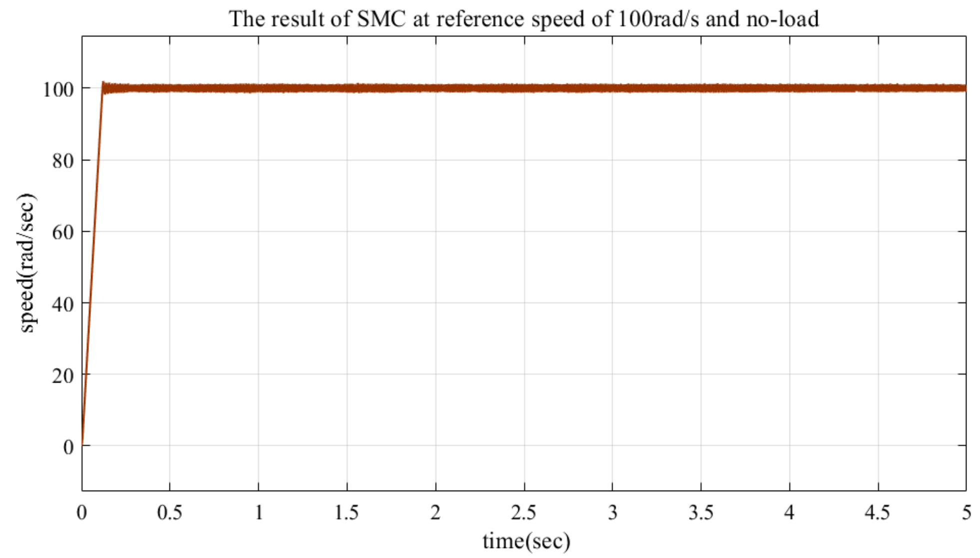


```
Command Window
>> stepinfo(out.S4,out.t,100)

ans =

  struct with fields:

         RiseTime: 0.0926
     SettlingTime: 0.1163
      SettlingMin: 90.0121
      SettlingMax: 101.9928
        Overshoot: 1.9928
       Undershoot: 0
             Peak: 101.9928
         PeakTime: 0.1230

>>
```